

Technische Universität München

Fakultät für Medizin

**Studying Mechanisms of Diabetes Remission  
following Bariatric Surgery**

Lena Sophie Oppenländer

Vollständiger Abdruck der von der Fakultät für Medizin der Technischen Universität München zur Erlangung des akademischen Grades einer

**Doktorin der Naturwissenschaften**

genehmigten Dissertation

Vorsitzender: Prof. Dr. Helmut Friess

Prüfer der Dissertation:

1. Prof. Dr. Heiko Lickert
2. apl. Prof. Dr. Johannes Beckers

Die Dissertation wurde am 13.08.2021 bei der Technischen Universität München eingereicht und durch die Fakultät für Medizin am 12.07.2022 angenommen.





# Table of Contents

<b>ABSTRACT .....</b>	<b>1</b>
<b>LIST OF FIGURES .....</b>	<b>3</b>
<b>LIST OF ABBREVIATIONS .....</b>	<b>4</b>
<b>1. INTRODUCTION .....</b>	<b>9</b>
1.1 Metabolic Syndrome.....	9
1.2 Diabetes Mellitus.....	9
1.3 Glucose Homeostasis in Health and Disease.....	9
1.4 Intestinal Architecture.....	10
1.5 Regulation of Glucose and Energy Homeostasis by Intestinal Hormones.....	12
1.6 Intestinal Mal-Adaptations in Obesity .....	12
1.7 Pancreatic Architecture.....	13
1.8 Glucose Regulation by the Endocrine Pancreas .....	14
1.9 Pancreatic $\beta$ -cell Failure in Type-2 Diabetes .....	16
1.10 Current Treatment Options for Type-2 Diabetes .....	17
1.11 Gluco-Regulatory Mechanisms of Vertical Sleeve Gastrectomy .....	21
<b>2. SCOPE OF THE THESIS.....</b>	<b>24</b>
<b>3. RESULTS.....</b>	<b>25</b>
3.1 Preclinical Mouse Models Mimicking Human Diabetes and Obesity .....	25
3.2 Therapeutic VSG Intervention in Early Diabetes .....	29
3.2.1 VSG Improves Diet-Induced Obesity and Pre-Diabetes Dependent of Model.....	29
3.2.2 Impact of Intestinal and Pancreatic Morphological Adaptations after VSG.....	35
3.3 Therapeutic VSG Intervention in Clinically-Overt Diabetes.....	40

3.3.1 VSG Rescues Clinically-Overt Diabetes and Is Superior to Calorie Restriction.....	40
3.3.2 $\beta$ -Cell Pathophysiology in Extreme Diabetes .....	42
3.3.3 VSG Distinctively Modulates the Islet Transcriptome.....	45
3.3.4 VSG Restores $\beta$ -Cell Identity and Function.....	48
3.3.5 Mechanisms of $\beta$ -Cell Regeneration upon VSG.....	52
<b>4. DISCUSSION .....</b>	<b>62</b>
<b>4.1 Modeling Pre-Diabetes and Diabetes in Mice.....</b>	<b>62</b>
<b>4.2 Counteracting Pre-Diabetes through VSG intervention.....</b>	<b>64</b>
4.2.1 Similar Physiological Outcomes of VSG and Calorie-Restriction in Obesity-Linked Pre-Diabetes.	64
4.2.2 Morphological Adaptations are Dispensable for VSG Outcomes in Obesity-Linked Pre-Diabetes.	66
<b>4.3 Reversing Clinically-Overt Diabetes through VSG intervention .....</b>	<b>68</b>
4.3.1 Pathomechanisms of Clinically-Overt Diabetes .....	68
4.3.2 Restoring Glucose Regulation through VSG .....	69
4.3.3 Recovering $\beta$ -Cell Identity and Function through VSG .....	70
4.3.4 Mechanisms of Expanded $\beta$ -Cell Mass upon VSG .....	72
4.3.5 Novel VSG Target Genes in $\beta$ -Cells .....	73
4.3.6 Role of Extreme $\beta$ -Cells in Diabetes and after VSG .....	76
<b>4.4 Conclusions.....</b>	<b>78</b>
<b>5. MATERIALS AND METHODS .....</b>	<b>79</b>
<b>REFERENCES .....</b>	<b>95</b>
<b>ACKNOWLEDGEMENTS .....</b>	<b>109</b>
<b>PUBLICATIONS.....</b>	<b>110</b>









## Abstract

Obesity-linked type-2 diabetes mellitus (T2D) is a life-threatening epidemic disease affecting millions of people worldwide. T2D is characterized by insulin-resistance, hyperglycaemia, and the progressive failure of insulin secreting  $\beta$ -cells. Despite intensive research, current therapies for the treatment of early and advanced stages of T2D are not optimal yet. While pharmacological and substitutive approaches on the market do not promise cure, bariatric surgery including vertical sleeve gastrectomy (VSG) has gained reputation for generating high T2D remission rates and lowering body weight. The mechanisms of bariatric surgery are complex and thought to involve synergistic beneficial effects of changes in peripheral insulin sensitivity, the gut-brain axis, microbiota, bile acids as well as local endocrine tissue adaptations. However, its invasiveness hinders the application to a broad range of patients. Thus, research aims at identifying the underlying molecular mechanisms of T2D remission upon VSG in order to identify targets for the development of novel pharmacological approaches mimicking bariatric surgery. Different stages of the disease require different therapeutic strategies. To this end, we used a classical diet-induced obesity (DIO) pre-diabetes mouse model and the *db/db* mouse modeling far-progressed, severe T2D to advance the mechanistic knowledge of VSG-mediated T2D remission and to discover novel gluco-regulatory targets of VSG. In pre-diabetes, we show that VSG is equally effective as pair-feeding (PF) in lowering glycaemia supporting dietary interventions for the rescue of very early diabetic conditions as well. Further, our findings reveal that morphological and cellular adaptations in endocrine intestinal epithelial and islet tissues are not mechanistically required to restore glycaemia upon VSG in our DIO models. In a mouse model of clinically-overt T2D, we provide the first prove that VSG is able to rapidly rescue severe, late-stage T2D conditions within only two weeks of intervention and reveal its superiority over calorie restriction. PF failed to improve far-progressed T2D, while VSG normalized glycaemia and markedly enhanced insulin secretion. Using state-of-the-art single-cell RNA-sequencing, our data provides the first highly-resolved transcriptional profile of islet cell types including  $\beta$ -cells. VSG improved  $\beta$ -cell identity, function, and induced several adaptive responses in  $\beta$ -cells including the unfolded protein response (UPR) and ER-associated degradation (ERAD) most likely to support high insulin secretion rates present after VSG. Mechanistically, we show that VSG expands  $\beta$ -cell mass by triggering additive mechanisms of 1)  $\beta$ -cell redifferentiation from a dysfunctional to a functional state and 2)  $\beta$ -cell replication. Finally, we discovered novel VSG targets intrinsic to  $\beta$ -cells including immune- and pregnancy-factors that might potentially drive the gluco-regulatory benefits of VSG in far-progressed T2D. In summary, our study reveals the potency of VSG

to promote T2D remission in early and late stages of T2D and resolves unique  $\beta$ -cell intrinsic adaptations including novel VSG targets that parallel the recovery of  $\beta$ -cell function after VSG. Future research will show if these targets can be used to develop novel pharmacological therapies to restore  $\beta$ -cell function in T2D.

## List of Figures

Figure 1: Intestinal architecture and cellular composition .....	11
Figure 2: Morphology and cellular composition of islets of Langerhans .....	14
Figure 3: Glucose-stimulated insulin secretion.....	15
Figure 4: Concept of $\beta$ -cell dedifferentiation.....	17
Figure 5: The two most commonly performed bariatric surgical procedures: Roux-en-Y gastric bypass (RYGB) and vertical sleeve gastrectomy (VSG).....	20
Figure 6: HFD feeding in B6J and B6N mice and leptin-receptor deficiency ( <i>db/db</i> ) in BKS mice results in obesity.....	26
Figure 7: HFD-fed B6N mice show a pre-diabetic phenotype, while <i>db/db</i> mice reveal overt diabetes characteristics.....	28
Figure 8: VSG and PF result in body weight loss in DIO mouse models.....	30
Figure 9: VSG and PF improve glycaemia in DIO mouse models dependent of strain.....	33
Figure 10: VSG does not impact small intestinal morphology in a B6J DIO model.....	36
Figure 11: EEC density is not affected by VSG in a DIO model.....	37
Figure 12: Pancreatic islet morphology is not affected by VSG in pre-diabetes DIO models.....	38
Figure 13: VSG does not alter $\beta$ - or $\alpha$ -cell mass in pre-diabetes DIO models.....	39
Figure 14: VSG but not PF restores normoglycaemia and enhances $\beta$ -cell function in overt diabetic <i>db/db</i> mice independent of body weight.....	41
Figure 15: Diabetic stress alters the $\beta$ -cell transcriptome but not that of $\alpha$ -, $\delta$ -, and PP-cells in <i>db/db</i> mice.....	43
Figure 16: Islets of <i>db/db</i> mice reveal extreme $\beta$ -cell dedifferentiation.....	44
Figure 17: The transcriptome of $\alpha$ -, $\delta$ -, and PP-cells is unchanged after VSG.....	45
Figure 18: VSG and PF differently affect the $\beta$ -cell transcriptome.....	47
Figure 19: VSG but not PF improves $\beta$ -cell identity and function.....	49
Figure 20: VSG enhances the UPR and ERAD to counteract ER-stress in $\beta$ -cells.....	51
Figure 21: <i>db/db</i> mice present heterogeneous $\beta$ -cell states.....	53
Figure 22: VSG improves transcriptional signature of mature and dedifferentiated $\beta$ -cells.....	54
Figure 23: VSG induces $\beta$ -cell redifferentiation and shifts towards extreme $\beta$ -cell states.....	56
Figure 24: Extreme $\beta$ -cells show a characteristic profile marked by high expression of insulin machinery genes.....	57
Figure 25: VSG expands $\beta$ -cell mass.....	59
Figure 26: The $\beta$ -cell transcriptome reveals unique targets of VSG.....	61

## List of Abbreviations

5-HT	5-Hydroxytryptamine (serotonin)
Adra2a	Adrenoreceptor alpha A
Aldh1a3	Aldehyde Dehydrogenase 1 Family Member A3
Adob	Aldolase B
BW	Body weight
Cacna1a	Calcium voltage gated channel subunit alpha 1A
Car8	Carbonic anhydrase 8
CCK	Cholecystokinin
Ccnd2	Cyclin D2
CD	Control diet
Cd81	Cluster of differentiation 81
Cdkn1a	Cyclin dependent kinase inhibitor 1A
cDNA	Copy DNA
ChgA	Chromogranin A
ChgB	Chromogranin B
Cldn4	Claudin 4
Cltrn	Collectrin
Cpe	Carboxypeptidase E
Cxcl1	C-X-C Motif Chemokine 1
DAPI	40, 6-diamidin-2-phenylindol
DIO	Diet-Induced Obesity
Dnajb2	DnaJ Heat Shock Protein Family (Hsp40) Member B2
DPP-IV	Dipeptidyl Peptidase-4
DPT	Diffusion Pseudotime
EEC	Enteroendocrine cell
EC	Enterochromaffin cell
EdU	5-ethynyl-2'-deoxyuridine
Eif2ak3/PERK	Eukaryotic translation initiation factor 2 alpha kinase 3
ELISA	Enzyme-linked immunosorbent assay
ER	Endoplasmic Reticulum
ERAD	ER-associated degradation

Erlin1	ER lipid raft associated 1
Ffar1	Free fatty acid receptor 1
Foxa2	Forkhead box transcription factor A2
FoxO1	Forkhead box protein O1
FVF	Foxa2-Venus fusion
Gast	Gastrin
Gc	Vitamin D binding protein
Gcg	Glucagon
GEM	Gel Bead-in-Emulsion
GIP	Glucose-Dependent Insulinotropic Polypeptide
GIPR	Glucose-Dependent Insulinotropic Polypeptide Receptor
Ghrl	Ghrelin
GLP-1	Glucagon Like Peptide 1
GLP-1R	Glucagon Like Peptide 1 Receptor
GO	Gene Ontology
Gpx3	Glutathione peroxidase 3
GRP78	78-kDa glucose-regulated protein
GSIS	Glucose Stimulated Insulin Secretion
Herpud1	Homocysteine-responsive endoplasmic reticulum-resident ubiquitin-like domain member 1 protein
HFD	High-fat, high-sugar diet
Hsp40	DnaJ Heat Shock Protein Family
Hspa5	Heat shock protein family A member 5
Ins1/2	Insulin
ISC	Intestinal stem cell
Isl1	Islet 1
IST	Insulin secretion test
KEGG	Kyoto Encyclopedia of Genes and Genomes
Ki67	Proliferation-related Ki67 antigen
LeptinR	Leptin receptor
LncRNA	Long non-coding RNA
MafA	Transcription factor Mafa
Meg3	Mouse maternal expressed gene 3

MMTT	Mixed-meal tolerance test
mRNA	Messenger RNA
Mt1	Metallothionein 1
NeuroD1	Neuronal differentiation 1
Ngn3	Neurogenin 3
Nkx2.2	Homeobox Protein Nkx-2.2
Nkx6.1	Nk6 Homeobox1
NMR	Nuclear magnetic resonance spectroscopy
OPG	Osteoprotegerin
PAGA	Partition-Based Graph Abstraction
PCA	Principal component analysis
Pcsk1	Proprotein convertase 1
Pcsk2	Proprotein convertase 2
Pdx1	Pancreatic Duodenal Homeobox 1
PF	Pair-feeding
PP	Pancreatic Polypeptide
PYY	Peptide YY
QC	Quality control
RANK	Receptor activator of NFkB
RANKL	Receptor activator of NFkB Ligand
Rbp4	Retinol binding protein 4
RNA	Ribonucleic Acid
RYGB	Roux-en-Y gastric bypass
Saa3	Serum Amyloid Protein A3
ScRNA-seq	Single-cell RNA sequencing
Sel1l	SE11L adaptor subunit of ERAD E3 ubiquitin ligase
S.e.m.	Standard error of the mean
Slc2a2 (Glut2)	Solute carrier family 2 member 2
Slc5a10	Sodium/glucose cotransporter 5
SP-D	Pulmonary Surfactant Protein D
Sham	Sham-surgery
Snap25	Synaptosomal-associated protein 25 kDa
Snhg11	lncRNA Small nucleolar host gene 11

Sox4	SRY-box transcription factor 4
SST	Somatostatin
STZ	Streptocotozin
Syt7	Synaptotagmin 7
Syvn1/Hrd1	Synoviolin 1
T1D	Type 1 Diabetes
T2D	Type 2 Diabetes
TF	Transcription Factor
Tnfrsf11b	TNF Receptor Superfamily Member 11b
Trpm5	Transient receptor potential cation channel subfamily M member 5
Ucn3	Urocortin 3
UMAP	Uniform Manifold Approximation and Projection
UPR	Unfolded protein response
VSG	Vertical Sleeve Gastrectomy
Wfs1	Wolframsyndrome 1
WT	Wildtype
Xbp1	X-box binding protein 1





# 1. Introduction

## 1.1 Metabolic Syndrome

The Metabolic syndrome is an epidemic disease estimated to affect 25% of the worldwide population<sup>1</sup>. Its clinical term represents a group of conditions characterized by abdominal obesity, hypertension, dyslipidemia, hyperglycaemia and insulin resistance (ICD10-CM E88.81, 2021). Although the diagnosis criteria of the metabolic syndrome differ along countries and institutions, it centrally involves obesity and insulin resistance, culminating in an increased risk of developing type-2 diabetes mellitus (T2D).

## 1.2 Diabetes Mellitus

Diabetes mellitus comprises a group of diseases centrally involving metabolic dysregulation through chronic hyperglycaemia. The most common forms are type-1 diabetes mellitus (T1D) and T2D. Both underlie different pathomechanisms: T1D is triggered by the progressive destruction of  $\beta$ -cells through autoimmune mechanisms, while the causes for the development of T2D are multifactorial involving environmental factors, such as a sedentary lifestyle, poor diet, or obesity, as well as genetic predisposition<sup>2</sup>. T2D is a severe health concern that causes major health care problems. According to the International Diabetes Federation, 9.3% of the worldwide population was affected by T2D in 2019 with steadily growing prevalence (IDF Diabetes Atlas 9<sup>th</sup> edition, IDF 2019). T2D manifests itself by chronic hyperglycaemia caused by peripheral insulin resistance and pancreatic  $\beta$ -cell dysfunction and can lead to severe medical complications when untreated. The major co-morbidities involve cardiovascular diseases, polydipsia, polyphagia, kidney disease, foot ulcers or infections, which reduce life expectancy.

## 1.3 Glucose Homeostasis in Health and Disease

Regulated blood glucose levels during fed and fasted states are essential for life and health. Glucose homeostasis ensures the adequate energy supply to organs and is tightly regulated by an interplay of central control and systemic functions of different endocrine tissues, such as the gastrointestinal

tract and pancreas. However, their homeostatic function can easily be disturbed upon prolonged exposure to obesogenic and diabetogenic triggers. The particular role of the intestine and pancreas on energy and glucose homeostasis in health and under conditions of diabetes and obesity will be reviewed in the following chapters.

## **1.4 Intestinal Architecture**

The intestine plays a pivotal role in digestion, nutrient absorption into the blood stream and energy regulation. It is anatomically divided into small and large intestines. While the small intestinal segment is specialized in nutrient absorption and hormonal regulation of metabolism, the distally located large intestine mainly serves to reabsorb water and to secrete mucus<sup>3,4</sup>. The intestine is highly vascularized and innervated to ensure the delivery of nutrients as well as to convey endocrine and neuronal signals to target tissues. The small intestine is further subdivided into three parts along the proximal-distal axis, duodenum, jejunum and ileum differing in their cellular composition, morphology, and gene expression profile owing to their functional role along the gut axis<sup>5-8</sup>. The duodenum and jejunum mainly absorb nutrients, minerals, and soluble vitamins, while the ileum absorbs residual nutrients and takes up bile acids for redirection to the liver. The small intestine contains an epithelial layer, which is functionally compartmentalized into the crypts of Lieberkühn and villi (Fig.1). Crypts are intestinal epithelial invaginations into the submucosa and villi form luminal protrusions to enlarge the epithelial surface for maximized nutrient absorption. While the villus contains mature intestinal cells, the crypt harbors intestinal stem cells (ISC) and intestinal epithelial progenitors. Due to the high exposure to mechanical forces and chemicals, the intestinal epithelium renews within 4-5 days driven by constant division of ISCs at the crypt bottom<sup>9,10</sup>. ISCs give rise to progenitors of six intestinal cell lineages, nutrient-absorptive enterocytes (ECs), mucus-secreting goblet cells (GCs), chemosensory tuft and microfold cells, Paneth cells (PCs), and enteroendocrine cells (EECs)<sup>9</sup> (Fig.1). Enterocytes represent the most abundant cell lineage in the intestinal epithelium and are the only cell type undergoing several transient amplification steps before committing to the mature EC lineage<sup>9</sup>. PCs reside in proximity to ISCs at the crypt base to provide essential niche signals and to release antimicrobial peptides for the maintenance of the gut microbiome<sup>11,12</sup>, while all other intestinal cell types move from the crypt up the villus as the formation of new intestinal epithelial cells progresses. The major function of tuft and microfold cells comprises the recognition and defense of pathogens as well as the induction of immune responses<sup>13,14</sup>. With a

prevalence of 1%, EECs represent the minority of cells in the intestinal epithelium, but collectively represent the largest endocrine organ in the human body<sup>15</sup>.

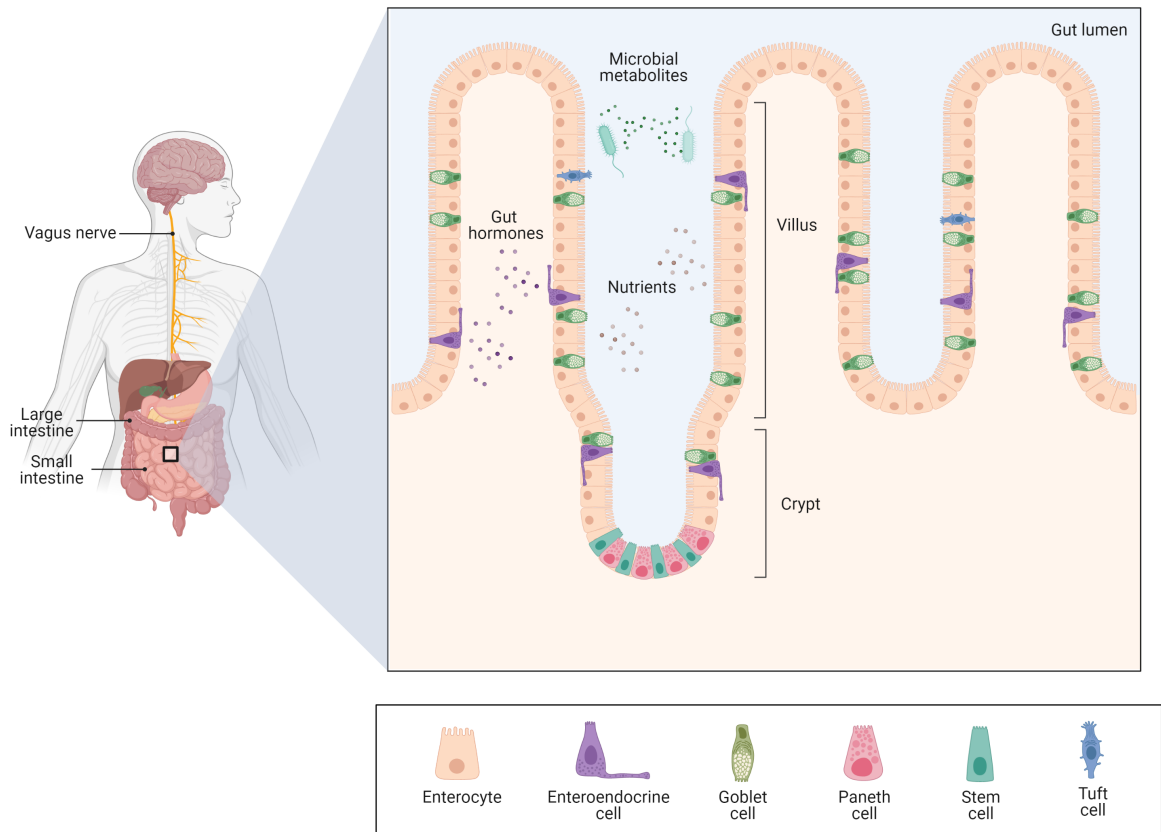


**Figure 1: Intestinal architecture and cellular composition.** The intestine is divided into the small and large intestine containing a mono-layered epithelium. Morphologically, the small intestinal epithelium forms villi and crypts. The crypts harbor ISCs, which give rise to progenitors of 5 lineages: Enterocytes, enteroendocrine cells, goblet cells, Paneth cells, and tuft cells. Together with ISCs, Paneth cells stay at the bottom of the crypt, while all other progenitors move up the crypt and villus. All cells undergo a maturation process in the crypt. Additionally, enterocytes proliferate in the so called transient-amplifying zone of the crypt. Cells reaching the tip of the villus undergo apoptosis and are shed off into the gut lumen. Graphic created using Biorender.

## 1.5 Regulation of Glucose and Energy Homeostasis by Intestinal Hormones

EECs are secretory, chemo-sensitive cells and play a pivotal role in hormonal regulation of metabolism<sup>16,17</sup>. They serve to sense luminal nutrients, bile acids and microbiota-derived molecules and respond by secreting hormones to transfer signals in an autocrine, paracrine and endocrine manner<sup>17,18</sup>. They have traditionally been classified according to their principal hormone expressed: D-cells (somatostatin), enterochromaffin cells (ECs) (Serotonin, 5-HT), enterochromaffin like (histamine), G-cell (gastrin, Gast), I-cells (cholecystokinin, Cck), K-cells (gastric inhibitory peptide, GIP), L-cells (glucagon-like peptide 1, GLP-1), M-cells (motilin), N-cells (neurotensin), S-cells (secretin) and X-cells (ghrelin). However, recent scRNA-seq studies discovered more complex EEC profiles involving about 20 different EEC subtypes with different hormonal combinations<sup>7,15,19-21</sup>. Additionally, these hormones display varying distribution patterns along the intestinal axis<sup>22,23</sup>. For instance, GLP-1 and PYY expressing EECs are predominantly found in the distal, while CCK expressing EECs are located in the proximal intestine. Under starved states, duodenal and gastric EECs progressively enhance the release of the hormone ghrelin. Blood ghrelin levels have been positively correlated with hunger sensation and, thus, ghrelin is thought to promote food ingestion<sup>24,25</sup>. Food intake, in turn, directly lowers ghrelin levels to reduce appetite and triggers the secretion of gut hormones. These exert different functions such as aiding digestion by prompting the secretion of gastric acid (gastrin, histamine)<sup>26</sup>, bile acids from the gallbladder, digestive enzymes and bicarbonate from the exocrine pancreas (CCK, secretin)<sup>27</sup> or inhibit food intake, and reduce gastric emptying (CCK, GLP-1, PYY)<sup>17</sup>. GLP-1 and GIP are the prominent gluco-regulatory hormones because of their incretin actions. GLP-1 and GIP exert insulinotropic effects by binding to their respective receptor on  $\beta$ -cells and, thus, contribute to postprandial insulin secretion and glycaemic control<sup>28</sup>.

## 1.6 Intestinal Mal-Adaptations in Obesity

The high turnover rate of the intestinal epithelium involves a remarkable ability to quickly adapt to nutritional changes<sup>29,30</sup>. In fact, overnutrition has been reported to trigger intestinal maladaptation and dysfunction<sup>17,31-33</sup>. Notably, these nutritional adaptations have been proven to originate from the intestinal stem cell niche<sup>31-33</sup>. Studies have shown that the consumption of calorie-dense food increased the number of absorptive enterocytes<sup>29,31,34,35</sup> and GCs<sup>31</sup> and impacts villus and/or crypt size<sup>31,32,36-38</sup> to increase nutritional uptake. More precisely, data from our laboratory (Aliluev et al.

2021, in press) revealed that the increased villus length is a result of enhanced EC and GC lineage allocation from ISCs as well as hyperproliferation of ISCs and progenitors of these two lineages with a concomitant increase in mature EC and GC numbers in HFHSD-fed mice<sup>31</sup>. Furthermore, while dysbalanced blood gut hormone levels have been well described in obesity for years<sup>31,39,40</sup>, the underlying mechanisms have been addressed to a lesser extent. Histological analyses revealed varying outcomes of EEC numbers in humans and different obesity mouse models ranging from lower<sup>31,40-42</sup> or higher proportions of EECs or specific subtypes<sup>43,44</sup> to an unchanged number of EECs<sup>32,38</sup>. These discrepancies most likely arose from the usage of different models or quantification methods. However, a previous report in a mouse model of diet-induced obesity (DIO) resolving EEC lineage formation using single-cell transcriptomics demonstrated that already early EEC progenitors are disturbed after HFHSD-feeding, which might affect EEC subtypes in different ways<sup>31</sup>.

## **1.7 Pancreatic Architecture**

The pancreas has a superior role in regulating glucose metabolism and digestion, exerted by two morphologically and functionally distinct compartments. The exocrine part of the pancreas forms the majority of pancreatic mass and consists of acinar cells aggregated to rosette-shaped bundles and ductal cells forming a tubular network within the pancreas. Acinar cells secrete digestive enzymes, while duct cells release a bicarbonate solution to neutralize stomach acids. These are in turn delivered to the duodenum via the ductal system for digestive support. The endocrine part of the pancreas forms small, roundish cell clusters referred to as islets of Langerhans, which are dispersed throughout (Fig. 2). High vascularization and innervation of islets by parasympathetic, sympathetic nerves ensures endocrine and neuronal communication between islets and other organs<sup>45</sup>. Islets consist of five different hormone-secreting cell types,  $\alpha$ -cells (glucagon),  $\beta$ -cells (insulin),  $\gamma$ -cells (pancreatic polypeptide),  $\delta$ -cells (somatostatin), and  $\epsilon$ -cells (ghrelin)<sup>46-48</sup> (Fig. 2). The interplay of these pancreatic hormones keep glycaemic levels in a narrow range of 4-6 mM in humans.

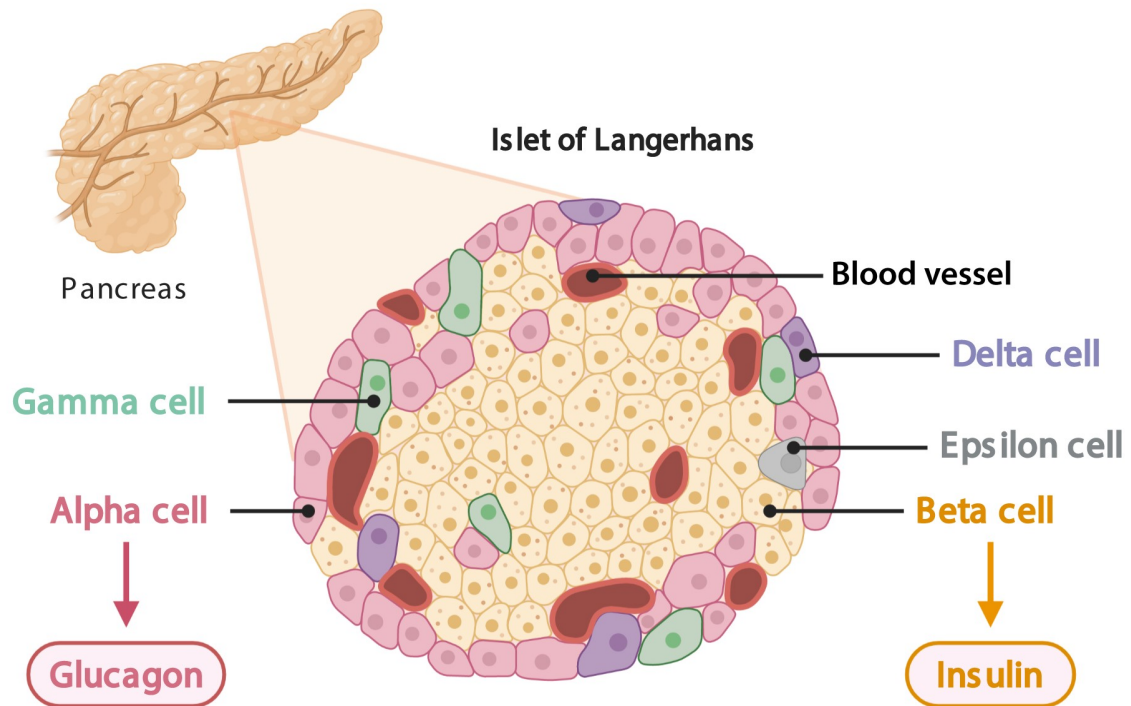


**Figure 2: Morphology and cellular composition of islets of Langerhans.** The pancreas comprises an exocrine and endocrine part. The endocrine part involves roundish cell clusters termed islets of Langerhans. These comprise insulin-secreting  $\beta$ -cells, glucagon-secreting  $\alpha$ -cells,  $\gamma$ -cells,  $\delta$ -cells, and  $\epsilon$ -cells. Islets are highly vascularized and innervated. This illustration is representative for a rodent islets. Graphic created using Biorender.

## 1.8 Glucose Regulation by the Endocrine Pancreas

Glycaemic homeostasis is mainly accomplished by counter-regulatory and balanced actions of insulin and glucagon and, thus, are the critical regulators of glycaemia. Insulin secreting  $\beta$ -cells represent the main cell type in adult mice. Functionally,  $\beta$ -cells sense blood glucose levels and accordingly secrete insulin to enable cellular glucose uptake in the body (Fig. 3). More precisely, the postprandial elevation of blood glucose leads to an increased flux of glucose into  $\beta$ -cells via the Glucose transporter type-2 (Glut2). Glucose is in turn metabolized via glycolysis and the tricarboxylic acid cycle to generate ATP. The relative increase in intracellular ATP leads to the closure of ATP-sensitive  $K^+$ -channels and subsequent depolarization. In turn, voltage-gated  $Ca^{2+}$ -channels open thereby allowing the influx of  $Ca^{2+}$  along the electrochemical gradient. Increased intracellular  $Ca^{2+}$ -levels trigger the

fusion of insulin-vesicles with the plasma membrane and enable the release of insulin into the circulation<sup>45,49-51</sup> (Fig. 3).

The process of postprandial insulin secretion is biphasic involving a rapid, strong first phase peak within 5-10 minutes and a slowly increasing second phase lasting for more than 30 minutes<sup>52</sup>. Once circulating insulin reaches target tissues, binding to the insulin receptor on the cell surface allows the uptake of circulating glucose for energy supply<sup>53-55</sup>. Besides the role as mediator for cellular glucose uptake, insulin signaling also dictates the hepatic function of glycaemic balance. High insulin levels during fed states signal the liver to store glucose (glycogenesis)<sup>56</sup>. Under fasted states, insulin secretion is low while pancreatic  $\alpha$ -cells enhance the release of glucagon to trigger hepatic glucose production by increased gluconeogenesis and glycogenolysis from internal stores<sup>57</sup>.

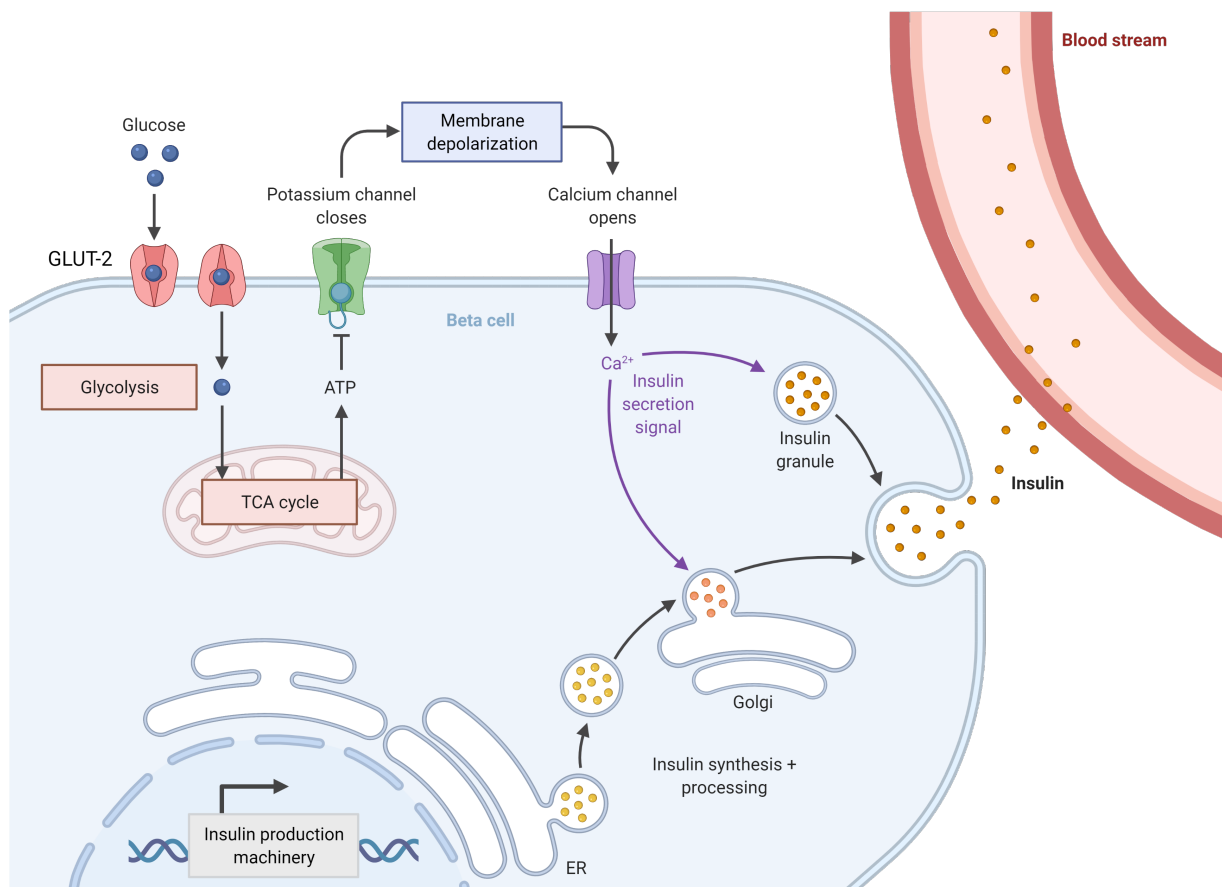


**Figure 3: Glucose-stimulated insulin secretion.** Insulin production via transcription in nucleus, translation in ER and processing in Golgi. Blood glucose enters  $\beta$ -cells through the transporter Glut-2. Downstream catabolism of glucose molecules via glycolysis and mitochondrial TCA-cycle generates ATP. High intracellular ATP-levels prompt the closure of  $K^+$ -channels resulting in membrane depolarization. Subsequently, voltage-gated  $Ca^{2+}$ -channels open thereby triggering the influx of  $Ca^{2+}$ -ions along the electrochemical gradient. High intracellular  $Ca^{2+}$ -levels promote signals for insulin secretion from vesicles into the circulation. Graphic created using Biorender.

## 1.9 Pancreatic $\beta$ -cell Failure in Type-2 Diabetes

Overnutrition and chronic hyperglycaemia have been linked to insulin resistance in peripheral tissues serving to protect cells from excess nutrient-induced metabolic stress. Concomitantly, insulin resistance and/or the hostile environment of westernized lifestyle *per se* fuel hypersecretion of insulin by pancreatic  $\beta$ -cells. In turn, hyperinsulinaemia induces adaptive  $\beta$ -cell proliferation in pre-diabetic and early T2D stages, while it ultimately leads to  $\beta$ -cell failure and glucose intolerance as the disease progresses<sup>58,59</sup>.  $\beta$ -cells are plastic and capable of adapting to environmental cues by functional and identity changes<sup>60</sup>. Recent cumulating research showed that failing  $\beta$ -cells in T2D lose their mature identity and undergo a process of dedifferentiation in both rodent and human forms of diabetes<sup>61-64</sup>. This process involves reduced expression levels of  $\beta$ -cell identity genes such as Transcription Factor Mafa (*Mafa*)<sup>65</sup> or Urocortin 3 (*Ucn3*)<sup>66</sup>, glucose metabolism, insulin processing, and secretory genes, as well the activation of normally repressed genes -  $\beta$ -cell disallowed genes<sup>60,64,67</sup> (Fig.4). There is evidence that dedifferentiated  $\beta$ -cells revert to a progenitor or immature state<sup>61,63,68</sup>. A recent single-cell RNA-sequencing study by Sachs et al. analyzed the  $\beta$ -cell transcriptome of Streptozotocin (STZ)-treated mice, a severe diabetes model, which chemically destroys the majority of  $\beta$ -cells and revealed novel insights in the progress of dedifferentiation. Sachs et al. showed that  $\beta$ -cells dedifferentiate through an immature state and that dedifferentiated  $\beta$ -cells govern a similar transcriptional signature as embryonic  $\beta$ -cells<sup>68</sup>. Being a promising entry-point for novel pharmacotherapies,  $\beta$ -cell dedifferentiation has intensively been investigated during the past years and led to the discovery of specific markers. The most prominent and initially discovered marker is Aldehyde Dehydrogenase 1 Family Member A3 (*Aldh1a3*)<sup>69</sup>. Further reports have shown that dedifferentiated  $\beta$ -cells start expressing the fetal islet hormone Gastrin (*Gast*)<sup>70</sup> and Cholecystokinin (*Cck*)<sup>68</sup>. Other recently described dedifferentiation markers are Vitamin D Binding Protein (*Gc*)<sup>67</sup>, Retinol Binding Protein 4 (*Rbp4*)<sup>71</sup>, Collectrin (*Cltn*), Glutathion Peroxidase 3 (*Gpx3*), Sodium/Glucose Cotransporter 5 (*Slc5a10*)<sup>68</sup>, and Cluster of Differentiation 81<sup>72</sup> (Fig. 4). Nevertheless, mechanistic understanding of  $\beta$ -cell dedifferentiation remains to be conclusively understood in order to fuel the discovery of novel drugs targeting de- and redifferentiation of  $\beta$ -cells for diabetes therapy.



## Diabetogenic stress



**Figure 4: Concept of  $\beta$ -cell dedifferentiation.** Prolonged diabetogenic stress impairs the identity and function of  $\beta$ -cells. During the process of dedifferentiation,  $\beta$ -cells downregulate maturity and functionality markers (e.g. MafA, Slc2a2) and upregulate dedifferentiation markers (e.g. Aldh1a3, Gastrin, or Slc5a10). Graphic created using Biorender.

### 1.10 Current Treatment Options for Type-2 Diabetes

Restoring metabolic control to achieve normoglycaemia greatly improves long-term prognoses and suggests early intervention therapies. Currently available therapies display different profiles in their effectiveness, invasiveness, and their risk of side-effects and comprise lifestyle-related, pharmacological and surgical interventions. Thus, they require a thorough, individualized medical assessment depending on the severity of T2D.

Lifestyle adjustments to a low-calorie, fiber-rich diet and high physical activity represent one of the first interventions for blood glucose management<sup>73,74</sup>. In fact, exercise increases glycaemic control in T2D, contributes to body weight loss, decreases cardiovascular risks, and may be able to prevent or delay T2D<sup>75-77</sup>. Combined exercise and calorie-restriction has been shown to improve insulin sensitivity and  $\beta$ -cell function<sup>78-80</sup>. Importantly, clinical studies have proven that decreased baseline glycaemia by dietary intervention is crucial for successful long-term body weight loss<sup>81</sup>. Nevertheless, lifestyle-related therapy of T2D alone bears major disadvantages. Difficulties to

maintain acquired dietary habits and exercise together with frequent occurrence of relapses makes sole lifestyle-related therapies insufficient for many patients on the long term<sup>82,83</sup> and often require the combination with pharmacological or surgical treatments.

Gut hormones represent the basis for many pharmacological approaches for diabetes therapy due to the fact that they exert important physiological functions in the systemic regulation of energy balance. GLP-1 is one of the most prominent hormones with metabolic function majorly being produced by subtypes of gastrointestinal enteroendocrine cells and to a lower extent by pancreatic  $\alpha$ -cells and in the brain through processing of the precursor polypeptide by prohormone convertase 1 (PC-1)<sup>22,84</sup>. Intestinal GLP-1 is secreted after meal ingestion and is rapidly degraded within few minutes by Dipeptidylpeptidase IV (DPP-IV). Consequently, only a minority of active GLP-1 reaches the systemic circulation<sup>22</sup> suggesting that GLP-1 acts locally via its receptor and/or through signal transmission by the nervous system. The GLP-1 receptor (GLP-1R) is expressed in the intestine as well as in central and systemic neurons and pancreatic  $\beta$ -cells<sup>22</sup>. Besides its direct function as incretin<sup>28</sup>, GLP-1 additionally exerts indirect effects on glycaemia such as slowing of gastric emptying, inhibiting glucagon secretion, and promoting satiety<sup>22</sup>. Due to its various beneficial metabolic effects, but short life in its native form, long-acting GLP-1 analogs (e.g. exenatide, liraglutide, lixisenatide), as well as DPP-IV inhibitors to increase incretin function (e.g. sitagliptin, vildagliptin, saxagliptin) have been developed to enhance therapeutic effects<sup>28,85,86</sup>. A novel promising pharmacological strategy, which is currently subject to investigations, is the generation of peptide conjugates combining the actions of two or more gut hormones for improved therapeutic action<sup>87,88</sup>. In several clinical and preclinical studies, co-agonism of the GLP-1R and GIP-receptor (GIPR) by a unimolecular dual incretin peptide has been reported superior glycaemic and body weight lowering actions and less side-effects compared to treatment with GLP-1 or GIP agonists alone<sup>89-91</sup>. The latter and many more polyhormone pharmacy approaches hold potential to improve diabetes management in future<sup>87</sup>.

Several classical glucose-lowering agents have been licensed the past decades. Metformin is the first-line anti-diabetic pharmacotherapy with multifaceted insulin-dependent and independent actions. It has a long-term safety record and reduces fasting plasma glucose by 2-4 mmol/l with tolerable side-effects in the majority of the patients<sup>85</sup>. Sodium-glucose linked transporter 2 (SGLT2) inhibitors (e.g. dapagliflozin, canagliflozin, empagliflozin) reduce the renal reuptake of glucose thereby decreasing glucotoxicity. Similarly,  $\alpha$ -glucosidase inhibitors (AGIs) delay carbohydrate digestion and prevent extreme blood glucose excursions by inhibiting the cleavage of di- and oligosaccharides into monosaccharides in the brush border of intestinal enterocytes<sup>85</sup>. However, SGLT2 inhibitors and AGIs are restricted to glucose lowering effects and do not directly impact on other pathomechanisms

underlying T2D<sup>85</sup>. Conclusively, current pharmacological treatment modalities are able to improve blood glycaemia to a certain extent but cannot revert diabetic conditions and always bear the risk of unwanted side effects. Consequently, further development and research is required to improve drug efficacy for diabetes treatment.

Bariatric surgery is at present the most potent treatment of T2D and related comorbidities. It is recommended for patients with a BMI of greater than 35 kg/m<sup>2</sup> and when glycaemia is insufficiently controlled by lifestyle and medical therapies<sup>92</sup>. These surgical procedures represent the only intervention that can achieve full T2D remission, with rates of up to 80 %, <sup>92-94</sup> and long-term body weight reductions of 20% and more<sup>95</sup>. The most popular procedures are VSG and Roux-en-Y gastric bypass (RYGB) (Fig. 5). Of them, VSG is most frequently used<sup>96</sup> and involves the excision of 80% of the stomach along the greater curvature leaving a gastric sleeve. RYGB additionally involves a gastrojejunal anastomosis so that food bypasses the duodenum (Fig. 5). Albeit its promising efficacy, bariatric surgery is highly invasive and can involve surgical and postsurgical complications. This is why bariatric surgery requires strict pre-surgical medical assessment and is only accessible for patients suffering from severe obesity and T2D. Consequently, identifying mechanisms that underlie the beneficial metabolic effects of bariatric surgery is of utmost importance to develop novel pharmacotherapies that mimic the bariatric surgical effects in order to circumvent surgical side-effects and to make it accessible to a broad spectrum of patients.

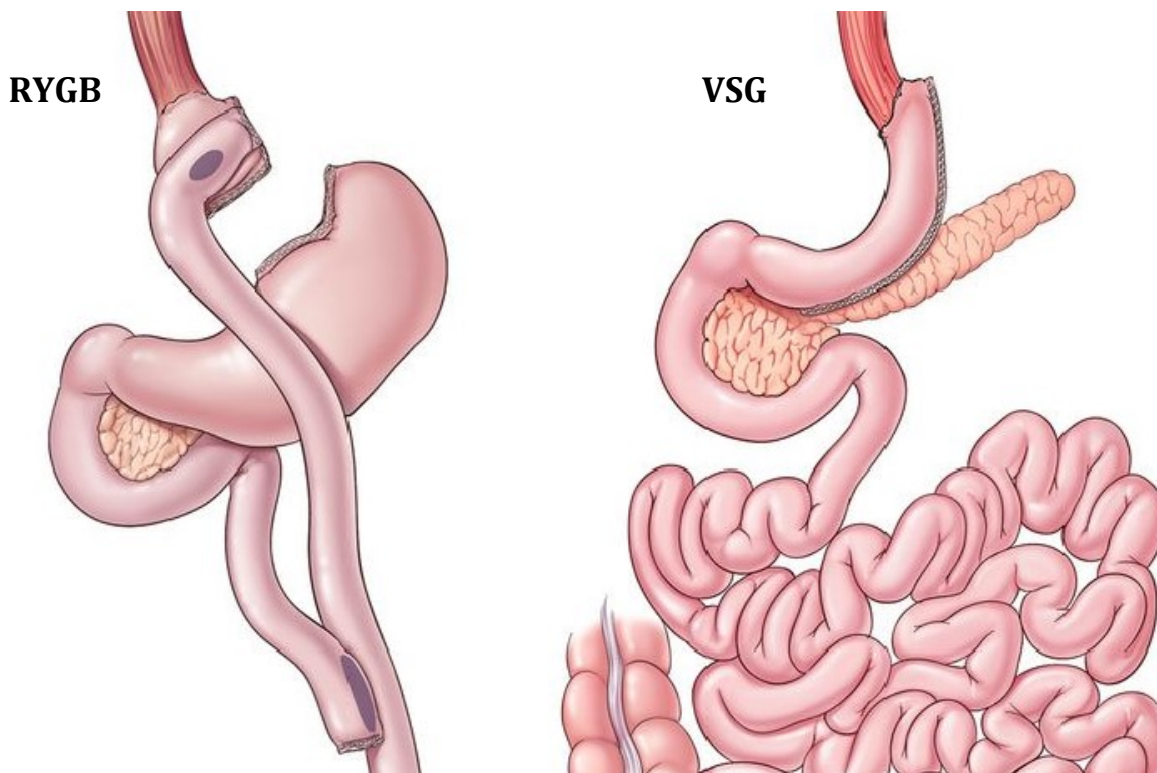



**Figure 5: The two most commonly performed bariatric surgical procedures: Roux-en-Y gastric bypass (RYGB) and vertical sleeve gastrectomy (VSG).** RYGB involves a by-pass of stomach and duodenum by gastro-jejunal anastomosis. VSG involves the excision of 80% of the stomach. Picture modified with permission of Cleveland Clinic.

Initially attributed to sole calorie-restrictive and mal-absorptive mechanisms, bariatric surgery is nowadays seen as metabolic surgery due to synergistically acting physiological adaptations taking place after surgery<sup>97,98</sup>. Bariatric surgery decreases food intake, food reward and increases satiety most likely driven by neuronal and hormonal gut-brain cross-talk<sup>99</sup>. Revealing insight was made in a study by Stefater and colleagues. They reported that obese rats that had achieved a normal body-weight after VSG and that had additionally been food-restricted, re-gained weight to healthy post-surgical levels but did not chose to overeat to pre-surgical levels when returned to an ad libitum diet<sup>100</sup>. In fact, bariatric surgical intervention triggers a remarkable switch to favorable levels of gut hormones, for instance increases in postprandial levels of GLP-1, PYY, CCK and decreases in ghrelin levels that likely explain some metabolic effects of bariatric surgery<sup>99</sup>. However, studies trying to narrow down surgical effects to single hormones were not successful supporting a holistic view of metabolic changes instead of hormones alone<sup>101-105</sup>. In how far combinations of gut hormones

account for the effects of VSG or whether the contribution of gut hormones has been overestimated by the field is still topic of debates.

VSG induces beneficial changes in liver-derived circulating bile acid profiles and the gut microbial composition<sup>27,106,107</sup>. In this context, it is important to briefly review the roles of the gut microbiome and bile acids. A diverse gut microbiome is essential for the maintenance of human health including processing of foods and nutrients, intestinal barrier integrity, and host immune defense<sup>108,109</sup>. Of note, there is a strong mutual impact of bile acids and the gut microbiome<sup>110</sup>. Bile acids regulate the growth and composition of the gut microbiome<sup>108,111</sup>, while the gut microbiota are involved in the biotransformation of bile acid species<sup>112</sup>. Both of them, changes in microbiota and bile acids have been correlated with postsurgical improvements in body-weight and insulin sensitivity<sup>107,113,114</sup>. What exact microbiota and microbial metabolites drive these effects is still topic of many investigations<sup>114</sup>.

### **1.11 Gluco-Regulatory Mechanisms of Vertical Sleeve Gastrectomy**

Mechanistic research mostly comes from rodent VSG models, which resemble similar weight-loss and metabolic improvements as observed in humans. A remarkable ability of VSG is to rapidly improve glucose regulation within a few days after surgery before the majority of weight-loss occurs. This observation led to the assumption that early glycaemic effects are body-weight independent. However, factors mediating these effects are still elusive and controversially discussed. While some suggest neurohumoral signals<sup>97-99</sup>, others hypothesize that acute post-surgical calorie restriction mediates early glycaemic effects<sup>115,116</sup> or a combination of both. Another subject to debate is whether improved peripheral insulin sensitivity or direct  $\beta$ -cell recovery is the initial and primary driver of glycaemic recovery after VSG. A study by the Ben-Zvi laboratory highlighted changes in hepatic insulin sensitivity as the primary driver of improved post-surgical glycaemia and proposed that the recovered  $\beta$ -cell markers observed in that study are a consequence of peripheral mechanisms<sup>117</sup>. In contrast, the Seeley laboratory revealed distinctive beneficial functional changes in the islet transcriptome after VSG and suggests that islet intrinsic  greatly contribute to postsurgical glycaemic recovery<sup>118</sup>. Nevertheless, it seems plausible that both peripheral and islet intrinsic gluco-regulatory mechanisms occur simultaneously and beneficially influence each other.

VSG might improve glycaemia through various possible mechanisms involving different tissues. The gastrointestinal tract and the flow of ingested food is directly affected by VSG, which triggers enteroplastic and functional changes. First of all, the resection of a large portion of the stomach including ghrelin-producing cells itself suggests a link to reduced ghrelin-levels observed after VSG and the decreased sensation of hunger after VSG<sup>119</sup>. Furthermore, the faster transit of food from the stomach to the intestine has been shown to enhance the stimulation of distally located EECs including GLP-1 expressing cells and is thus thought to contribute to the increased postprandial GLP-1 response<sup>120</sup>. However, analyses of the EEC transcriptome showed that VSG does not trigger intrinsic transcriptional changes. This suggests that altered EEC function is most likely not origin of increased post-surgical GLP-1 levels<sup>120,121</sup> but increased stimulation and density of EECs after VSG. In fact, one report showed that VSG induces plastic changes in the intestine, in particular an increase in the density of GLP-1 expressing EECs without inducing hyperplasia<sup>122</sup>. This finding tempts to speculate that VSG might influence EEC differentiation or proliferation. In fact, a recent study by the Sandoval lab revealed that enhanced bile acid levels observed after VSG resulted in increased farnesoid-X receptor (FXR) signaling in ISCs to promote EEC differentiation thereby increasing the number of GLP-1 expressing EECs<sup>123</sup>. Additionally, another recent study discovered that the stomach harbors GLP-1 expressing cells, which detectably contributed to post-prandial GLP-1 responses and that VSG increased the density of gastric GLP-1 expressing cells likely contributing to GLP-1 effects after VSG<sup>124</sup>. Despite intensive research on the enhanced GLP-1 level after bariatric surgery and its origin, the conclusive proof on the actual contribution to post-surgical metabolic improvements is still missing. An initial study using animals with a genetic deletion of the GLP-1R showed that VSG was equally efficient as in WT animals suggesting that GLP-1 signaling does not represent the sole mechanism explaining the effectiveness of VSG<sup>103</sup>. Subsequent research investigating the tissue-specific role of GLP-1Rs, as well as the source (intestinal and pancreatic) of postsurgical GLP-1-levels on certain aspects of metabolic improvements has been controversial. A study by Kim et al. using conditional intestinal or pancreatic GLP-1 knock-out mouse models, revealed that VSG was still effective in absence of intestinal GLP-1, whereas pancreatic deletion of GLP-1 led to an inability of VSG to improve glycaemia<sup>125</sup>. Furthermore, VSG was ineffective in rescuing glycaemia in mice with  $\beta$ -cell specific deletion of the GLP-1R compared to controls<sup>126</sup>. Other studies delineated the contribution of  $\alpha$ -cell paracrine-acting GLP-1 rather than intestinal GLP-1 on the incretin effect<sup>127,128</sup> and showed that VSG increased  $\alpha$ -cell GLP-1, yet requiring the  $\beta$ -cell GLP-1R<sup>126</sup>. These findings reveal that localized paracrine GLP-1 signaling between  $\alpha$ - and  $\beta$ -cells contributes to the gluco-regulatory effects observed after VSG instead of intestinal GLP-1, as initially speculated.

There is ample research that has proven causality between increased bile acid signaling and improved glycaemia. Besides aiding lipid metabolism, bile acids are involved in several metabolic processes via their receptors FXR and Takeda G-protein-coupled receptor 5 (TGR5) mediating bile acid production and metabolic functions<sup>129</sup>. Both receptors are widely expressed including liver, muscle and fat tissue as well as the intestinal epithelial cells and pancreatic endocrine cells. While intestinal TGR5 activation on GLP-1 expressing EECs potentiates postprandial GLP-1 secretion<sup>130</sup>, islet TGR5 activation mediates  $\alpha$ -/ $\beta$ -cell cross-talk and enhances the paracrine release of GLP-1 from  $\alpha$ -cells to potentiate GSIS from  $\beta$ -cells<sup>131</sup>. Interestingly, there is a report linking TGR5 with glucoregulatory effects of VSG. Using TGR5-deficient mice McGavigan et al. showed that VSG successfully decreased body weight but was unable to fully improve glucose regulation implying a specific glucoregulatory role after VSG<sup>132</sup>.

FXR is a regulator of whole-body energy homeostasis by a complex not yet fully understood network<sup>133</sup>. For instance, hepatic FXR expression depends on the nutritional status and is implicated in hepatic gluconeogenesis by regulating expression of metabolic genes, such as Glucose-6 phosphatase (*G6pc*)<sup>134,135</sup>. In  $\beta$ -cells, FXR signaling has been shown to activate insulin secretion likely by inhibition of K-ATP channels, which consequently facilitates stimulus-secretion coupling<sup>136</sup>. In VSG, FXR has been proven a target to mediate post-surgical body weight loss and normalization of glycaemia<sup>137</sup>. However, conclusive downstream mechanisms in the context of bile acid signaling and VSG still need to be determined.

## 2. Scope of the Thesis

Intervention of early and late stage diabetes is crucial for long-term prognoses. While current pharmacological treatment modalities are only modestly efficacious, VSG promises high T2D remission rates, but involves a risk of surgical and postsurgical complications. Therefore, it is of utmost importance to identify novel mechanisms and targets underlying the metabolic improvements of VSG. Pharmacotherapies mimicking the metabolic effects of VSG could promise the replacement of invasive surgeries and would make the effects of VSG accessible to a broad spectrum of patients. Mechanistic research in animal models is the basis of achieving this goal and facilitates the discovery of novel therapeutic targets. Therefore, the **first (1) aim of this thesis was to assess the physiological relevance of different pre-diabetes and diabetes mouse models for pre-clinical intervention studies**. Different genetic and diet-induced diabetes/obesity models mirror distinct physiological phenotypes and stages of the disease. We intended to assess the susceptibility of different mouse backgrounds, B6J (*Foxa2-Venus-Fusion*) and B6N (WT), to develop HFD-induced obesity-linked diabetes. Furthermore, we compared these two HFD models with a genetic mouse model (Leptin-receptor deficiency, *db/db*) of severe obesity-linked diabetes in order to evaluate the suitability for VSG intervention. The **second (2) objective was to address pancreatic and intestinal plasticity as possible mediators for VSG effects under pre-diabetic conditions**. Literature has proven that pancreatic islets and the intestinal epithelium undergo rapid morphological and functional maladaptations after HFD feeding. Thus, we intended to investigate whether VSG restores these adaptations or induces distinct morphological or compositional changes in pancreatic islets and the intestinal epithelium. These changes might represent early functional adaptations after VSG and the basis of downstream metabolic mechanisms. Our **third (3) goal was to identify novel mechanisms and targets of VSG-mediated  $\beta$ -cell recovery upon overt diabetes**. The effectiveness of VSG has largely been described in animal models of pre-diabetes and obesity. Here, we used the genetic *db/db* mouse model, which mirrors clinically relevant features of late-stage obesity-linked diabetes and displays severe  $\beta$ -cell failure and dedifferentiation. We first of all sought to test whether VSG is able to rescue an end-stage diabetes phenotype. On the basis of this, we intended to extensively characterize the recovery of functional  $\beta$ -cell mass using single-cell RNA-sequencing (scRNA-seq). In particular, we sought to investigate whether VSG is capable of triggering proliferation and/or redifferentiation of dysfunctional  $\beta$ -cells as well as to unravel novel mechanisms and driving genes of VSG-mediated recovery of  $\beta$ -cell function.



### 3. Results

The results of this thesis were obtained in collaboration with the Institute of Computational Biology. (Subarna Palit, Prof. Dr. Dr. Fabian Theis), the Core facility of single-cell RNA sequencing (Dr. Michael Sterr), the Institute of Diabetes and Obesity (Prof. Dr. Kerstin Stemmer) and the Research Unit of Analytical Pathology (Dr. Annette Feuchtinger) at Helmholtz Center Munich. Surgeries were performed by Prof. Dr. Kerstin Stemmer. Biological experiments were performed by the candidate. The bioinformatical single-cell RNA sequencing analysis was done by Subarna Palit and subsequent interpretation by the candidate and Subarna Palit. Automated islet cell quantification was performed in collaboration with Dr. Annette Feuchtinger. Contributions are indicated in figure legends.

Data obtained from *db/db* mice is the basis for the following manuscript in revision at Molecular Metabolism:

Vertical sleeve gastrectomy triggers fast  $\beta$ -cell recovery upon overt diabetes by Lena Oppenländer\*, Subarna Palit\*, Kerstin Stemmer, Tobias Greisle, Michael Sterr, Annette Feuchtinger, Ciro Salinno, Aimée Bastidas-Ponce, Anika Böttcher, Ansarullah, Fabian Theis and Heiko Lickert (status 26.07.2021).

(\*indicates equal contribution)

Single-cell RNA-seq-based graphs from the collaboration with the Institute of Computational Biology was shared with courtesy of Subarna Palit. Figures from the manuscript were used with permission of the journal Molecular Metabolism (21.07.2021).

#### 3.1 Preclinical Mouse Models Mimicking Human Diabetes and Obesity

DIO models have been used since years to mimic the development of the metabolic syndrome including obesity, insulin resistance, and diabetes. However, the extent of the disease phenotype highly varies depending on the mouse strain used, the duration and composition of diet, as well as environmental factors<sup>138-142</sup>. In contrast, the genetic obesity-linked diabetes model involving C57BKS/J mice lacking the leptin-receptor (*db/db*)<sup>143</sup> results in less variable phenotypes considering the equal genetic pressure. Defects of leptin signaling in *db/db* mice causes an extreme hyperphagic

eating behavior driving the development of obesity, T2D and co-morbidities with age and premature death<sup>144,145</sup>.

Here, we intended to directly compare the severity of disease phenotypes in a HFD-induced obesity model in two mouse strains, B6J and B6N mice, and the *db/db* model. WT mice of the respective strain, B6J, B6N, and BKS, served as healthy controls. HFD-feeding in both strains, B6J and B6N mice, resulted in significant increases in body weight and adiposity, while B6N mice achieved a higher body weight than B6J mice. In contrast, the hyperphagia-driven obesity in *db/db* mice showed the strongest phenotype compared with the DIO models (Fig. 6a,b).

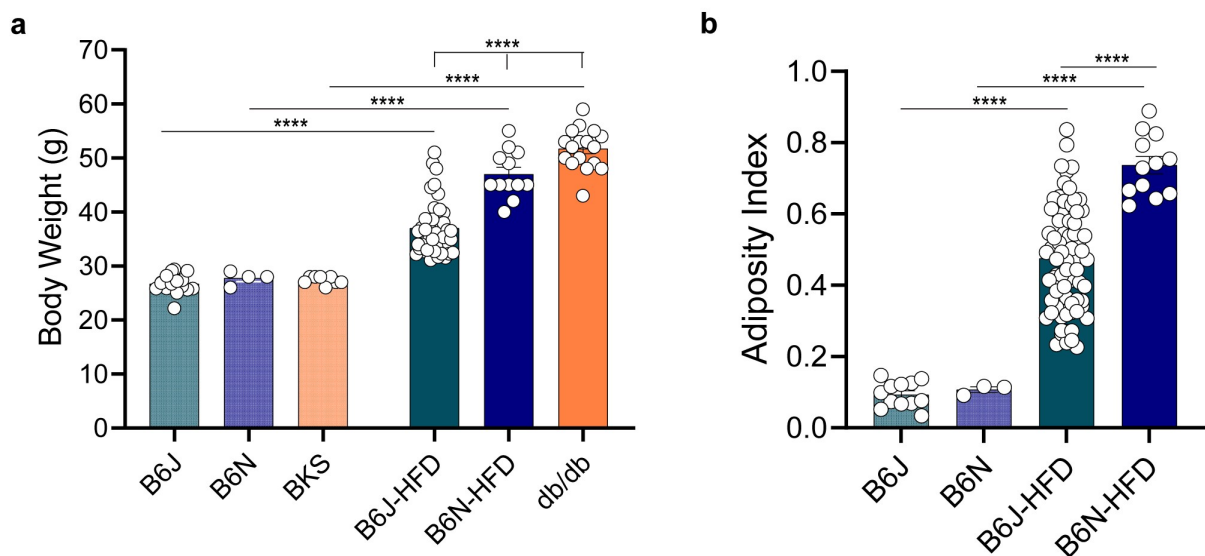


**Figure 6: HFD feeding in B6J and B6N mice and leptin-receptor deficiency (*db/db*) in BKS mice results in obesity.** (a) Body weight ( $n_{B6J}=16$ ,  $n_{B6N}=4$ ,  $n_{BKS}=8$ ,  $n_{B6J-HFD}=44$ ,  $n_{B6N-HFD}=12$ ,  $n_{db/db}=16$ ) and (b) adiposity index ( $n_{B6J}=12$ ,  $n_{B6N}=3$ ,  $n_{B6J-HFD}=23$ ,  $n_{B6N-HFD}=12$ ) in a DIO model of B6J and B6N mice fed a HFD for 12-15 weeks, and a genetic diabetes-obesity model of *db/db* mice (16-18 weeks old) compared to chow-fed controls (B6J and B6N). Statistical significance for (a) body weight: B6J vs. B6J-HFD ( $p<0.0001$ ), B6N vs. B6N-HFD ( $p<0.0001$ ), BKS vs. *db/db* ( $p<0.0001$ ), B6J-HFD vs. B6N-HFD ( $p<0.0001$ ), B6N-HFD vs. *db/db* ( $p<0.0001$ ), B6J-HFD vs. *db/db* ( $p<0.0001$ ). Statistical significance for (b) adiposity index: B6J vs. B6J-HFD ( $p<0.0001$ ), B6N vs. B6N-HFD ( $p<0.0001$ ), B6J-HFD vs. B6N-HFD ( $p<0.0001$ ). Statistical testing was performed using One-way-ANOVA and Bonferroni correction. Data is presented as mean  $\pm$  s.e.m.

Blood glycaemia is a suitable measure for the classification of different stages of diabetes. In fact, the progression of diabetes correlates with growing fasting and postprandial blood glucose levels. Here, HFD-feeding in B6J and B6N mice did not significantly affect fasting glycaemia, while *db/db* mice revealed highly increased glycaemic levels of more than 500 mg/dl compared to controls (Fig. 7a). During a mixed-meal challenge, B6J HFD-fed mice showed slightly higher glycaemic excursions compared with controls, albeit not statistically significant. HFD-fed B6N did not develop

hyperglycaemia. In contrast, *db/db* mice revealed extremely hyperglycaemic levels after a mixed-meal challenge (Fig. 7c). In early stages of diabetes,  $\beta$ -cells hypersecrete insulin to counteract peripheral insulin resistance. Upon continued diabetogenic stress,  $\beta$ -cells fail to secrete insulin in advanced stages. Here, B6J HFD-fed mice presented slightly higher fasting and postprandial insulin levels, although statistically not significant. B6N mice fed a HFD responded with markedly enhanced fasting and postprandial insulin levels (Fig. 7b,d). These observations suggest that both, B6J and B6N mouse strains, reflect models of obesity and pre-diabetes. Of note, B6N mice compensate diabetogenic stress by enhancing insulin secretion more than the B6J mouse strain and might better model the  $\beta$ -cell compensation stage during diabetes progression. By contrast, *db/db* mice revealed increased fasting and postprandial insulin levels, albeit insufficient to counteract the overt hyperglycaemia (Fig. 7a-d). Thus, *db/db* mice model a clinically-overt diabetes phenotype.

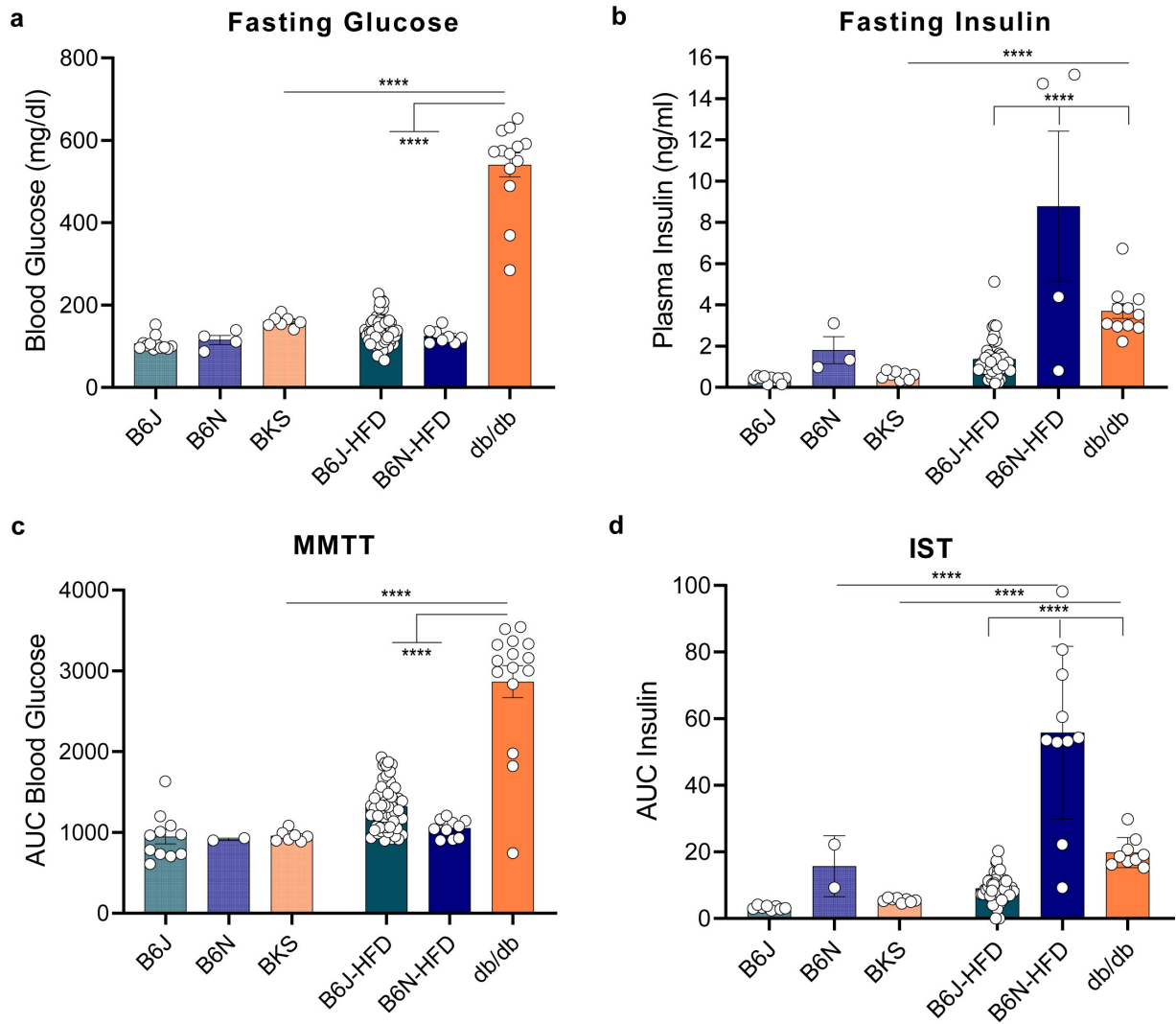


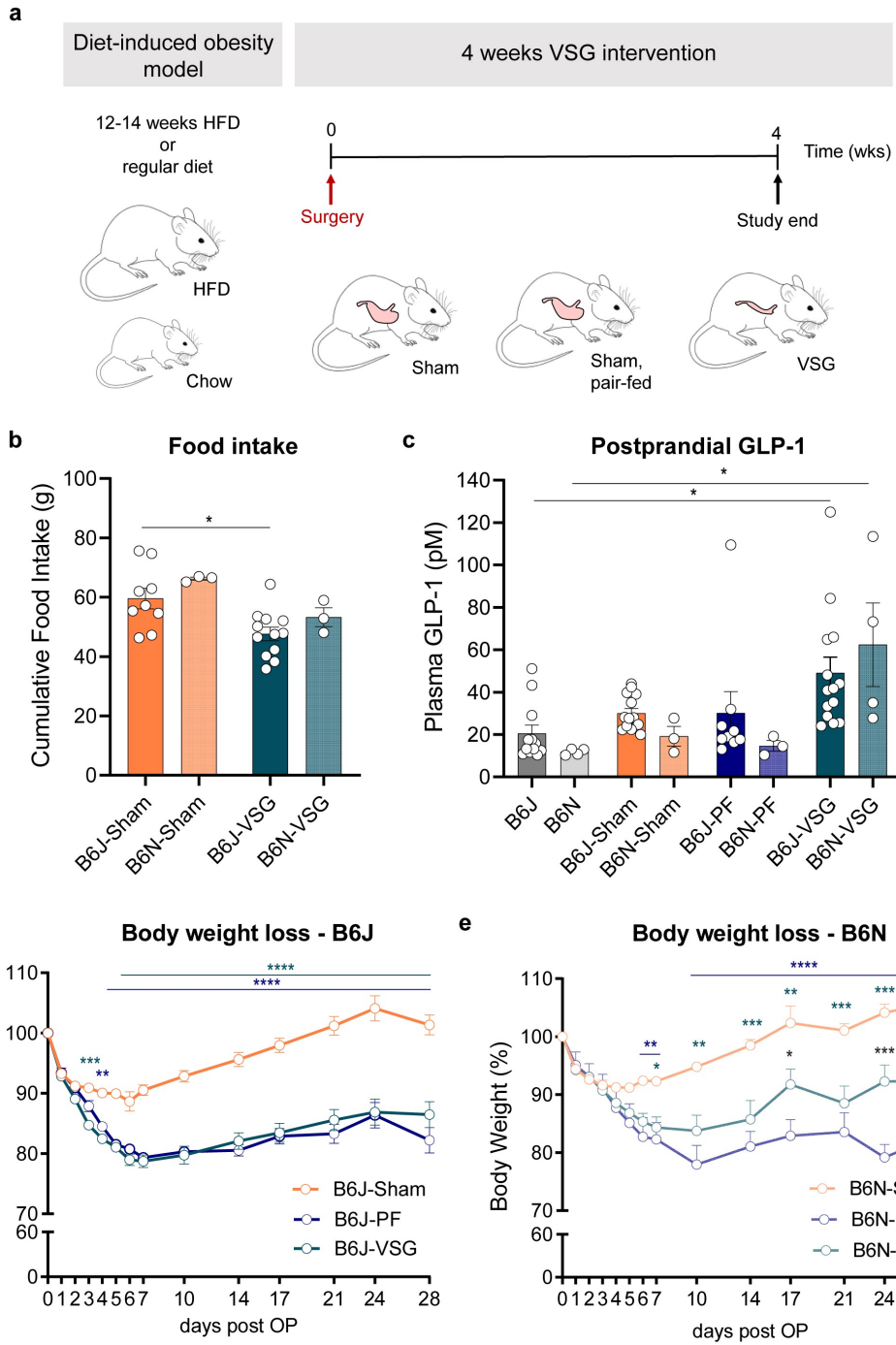
**Figure 7: HFD-fed B6N mice show a pre-diabetic phenotype, while *db/db* mice reveal overt diabetes characteristics.** (a) Blood glucose levels after 6h starvation in B6J and B6N HFD-fed mice and *db/db* mice compared to controls ( $n_{B6J}=12$ ,  $n_{B6N}=4$ ,  $n_{BKS}=7$ ,  $n_{B6J-HFD}=55$ ,  $n_{B6N-HFD}=8$ ,  $n_{db/db}=12$ ). BKS vs. *db/db* ( $p<0.0001$ ), *db/db* vs. B6J-HFD ( $p<0.0001$ ), *db/db* vs. B6N-HFD ( $p<0.0001$ ). (b) Plasma insulin levels after 6h starvation in B6J and B6N HFD-fed mice and *db/db* mice compared to controls ( $n_{B6J}=10$ ,  $n_{B6N}=3$ ,  $n_{BKS}=8$ ,  $n_{B6J-HFD}=46$ ,  $n_{B6N-HFD}=4$ ,  $n_{db/db}=11$ ). BKS vs. *db/db* ( $p<0.0001$ ), *db/db* vs. B6J-HFD ( $p<0.0001$ ), *db/db* vs. B6N-HFD ( $p<0.0001$ ), B6J-HFD vs. B6N-HFD ( $p<0.0001$ ). (c) AUC blood glucose levels during a 120 min MMTT in B6J and B6N HFD-fed mice and *db/db* mice compared to controls ( $n_{B6J}=11$ ,  $n_{B6N}=2$ ,  $n_{BKS}=7$ ,  $n_{B6J-HFD}=33$ ,  $n_{B6N-HFD}=10$ ,  $n_{db/db}=15$ ). BKS vs. *db/db* ( $p<0.0001$ ), *db/db* vs. B6J-HFD ( $p<0.0001$ ), *db/db* vs. B6N-HFD ( $p<0.0001$ ). (d) AUC plasma insulin levels during a 120 min insulin-secretion test (IST) after oral gavage of a mixed-meal in B6J and B6N HFD-fed mice and *db/db* mice compared to controls ( $n_{B6J}=8$ ,  $n_{B6N}=2$ ,  $n_{BKS}=8$ ,  $n_{B6J-HFD}=47$ ,  $n_{B6N-HFD}=10$ ,  $n_{db/db}=9$ ). BKS vs. *db/db* ( $p<0.0001$ ), B6N vs. B6N-HFD ( $p<0.0001$ ), *db/db* vs. B6J-HFD ( $p<0.0001$ ), *db/db* vs. B6N-HFD ( $p<0.0001$ ), B6J-HFD vs. B6N-HFD ( $p<0.0001$ ). Statistical testing was performed using One-way-ANOVA for single parameters, Two-way-ANOVA for longitudinal data and Bonferroni correction. Data is presented as mean  $\pm$  s.e.m.

## **3.2 Therapeutic VSG Intervention in Early Diabetes**

While the urgency of diabetes intervention in early stages of the disease is widely known, appropriate treatments that can halt the progression of diabetes in the long-term are still missing. To date, bariatric surgery including VSG is the most potent and sustainable treatment of obesity and diabetes. However, due to the high invasiveness of these procedures, surgery is clinically indicated solely for patients presenting severe states of obesity-driven diabetes. Therefore, current research aims at identifying the underlying mechanisms of VSG. These hold potential for the development of pharmacotherapies mimicking bariatric surgery, which can in turn be more easily applied to a broad spectrum of diabetes and obesity patients.

### **3.2.1 VSG Improves Diet-Induced Obesity and Pre-Diabetes Dependent of Model**

Here, we assessed the ability of VSG to reverse obesity, halt the progression of diabetes and explored possible downstream mechanisms of VSG in DIO-pre-diabetes mouse models. To this end, HFD-fed B6J and B6N mice underwent a VSG intervention for 28 days. Mice were homogeneously allocated to VSG, Sham surgery and Sham surgery including subsequent pair-feeding (PF) (Fig. 8a). Food intake of PF mice was matched to that of VSG mice to control energy consumption and body weight. Sham surgery itself controlled for surgical stress including handling, anesthesia, wound healing, and postsurgical medication. Chow-fed B6J and B6N animals were considered as healthy controls. Here, VSG-treated mice of both strains reduced their food intake by 20% compared to Sham controls, albeit not statistically significant in B6N mice due to low animal numbers (Fig. 8b). Enhanced postprandial GLP-1 responses are a characteristic feature of a successful VSG procedure. High GLP-1 levels are explained by the accelerated transit of food through the intestine to distally located GLP-1 secreting EECs after VSG<sup>120</sup>. In fact, VSG-treated mice of both strains revealed the characteristic postprandial increase in GLP-1 secretion compared to WT controls indicating that VSG was successful (Fig. 8c). Furthermore, VSG and PF equally reduced the postsurgical body weight by 20% compared to Sham controls in B6J and B6N HFD-models (Fig. 8d,e). Collectively, our data shows that VSG and PF are equally effective in reducing body weight in DIO models but solely VSG led to characteristic hormonal adaptations of GLP-1 and decreased food intake.



Caption on the next page.

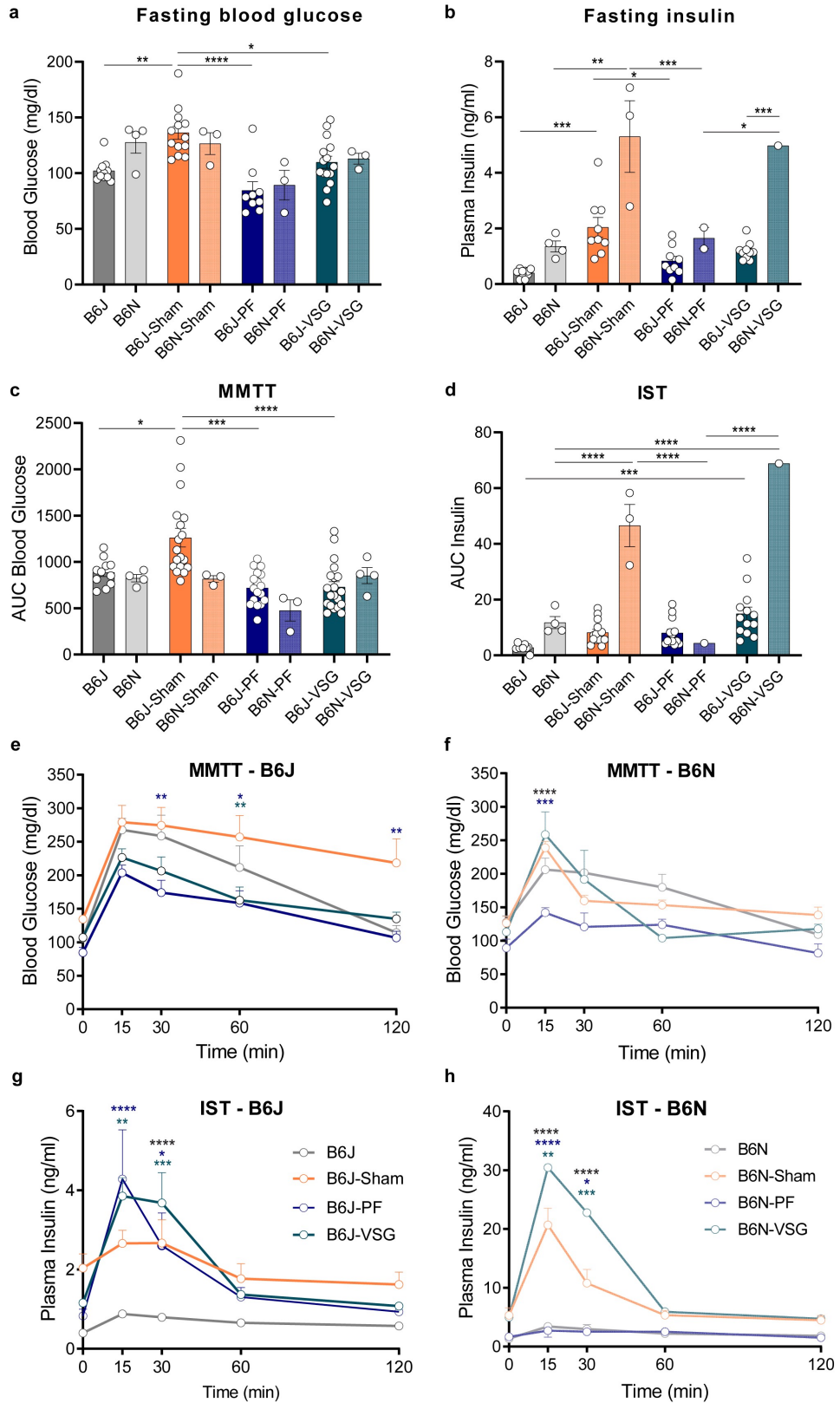
**Figure 8: VSG and PF result in body weight loss in DIO mouse models. (a)** Experimental scheme of DIO and subsequent VSG surgery in B6J and B6N mice. **(b)** Cumulative food intake over 28 days after surgery in Sham and VSG mice ( $n_{B6J-Sham}=9$ ,  $n_{B6N-Sham}=3$ ,  $n_{B6J-VSG}=12$ ,  $n_{B6N-Sham}=3$ ). B6J-Sham vs. B6J-VSG,  $p=0.0221$ . **(c)** Postprandial plasma GLP-1 levels 28 days after surgery in WT, Sham, PF, and VSG mice ( $n_{B6J}=12$ ,  $n_{B6N}=4$ ,  $n_{B6J-Sham}=14$ ,  $n_{B6N-Sham}=3$ ,  $n_{B6J-PF}=9$ ,  $n_{B6N-PF}=3$ ,  $n_{B6J-VSG}=14$ ,  $n_{B6N-VSG}=4$ ). B6J vs B6J-VSG ( $p=0.0374$ ), B6N vs. B6N-VSG ( $p=0.0432$ ). **(d)** Postsurgical body weight loss in B6J mice ( $n_{B6J-Sham}=16$ ,  $n_{B6J-PF}=9$ ,  $n_{B6J-VSG}=14$ ). Statistical significance of B6J-VSG vs. B6J-Sham shown by green asterisks (day 3:  $p<0.001$ , day 4-28:  $p<0.0001$ ). Statistical significance of B6J-PF vs- B6J-Sham shown by purple asterisks (day 4:  $p<0.01$ , day 5-28:  $p<0.0001$ ). **(e)** Postsurgical body weight loss in B6N mice ( $n_{B6N-Sham}=3$ ,  $n_{B6N-PF}=3$ ,  $n_{B6N-VSG}=4$ ). Statistical significance of B6N-VSG vs. B6N-Sham shown by green asterisks (day 7:  $p=0.0293$ , day 10:  $p=0.0013$ , day 14:  $p=0.0002$ , day 17:  $p=0.0021$ , day 21:  $p=0.0002$ , d24:  $p=0.0005$ , day 28:  $p<0.0001$ ). Statistical significance of B6N-PF vs. B6N-Sham shown by purple asterisks (day 6:  $p=0.0058$ , day 7:  $p=0.0040$ , day 10-28:  $p<0.0001$ ). Statistical significance of B6N-VSG vs. B6N-PF shown by black asterisks (day17:  $p=0.0133$ , day 24:  $p=0.0001$ , day 28:  $p=0.0084$ ). Statistical testing was performed using One-way-ANOVA for single parameters, Two-way-ANOVA for longitudinal data and Bonferroni correction. Data is presented as mean  $\pm$  s.e.m.

In order to test the ability of VSG to improve glycaemic regulation in B6J and B6N DIO-pre-diabetes models, VSG-treated mice of both strains underwent a mixed-meal challenge. Here, only VSG mice of the B6J but not B6N DIO model achieved an improved glucose regulation, which was equivalent to the effects observed upon PF. In particular, B6J-VSG and B6J-PF mice showed normalized fasting blood glucose levels and glucose excursions similar to WT controls during an MMTT (Fig. 9a,c,f). Glucose excursions in B6J-VSG and B6J-PF mice were less pronounced and levels returned to baseline more rapidly than in B6J-Sham animals during the MMTT (Fig. 9e). Of note, PF and VSG had no effects on glycaemia in the B6N DIO model, except for PF, which lowered the initial glycaemic peak 15 min after an oral application of a mixed-meal compared with Sham and VSG (Fig. 9f). These findings suggest 1) that VSG and PF are equally efficient in normalizing glycaemia to WT-levels under early pre-diabetic conditions and 2) that these effects become only overt in models of hyperglycaemia, such as the B6J-DIO model.

Although mice of the B6N strain had generally higher insulin levels than those of the B6J strain, VSG and PF interventions yielded similar effect sizes in both models. VSG did not alter fasting insulin levels but significantly enhanced the postprandial insulin secretion compared to WT levels in both, B6J and B6N, DIO models (Fig. 9b,d). Differences in fasting postprandial insulin levels were not statistically significant in VSG compared to Sham mice of both models. In contrast, PF remarkably reduced the fasting insulin levels in both DIO models, while only B6N-PF but not B6J-PF mice presented decreased postprandial insulin levels compared to Sham controls (Fig. 9b,d). Thus, VSG and PF impact insulin secretion in opposite directions during the fasted state suggesting that both interventions might govern different mechanisms targeting insulin secretion.

Moreover, VSG and PF improved the regulation of insulin secretion in the B6J DIO model. Generally, Sham groups of both strains displayed hyperinsulinemia. However, B6J-Sham animals showed a dysregulated postprandial insulin secretion lacking the characteristic initial peak and presented a delayed return to baseline levels, while B6N-Sham mice still displayed a phasic insulin secretion profile (Fig. 9g,h). Thus, in accordance with results from figure 7, HFD-feeding results in a stronger phenotype of  $\beta$ -cell failure in B6J mice and a hyperinsulinemic, compensatory phenotype in B6N mice. Here, VSG and PF enhanced the postprandial insulin secretion and restored a phasic secretion in the B6J DIO model. Likewise, VSG markedly increased postprandial insulin levels in the B6N DIO model. However, PF yielded opposite effects in the B6N DIO model presenting decreased postprandial insulin profiles (Fig. 9g,h). Of note, all data on insulin levels obtained from B6N VSG and PF groups need to be interpreted carefully due to insufficient numbers of replicates.





Caption on next page.

**Figure 9: VSG and PF improve glycaemia in DIO mouse models dependent of strain. (a)** Fasting blood glucose levels ( $n_{B6J}=11$ ,  $n_{B6N}=4$ ,  $n_{B6J-Sham}=13$ ,  $n_{B6N-Sham}=3$ ,  $n_{B6J-PF}=9$ ,  $n_{B6N-PF}=3$ ,  $n_{B6J-VSG}=15$ ,  $n_{B6N-VSG}=3$ ) and **(b)** fasting insulin levels 28 days after surgical intervention in diet-induced obese B6J and B6N mice ( $n_{B6J}=10$ ,  $n_{B6N}=4$ ,  $n_{B6J-Sham}=9$ ,  $n_{B6N-Sham}=3$ ,  $n_{B6J-PF}=9$ ,  $n_{B6N-PF}=2$ ,  $n_{B6J-VSG}=10$ ,  $n_{B6N-VSG}=1$ ). HFD-feeding in B6J but not B6N mice led to an increase in fasting blood glucose levels and only PF and VSG in B6J mice significantly decreased fasting blood glucose levels (B6J vs. B6J-Sham ( $p=0.0019$ ), B6J-Sham vs. B6J-PF ( $p<0.0001$ ), B6J-VSG vs. B6J-Sham ( $p=0.0181$ )). HFD-feeding increased fasting insulin levels in B6J and B6N DIO models (B6J vs. B6J-Sham ( $p=0.0009$ ), B6N vs. B6N-Sham ( $p<0.0001$ )). Only PF decreased fasting insulin levels compared to Sham controls (B6J-PF vs. B6J-Sham ( $p=0.0459$ ), B6N-PF vs. B6N-Sham ( $p=0.0001$ )). Fasting insulin levels after VSG were significantly lower in B6J than B6N mice ( $p=0.0007$ ). PF decreased fasting insulin levels more than VSG in the B6N DIO model ( $p=0.0260$ ). **(c)** Area under the curve of blood glucose levels during an MMTT ( $n_{B6J}=11$ ,  $n_{B6N}=4$ ,  $n_{B6J-Sham}=18$ ,  $n_{B6N-Sham}=3$ ,  $n_{B6J-PF}=17$ ,  $n_{B6N-PF}=3$ ,  $n_{B6J-VSG}=20$ ,  $n_{B6N-VSG}=4$ ), B6J vs. B6J-Sham ( $p=0.0149$ ), B6J-Sham vs. B6J-PF ( $p<0.0001$ ), B6J-Sham vs. B6J-VSG ( $p<0.0001$ ). **(d)** Area under the curve of insulin levels during an IST ( $n_{B6J}=9$ ,  $n_{B6N}=4$ ,  $n_{B6J-Sham}=14$ ,  $n_{B6N-Sham}=3$ ,  $n_{B6J-PF}=14$ ,  $n_{B6N-PF}=1$ ,  $n_{B6J-VSG}=13$ ,  $n_{B6N-VSG}=1$ ), B6J vs. B6J-VSG ( $p=0.0006$ ), B6N vs. B6N-Sham ( $p<0.0001$ ), B6N vs. B6N-VSG ( $p<0.0001$ ), B6N-Sham vs. B6N-PF ( $p<0.0001$ ), B6N-PF vs. B6N-VSG ( $p<0.0001$ ). **(e,f)** Postsurgical blood glucose profiles during an MMTT in (e) B6J and (f) in B6N DIO models ( $n_{B6J}=11$ ,  $n_{B6N}=4$ ,  $n_{B6J-Sham}=14$ ,  $n_{B6N-Sham}=3$ ,  $n_{B6J-PF}=9$ ,  $n_{B6N-PF}=3$ ,  $n_{B6J-VSG}=15$ ,  $n_{B6N-VSG}=3$ ). Statistical significance of B6J-VSG vs. B6J-Sham shown by green asterisks (60 min:  $p=0.0032$ ), B6J-PF vs. B6J-Sham shown by purple asterisks (30 min:  $p=0.0067$ , 60 min:  $p=0.0119$ , 120 min:  $p=0.0082$ ). B6N-PF vs. B6N-Sham shown by purple asterisks (15 min:  $p=0.0008$ ), B6N-VSG vs. B6N-PF shown by black asterisks (15 min:  $p<0.0001$ ). **(g,h)** Postsurgical plasma insulin profiles during an IST in (g) B6J and (h) B6N DIO models ( $n_{B6J}=10$ ,  $n_{B6N}=4$ ,  $n_{B6J-Sham}=9$ ,  $n_{B6N-Sham}=3$ ,  $n_{B6J-PF}=9$ ,  $n_{B6N-PF}=2$ ,  $n_{B6J-VSG}=12$ ,  $n_{B6N-VSG}=1$ ). Statistical significance of B6N-VSG vs. B6N-Sham shown by green asterisks (15 min:  $p=0.0022$ , 30 min:  $p=0.0002$ ), B6N-PF vs. B6N-Sham shown by purple asterisks (15 min:  $p<0.0001$ , 30 min:  $p=0.0118$ ), B6N-VSG vs. B6N-PF shown by black asterisks (15 min:  $p<0.0001$ , 30 min:  $p<0.0001$ ). Statistical testing was performed using One-way-ANOVA for single parameters and Two-way-ANOVA for longitudinal data and Bonferroni correction. Data is presented as mean  $\pm$  s.e.m.

Collectively, our data shows that VSG and PF are equally suitable interventions to normalize glycaemia in pre-diabetic conditions. VSG commonly enhanced  $\beta$ -cell function, while PF yielded opposing outcomes in B6J and B6N DIO-pre-diabetes models suggesting different mechanisms of action for VSG and PF interventions.

### **3.2.2 Impact of Intestinal and Pancreatic Morphological Adaptations after VSG**

Intestinal and pancreatic tissues involve the ability to adapt to varying nutritional demands. The intestinal epithelium and pancreatic islets have widely been reported to expand in mass to meet metabolic demand during diet-induced early stages of diabetes<sup>34,35,146</sup>. In particular, HFD-feeding has been shown to induce hyper-proliferation of enterocytes thereby increasing nutrient absorption<sup>31</sup>. Here, we tested whether VSG reverses obesity-driven intestinal expansion to reduce the capacity of nutrient absorption and systemic availability in our B6J-DIO model. This might present a possible mechanism driving the beneficial effects of VSG on body weight and glucose regulation. While our data confirmed the expansion of the intestine after HFD-feeding, as such, an increased small intestinal weight in Sham compared to B6J control mice, VSG did not impact intestinal mass or crypt-villus morphology. In particular, VSG did not alter small intestinal weight or length (Fig. 10a,b), the number of cells per crypt, the depth or width of crypts compared to Sham controls (Fig. 10c-e). Of note, PF significantly reduced the number of cells per crypt compared to Sham and VSG groups, which was, however, not mirrored by significant changes in crypt width or depth (Fig. 10c-e). We next explored the possibility of VSG to alter intestinal proliferation that can directly affect villus length and thus the capacity of nutrient absorption. VSG did not alter small intestinal proliferation or villus length (Fig. 10f-h). PF intervention increased small intestinal proliferation compared to Sham controls, however, this effect did not translate into larger villi (Fig. 10f-h). Collectively, these findings suggest that the beneficial effects of VSG on body weight and glucose regulation do not require mechanisms that involve changes in small intestinal morphology in the B6J-DIO model.

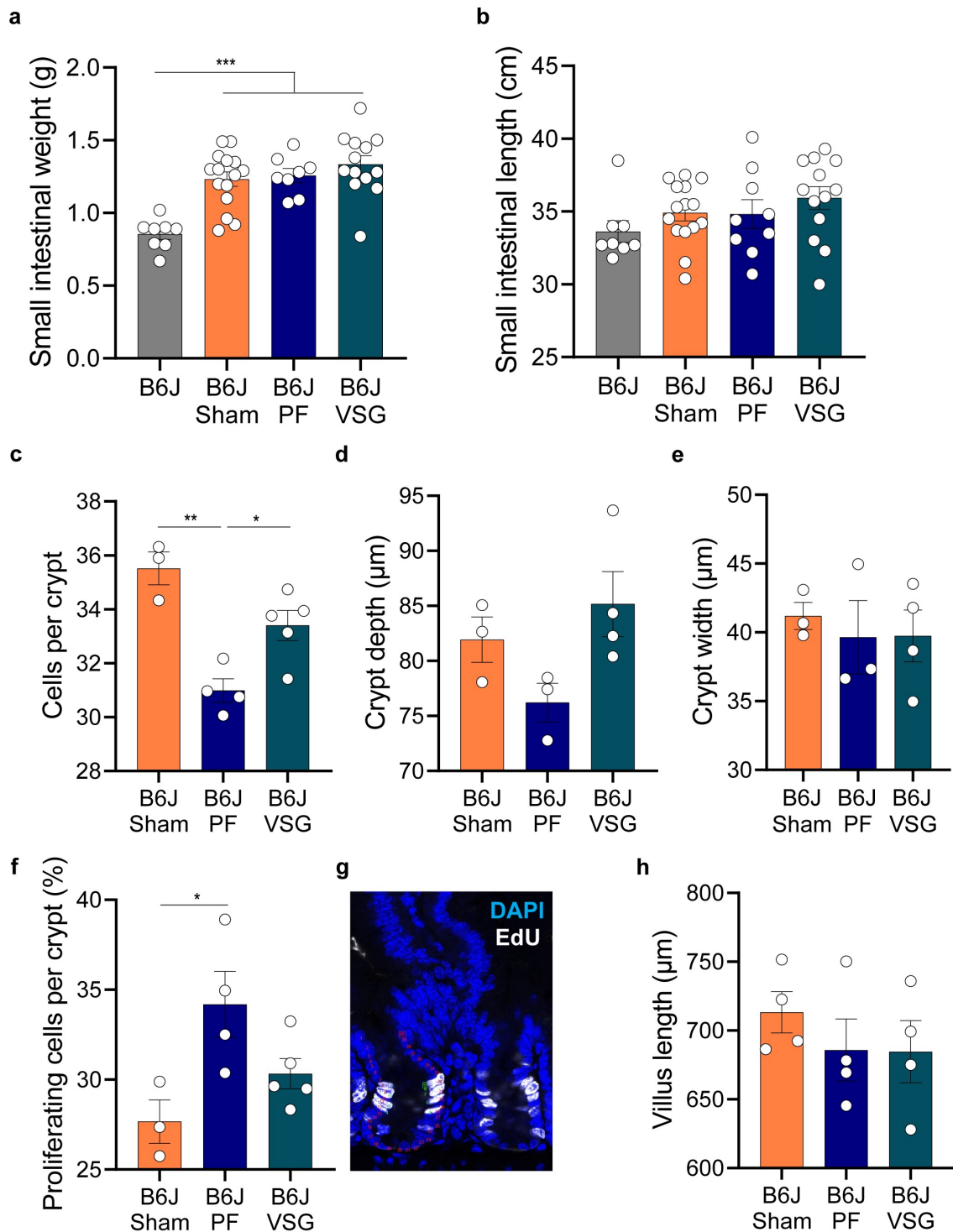


**Figure 10: VSG does not impact small intestinal morphology in a B6J DIO model.** (a,b) Postsurgical small intestinal (a) weight and (b) length in the B6J DIO model (a,b:  $n_{\text{B6J}}=8$ ,  $n_{\text{B6J-Sham}}=16$ ,  $n_{\text{B6J-PF}}=9$ ,  $n_{\text{B6J-VSG}}=13$ ). HFD-feeding resulted in an increased small intestinal weight but not length independent of treatments (B6J vs. B6J-Sham ( $p=0.0001$ ), B6J vs. B6J-PF ( $p=0.0003$ ), B6J vs. B6J-VSG ( $p=0.0001$ )). (c) Number of cells per crypt is decreased after

PF intervention ( $n_{B6J-Sham}=3$ ,  $n_{B6J-PF}=4$ ,  $n_{B6J-VSG}=5$ , B6J-Sham vs. B6J-PF ( $p=0.0012$ ) and B6J-VSG vs. B6J-PF ( $p=0.0277$ )). **(d,e)** Small intestinal (d) crypt depth and (e) crypt width were unchanged after VSG and PF intervention ( $n_{B6J-Sham}=3$ ,  $n_{B6J-PF}=3$ ,  $n_{B6J-VSG}=4$ ). **(f)** Barplot showing the percentage of proliferating crypt cells per group after a 4h EdU pulse ( $n_{B6J-Sham}=3$ ,  $n_{B6J-PF}=4$ ,  $n_{B6J-VSG}=5$ ) and **(g)** representative microscopy image showing the quantification of proliferating EdU+ crypt cells. PF increased the fraction of proliferating crypt cells (B6J-Sham vs. B6J-PF:  $p=0.0310$ ). **(h)** Small intestinal villus length was unchanged after VSG and PF intervention ( $n_{B6J-Sham}=4$ ,  $n_{B6J-PF}=4$ ,  $n_{B6J-VSG}=4$ ). Statistical testing was performed using One-way-ANOVA and Bonferroni correction. Data is presented as mean  $\pm$  s.e.m.

Gut hormones are continuously being investigated in the field of bariatric surgery to mediate gluco-regulatory and body weight lowering effects. Many laboratories including ours have shown substantial postprandial increases in intestinal GLP-1 levels after VSG across species. This phenomenon has been attributed to increased EEC stimulation and EEC density after VSG, instead of enhanced EEC function<sup>120,122,123</sup>. Here, we tested whether VSG had similar effects on the density of ChgA<sup>+</sup> cells (marking mainly enterochromaffin EECs) and GLP-1<sup>+</sup> EECs in our B6J DIO model. In fact, VSG did not significantly alter the fraction of ChgA<sup>+</sup> EECs in the villus or the number of GLP-1<sup>+</sup> EECs per crypt in the ileum. PF increased the percentage of ChgA<sup>+</sup> EECs compared to Sham controls (Fig. 11a-c). These findings indicate that the high postprandial GLP-1 levels we observed after VSG did likely not result from an increased density of GLP-1<sup>+</sup> EECs in our B6J DIO model as previously reported in similar models or might result from methodological discrepancies between our EEC analyses and those of published studies<sup>122,123</sup>.

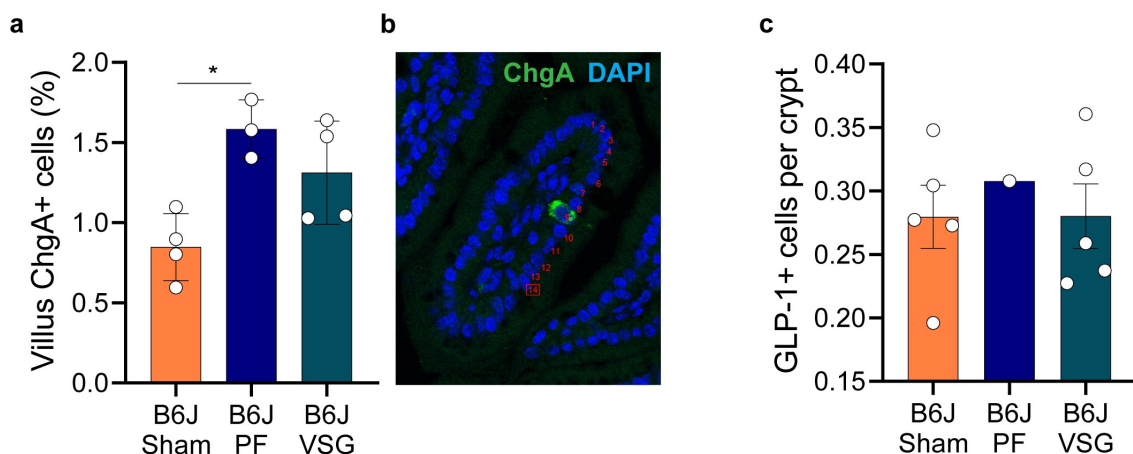


**Figure 11: EEC density is not affected by VSG in a DIO model.** **(a)** Fraction of ChgA<sup>+</sup> EECs in small intestinal villi after VSG and PF intervention ( $n_{B6J-Sham}=4$ ,  $n_{B6J-PF}=3$ ,  $n_{B6J-VSG}=4$ ) and **(b)** representative microscopy image showing the quantification of ChgA<sup>+</sup> cells. PF increased the proportion of ChgA<sup>+</sup> EECs (B6J-PF vs. B6J-Sham:  $p=0.0153$ ). **(c)** Number of GLP-1<sup>+</sup> EECs per crypt is unchanged after PF and VSG interventions ( $n_{B6J-Sham}=5$ ,  $n_{B6J-PF}=1$ ,  $n_{B6J-VSG}=5$ ). Statistical testing was performed using One-way-ANOVA and Bonferroni correction. Data is presented as mean  $\pm$  s.e.m.

$\beta$ -cell function and mass are the primary determinants of insulin levels. Both of them are compromised in diabetes pathophysiology. Here, VSG markedly increased insulin secretion in B6J and B6N DIO pre-diabetes models. Three mechanisms of expansion of adult  $\beta$ -cell mass are currently debated and comprise replication of existing  $\beta$ -cells,  $\alpha$ - to  $\beta$ -cell trans-differentiation or neogenesis from ductal epithelial progenitors<sup>147</sup>. In order to understand the source of enhanced insulin secretion after VSG, we quantitatively assessed the density and size of islets in B6J and B6N DIO models. Notably, B6N HFD-fed mice generally displayed a denser distribution of islets compared to the B6J DIO model (Fig. 12a). Further, VSG did not increase the frequency of islets or alter the abundance of small-, medium- and large-sized islets (Fig. 12a,b). PF slightly increased the fraction of small islets in the B6J DIO model (Fig. 12b). These findings suggest that the mechanisms of VSG to enhance insulin secretion do not rely on major increases in islet mass in pre-diabetic DIO models. The observation that VSG did not result in proportional increases in small versus larger islets contradicts hypotheses based on  $\beta$ -cell neogenesis.

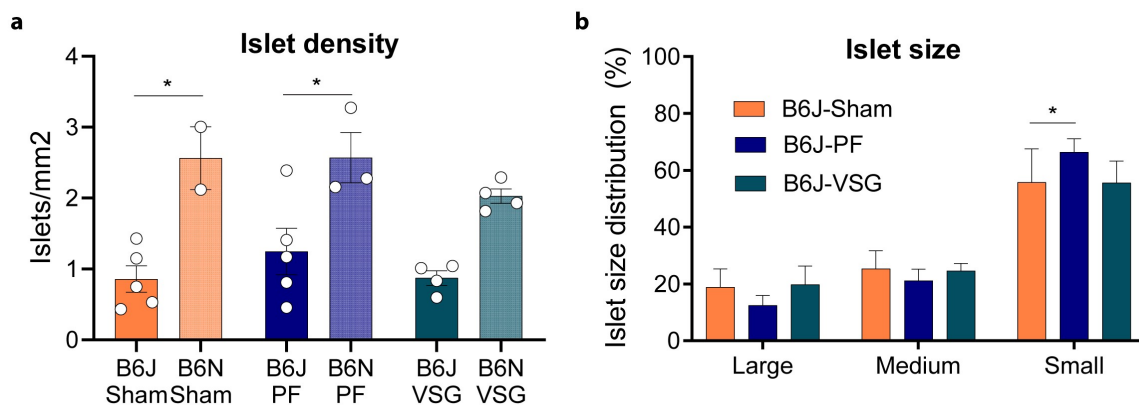


**Figure 12: Pancreatic islet morphology is not affected by VSG in pre-diabetes DIO models. (a)** Pancreatic islet density after VSG and PF interventions in B6J and B6N DIO models ( $n_{B6J-Sham}=5$ ,  $n_{B6N-Sham}=2$ ,  $n_{B6J-PF}=5$ ,  $n_{B6N-PF}=3$ ,  $n_{B6J-VSG}=4$ ,  $n_{B6N-VSG}=4$ ). B6N mice showed higher density of islets compared to the B6J strain (B6J-Sham vs. B6N-Sham:  $p=0.0119$ , B6J-PF vs. B6J-Sham:  $p=0.0318$ ). **(b)** Barplot showing the fractional distribution of small, medial and large sized islets after VSG and PF interventions in a B6J DIO model ( $n_{B6J-Sham}=5$ ,  $n_{B6J-PF}=5$ ,  $n_{B6J-VSG}=4$ ). B6J-PF significantly increased the proportion of small islets compared to B6J-Sham ( $p=0.0445$ ). Statistical testing was performed using One-way-ANOVA and Bonferroni correction. Data is presented as mean  $\pm$  s.e.m. Morphological analysis performed in collaboration with Dr. Annette Feuchtinger (Institute of Analytical Pathology).

We then explored the possibility of VSG to directly alter  $\beta$ - and  $\alpha$ -cell mass and replication. Here, VSG did not markedly alter the fraction of  $\beta$ - and  $\alpha$ -cells in B6J and B6N HFD-fed mice suggesting that VSG does not expand  $\beta$ -cell mass or induce trans-differentiation from  $\alpha$ - to  $\beta$ -cells (Fig. 13a,b). Further, VSG did not impact the frequency of proliferation in  $\beta$ - and  $\alpha$ -cells (Fig. 13c,d). PF resulted in a significantly reduced fraction of cycling  $\beta$ -cells compared to Sham controls in the B6J DIO model (Fig.

13c). Of note, due to batch-specific thresholds for the automated quantification of immuno-stained  $\alpha$ - and  $\beta$ -cells, treatment effects should solely be compared within each model. Collectively, our data demonstrates that the effects of VSG on insulin secretion do not originate from increases in islet or  $\beta$ -cell mass in pre-diabetic DIO models but might be of functional nature.

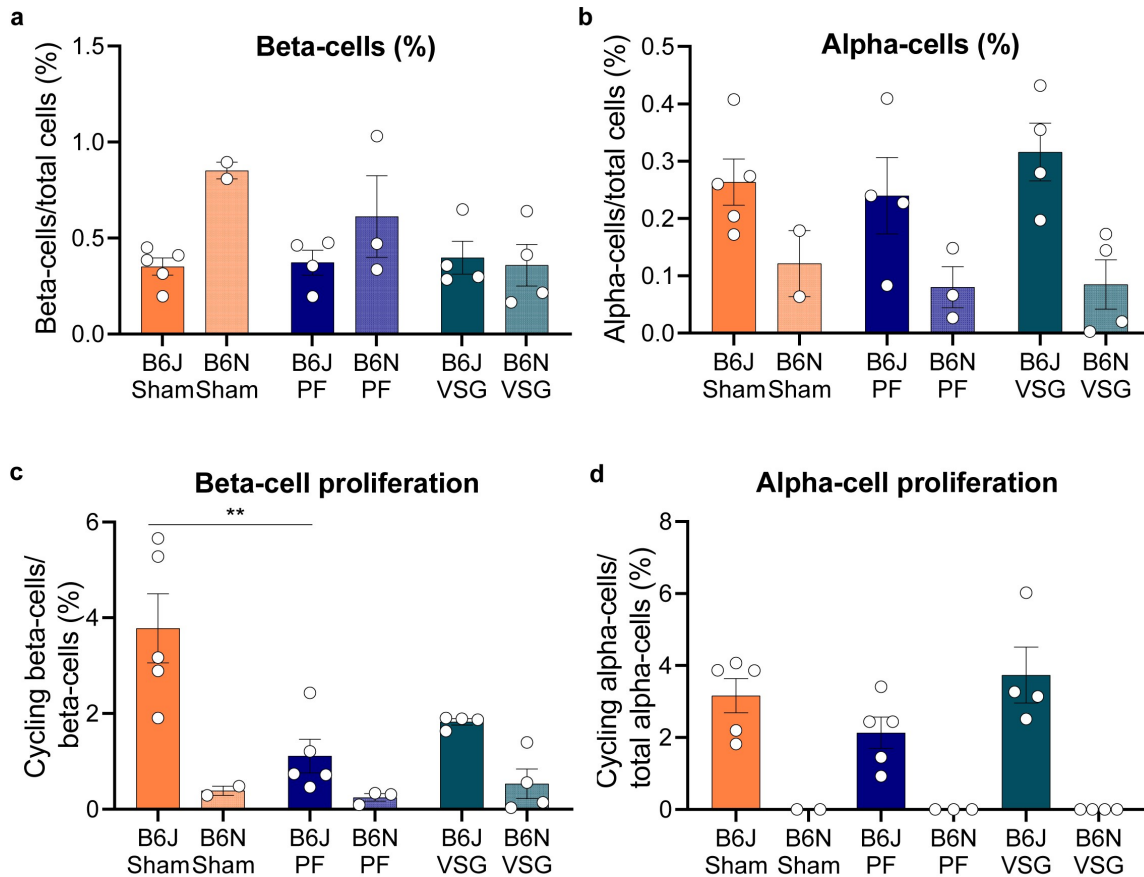


**Figure 13: VSG does not alter  $\beta$ - or  $\alpha$ -cell mass in pre-diabetes DIO models.** (a,b) Barplots showing postsurgical percentage of (a)  $\beta$ -cells and (b)  $\alpha$ -cells in B6J and B6N DIO models ( $n_{B6J-Sham}=5$ ,  $n_{B6N-Sham}=2$ ,  $n_{B6J-PF}=4$ ,  $n_{B6N-PF}=3$ ,  $n_{B6J-VSG}=4$ ,  $n_{B6N-VSG}=4$ ). VSG and PF interventions did not alter  $\beta$ - and  $\alpha$ -cell percentages. (c) Percentage  $\beta$ -cell proliferation and (d) percentage  $\alpha$ -cell proliferation after VSG and PF ( $n_{B6J-Sham}=5$ ,  $n_{B6N-Sham}=2$ ,  $n_{B6J-PF}=4$ ,  $n_{B6N-PF}=3$ ,  $n_{B6J-VSG}=4$ ,  $n_{B6N-VSG}=4$ ). B6J-Sham mice showed higher  $\beta$ -cell proliferation than B6N-Sham mice (B6J-Sham vs. B6N-Sham,  $p=0.0053$ ). PF significantly decreased  $\beta$ -cell proliferation in the B6J DIO model (B6J-PF vs. B6J-Sham,  $p=0.0037$ ). HFD-feeding resulted in higher  $\alpha$ -cell proliferation in B6J mice than B6N mice (B6J-Sham vs. B6N-Sham:  $p=0.0156$ , B6J-VSG vs. B6N-Sham:  $p=0.0006$ ). Statistical testing was performed using One-way-ANOVA and Bonferroni correction. Data is presented as mean  $\pm$  s.e.m. Morphological analysis performed in collaboration with Dr. Annette Feuchtinger (Institute of Analytical Pathology).

### 3.3 Therapeutic VSG Intervention in Clinically-Overt Diabetes

Mechanistic research on body weight and gluco-regulatory benefits upon VSG has mainly been conducted in DIO mouse models<sup>118</sup> or young (4-12 weeks old) *db/db* mice<sup>117,148</sup>. These models display features of obesity and early stages of diabetes, in which  $\beta$ -cells compensate diabetogenic stress by increasing insulin secretion and are useful to study early intervention mechanisms. However, in clinics, VSG is mostly carried out in patients of morbid obesity-linked diabetes and reports on VSG in animal models mimicking these clinical conditions are still missing. *db/db* mice present an inbuilt adaptive flexibility that enables them to adjust insulin production rates and  $\beta$ -cell mass relative to the metabolic demand in early stages, while they show progressive  $\beta$ -cell failure after 12 weeks of age<sup>144,149</sup>. Here, we used 16-18 weeks old *db/db* mice, which display a clinically overt phenotype of obesity-linked diabetes and involve pathomechanisms of  $\beta$ -cell dysfunction and dedifferentiation<sup>150,151</sup>. We aimed to test whether a two weeks VSG intervention is able to rescue a clinically-relevant condition of extreme diabetes and, if so, to study the reversal of  $\beta$ -cell dysfunction and dedifferentiation upon VSG.

#### 3.3.1 VSG Rescues Clinically-Overt Diabetes and Is Superior to Calorie Restriction

Overt obese-diabetic, 16-18 weeks old *db/db* mice were homogeneously allocated to VSG, Sham, and PF groups. BKS WT mice were considered as healthy control group and did not undergo surgery. Postsurgically, body weight, food intake and glycaemic regulation were monitored until study end, 14 days after surgery (Fig. 14a). VSG resulted in slight, albeit not statistically significant, reductions in food intake compared to Sham controls (Fig. 14b). All surgery groups irrespective of treatment lost around 10% of body weight within 14 days after surgery indicating that (post)surgical stress, but not VSG or PF interventions themselves, decreased body weight in *db/db* mice (Fig. 14c). VSG-treated mice presented slightly, but not significantly, increased postprandial plasma GLP-1 levels, a standard measure for successful VSG (Fig. 14d). To test gluco-regulatory effects of VSG dependent of gastrointestinal functions, mice underwent an MMTT. Albeit similar weight profiles in all groups, glycaemic regulation remarkably improved after VSG compared to Sham and PF groups within only two weeks of intervention. VSG, but not PF, normalized fasting glycaemia to WT-levels and significantly lowered glucose excursions during the MMTT (Fig. 14e,g). Moreover, VSG tremendously enhanced fasting and postprandial insulin secretion during the MMTT, an effect, which was not present in PF mice (Fig. 14f,h). Collectively, our data indicates that 1) VSG in hyperphagic *db/db* mice works independently of body weight reductions, 2) rapidly restores glycaemic control by enhancing



$\beta$ -cell function, and 3) is, unlike in early stages of diabetes, superior to PF after prolonged severe diabetes in *db/db* mice.

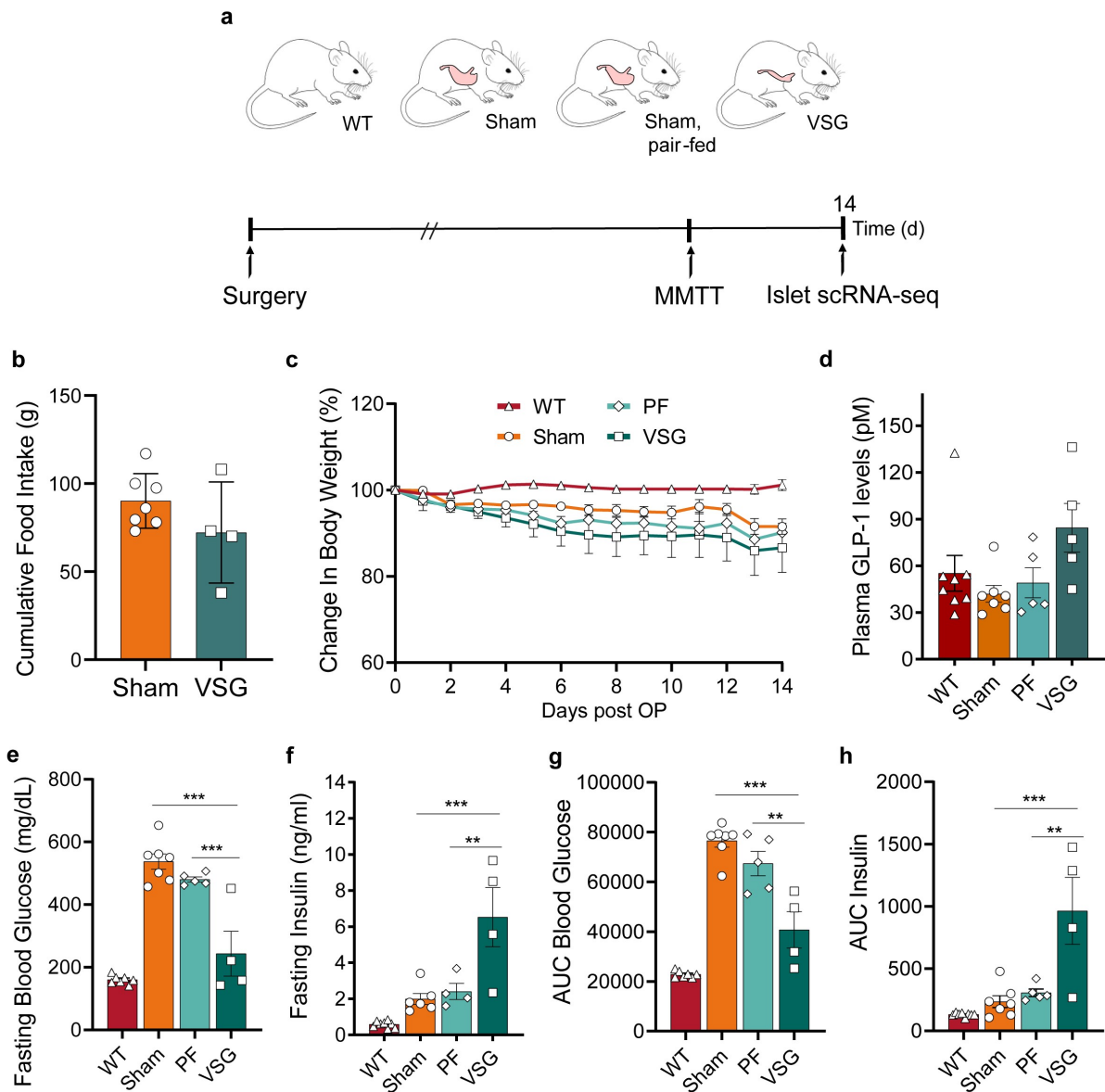


**Figure 14: VSG but not PF restores normoglycaemia and enhances  $\beta$ -cell function in overt diabetic *db/db* mice independent of body weight.** (a) Experimental scheme. 16-18 weeks old *db/db* mice were subjected to VSG, Sham surgery (Sham) and Sham surgery with subsequent PF. (b) Cumulative food intake over 14 days in Sham and VSG-treated mice ( $n_{\text{Sham}}=7$ ,  $n_{\text{VSG}}=4$ ). (c) Postprandial plasma GLP-1 levels ( $n_{\text{WT}}=7$ ,  $n_{\text{Sham}}=7$ ,  $n_{\text{PF}}=5$ ,  $n_{\text{VSG}}=5$ ). (d) Postsurgical relative loss of body weight ( $n_{\text{WT}}=8$ ,  $n_{\text{Sham}}=6$ ,  $n_{\text{PF}}=6$ ,  $n_{\text{VSG}}=4$ ). Differences between Sham, PF and VSG were not statistically significant. (e) Postsurgical fasting blood glycaemia ( $n_{\text{WT}}=7$ ,  $n_{\text{Sham}}=7$ ,  $n_{\text{PF}}=5$ ,  $n_{\text{VSG}}=4$ , WT vs. Sham ( $p<0.0001$ ), WT vs. PF ( $p<0.0001$ ), Sham vs. VSG ( $p<0.0001$ ), PF vs. VSG ( $p=0.0003$ )). (f) Postsurgical fasting

plasma insulin levels ( $n_{WT}=8$ ,  $n_{Sham}=6$ ,  $n_{PF}=4$ ,  $n_{VSG}=4$ , WT vs. VSG ( $p<0.0001$ ), Sham vs. VSG ( $p=0.0008$ ), PF vs. VSG ( $p=0.0047$ )). **(g,h)** Postsurgical area under the curve of (g) blood glucose ( $n_{WT}=7$ ,  $n_{Sham}=7$ ,  $n_{PF}=5$ ,  $n_{VSG}=4$ , Sham vs. VSG ( $p<0.0001$ ); PF vs. VSG ( $p=0.0011$ ) and (h) plasma insulin levels during an MMTT ( $n_{WT}=8$ ,  $n_{Sham}=7$ ,  $n_{PF}=5$ ,  $n_{VSG}=4$ , Sham vs. VSG ( $p=0.0002$ ); PF vs. VSG ( $p=0.0016$ ). Statistical testing was performed using One-way-ANOVA and Bonferroni correction. Data is presented as mean  $\pm$  s.e.m. Figures from Oppenländer et al., in revision at Molecular Metabolism.

### 3.3.2 $\beta$ -Cell Pathophysiology in Extreme Diabetes

While the metabolic characteristics of *db/db* mice are well reported, the detailed molecular mechanisms of prolonged severe diabetes in islets of *db/db* mice are not fully understood. Here, we used scRNA-seq to analyze islets of 18-20 weeks old Sham ( $n=2$ ) and WT mice ( $n=2$ ) to decipher islet cell type specific effects upon overt diabetes. We profiled 19,878 endocrine cells using scRNA-seq (WT:  $n=2$ , 10,725 cells; *db/db*:  $n=2$ , 9,153 cells). These were clustered into five main endocrine populations based on their predominant expression of hormonal markers,  $\alpha$ -cells (*Gcg*),  $\beta$ -cells (*Ins1*),  $\delta$ -cells (*Sst*), PP-cells (*Ppy*), and polyhormonal cells (combination of hormones), using Uniform Manifold Approximation and Projection (UMAP) and Louvain clustering (Fig. 15a). Our analysis showed an altered cell composition in diabetic islets with decreased proportions of  $\beta$ -cells and increased fractions of  $\alpha$ -,  $\delta$ -, PP- and polyhormonal cells compared to healthy WT islets (Fig. 15a). Differential gene expression revealed a large number of regulated genes in  $\beta$ -cells of *db/db* mice, while showing only very few regulated genes in  $\alpha$ -,  $\delta$ -, or PP-cells (Fig. 15b-e). This indicates that  $\beta$ -cells are most impacted in diabetes pathophysiology and more sensitive to diabetogenic stress than other islet cell types.

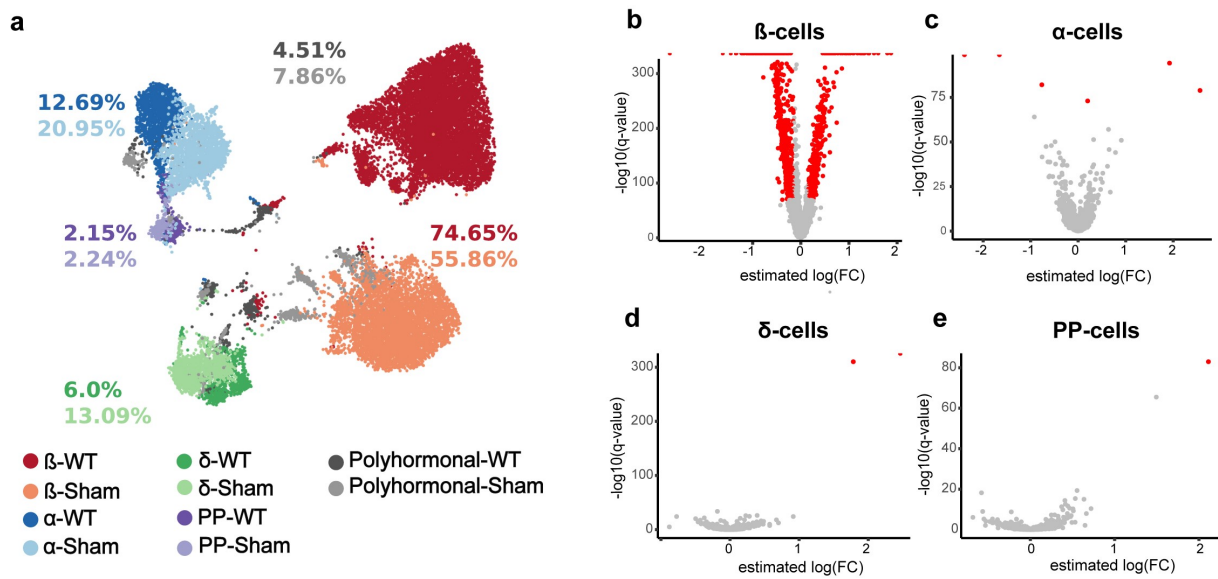


**Figure 15: Diabetic stress alters the  $\beta$ -cell transcriptome but not that of  $\alpha$ -,  $\delta$ -, and PP-cells in *db/db* mice. (a)** Plot of 19,878 pancreatic endocrine cells from WT mice (n=2) and Sham mice (n=2) in a UMAP distribution showing five main endocrine cell types in WT (darker tones) and Sham (lighter tones). Numbers present the percentage of each cell cluster in WT and Sham. **(b)** Volcano plots showing differentially expressed genes between WT and Sham in  $\beta$ -,  $\alpha$ -,  $\delta$ -, and PP-cells (threshold: absolute estimated logFC>0.15, B>150, adjusted p<0.01). Analysis and interpretation of scRNA-seq data in collaboration with Subarna Palit (Institute of Computational Biology). Figures from Oppenländer et al., in revision at Molecular Metabolism.

In order to further delineate the phenotype of  $\beta$ -cells of severely diabetic *db/db* mice, we transcriptionally characterized the identity and functionality of  $\beta$ -cells.  $\beta$ -cells of Sham presented reduced expression profiles of  $\beta$ -cell identity markers, such as *Ins1*, *Mafa*<sup>65</sup>, Pancreatic and duodenal homeobox 1 (*Pdx1*)<sup>66</sup>, Neuronal differentiation (*Neurod1*)<sup>152</sup>, and  $\beta$ -cell functional markers, Solute carrier family 2 (*Slc2a2*, also known as *Glut2*), Transient receptor potential cation channel subfamily M member 5 (*Trpm5*), and Proprotein convertase 1 (*Pcsk1*) (Fig. 16a).  $\beta$ -cell failure in T2D is characterized by progressive dysfunction and dedifferentiation in rodents<sup>61,69</sup> as well as humans<sup>64</sup>. The best-known and established marker for  $\beta$ -cell dedifferentiation, *Aldh1a3*<sup>69</sup>, was found highly upregulated and present in the great majority of  $\beta$ -cells of Sham mice. The expression of other dedifferentiation markers, for instance *Gast*<sup>70,153</sup>, *Gc67*, *Cd81*<sup>72</sup>, *Cltrn*<sup>68</sup>, and *Gpx3*<sup>68</sup> were markedly increased in Sham-derived  $\beta$ -cells (Fig. 16a). Immunohistochemical stainings of *Slc2a2*, *MafA*, *UCN3*, and *Aldh1a3* confirmed the observed mRNA expression patterns in islets of Sham mice (Fig. 16b-e). Collectively, our data reveals that Sham-derived  $\beta$ -cells progressively lose their function and identity and transition to a dedifferentiated state upon prolonged diabetic stress. Based on that, we believe

that aged *db/db* mice represent an ideal pre-clinical model to study the process of dedifferentiation, as well as regenerative mechanisms by therapeutic interventions.

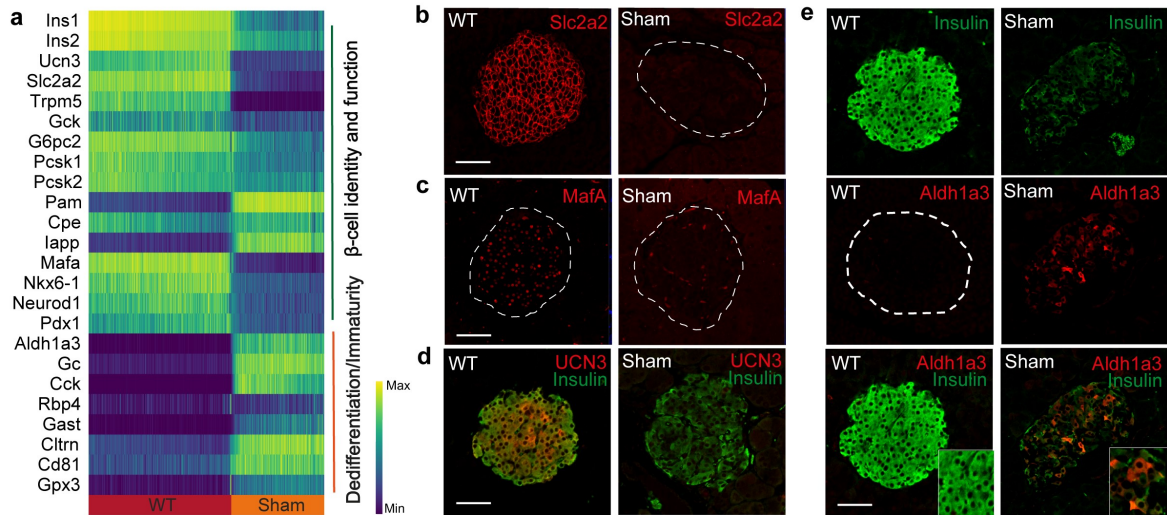


**Figure 16: Islets of *db/db* mice reveal extreme  $\beta$ -cell dedifferentiation.** (a) Changes in  $\beta$ -cell identity and function marker genes along a diffusion trajectory path from WT to Sham. Cells were ordered using a random-walk-based distance metric computed using diffusion pseudotime (DPT). Smaller clusters were removed to ensure smooth transitions. (b) Immunostainings of Slc2a2 (Glut-2), MafA, UCN3, Insulin and Aldh1a3 in  $\beta$ -cells of WT and Sham mice at study end. Scale is 50  $\mu$ m. All data is presented as mean  $\pm$  s.e.m. Analysis and interpretation of scRNA-seq data in collaboration with Subarna Palit (Institute of Computational Biology). Figures from Oppenländer et al., in revision at Molecular Metabolism.

### 3.3.3 VSG Distinctively Modulates the Islet Transcriptome

We next sought to explore islet intrinsic changes upon VSG that might underlie the marked glycaemic improvements. Prior studies used clinically less relevant pre-diabetes or early stage T2D models and did not resolve the effects of VSG on the transcriptome of specific islet cell types<sup>117,118,148</sup>. To address this gap in knowledge, we profiled 35,941 single pancreatic endocrine cells from VSG (n=2), Sham (n=2) and PF (n=1) *db/db* mice (Sham: 9153 cells, PF: 13,184 cells, VSG: 13,604 cells) 14 days after surgery and specifically addressed the transcriptional effect of VSG on distinct islet cell types. Pancreatic endocrine cells formed 5 distinct clusters based on the expression of canonical markers:  $\alpha$ -cells (*Gcg*),  $\beta$ -cells (*Ins1*),  $\delta$ -cells (*Sst*), PP-cells (*Ppy*), polyhormonal cells (hormone combination) (Fig. 17a). Subsequent differential genes expression analyses revealed that VSG did not greatly alter the transcriptome of  $\alpha$ -,  $\delta$ -, and PP-cells compared to Sham suggesting that VSG exerts its gluco-regulatory effects independent of the function of these cell types (Fig. 17b).

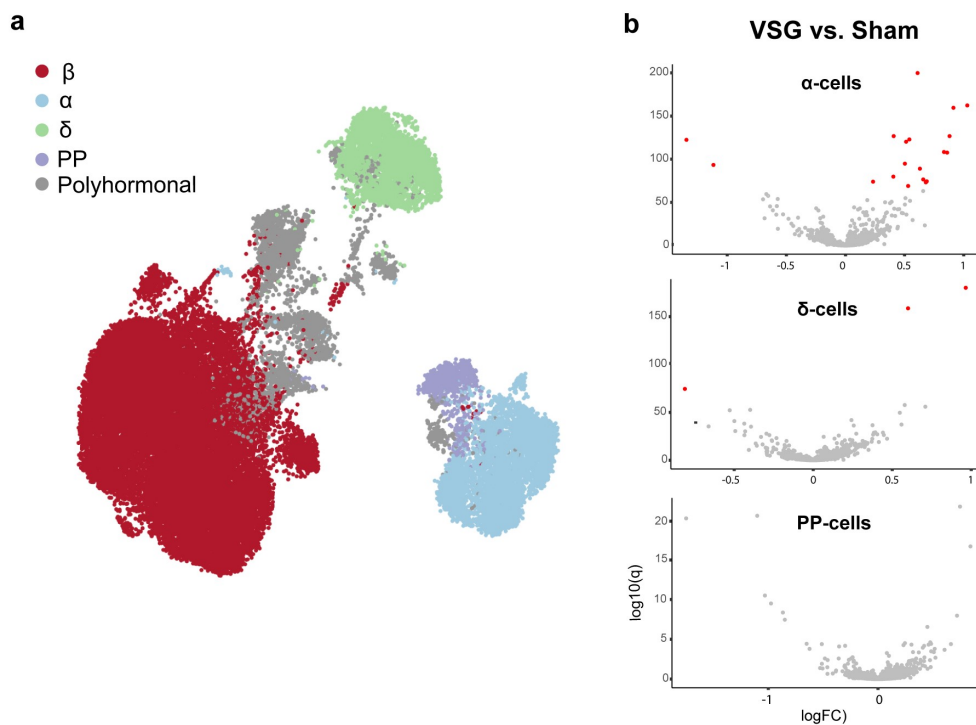
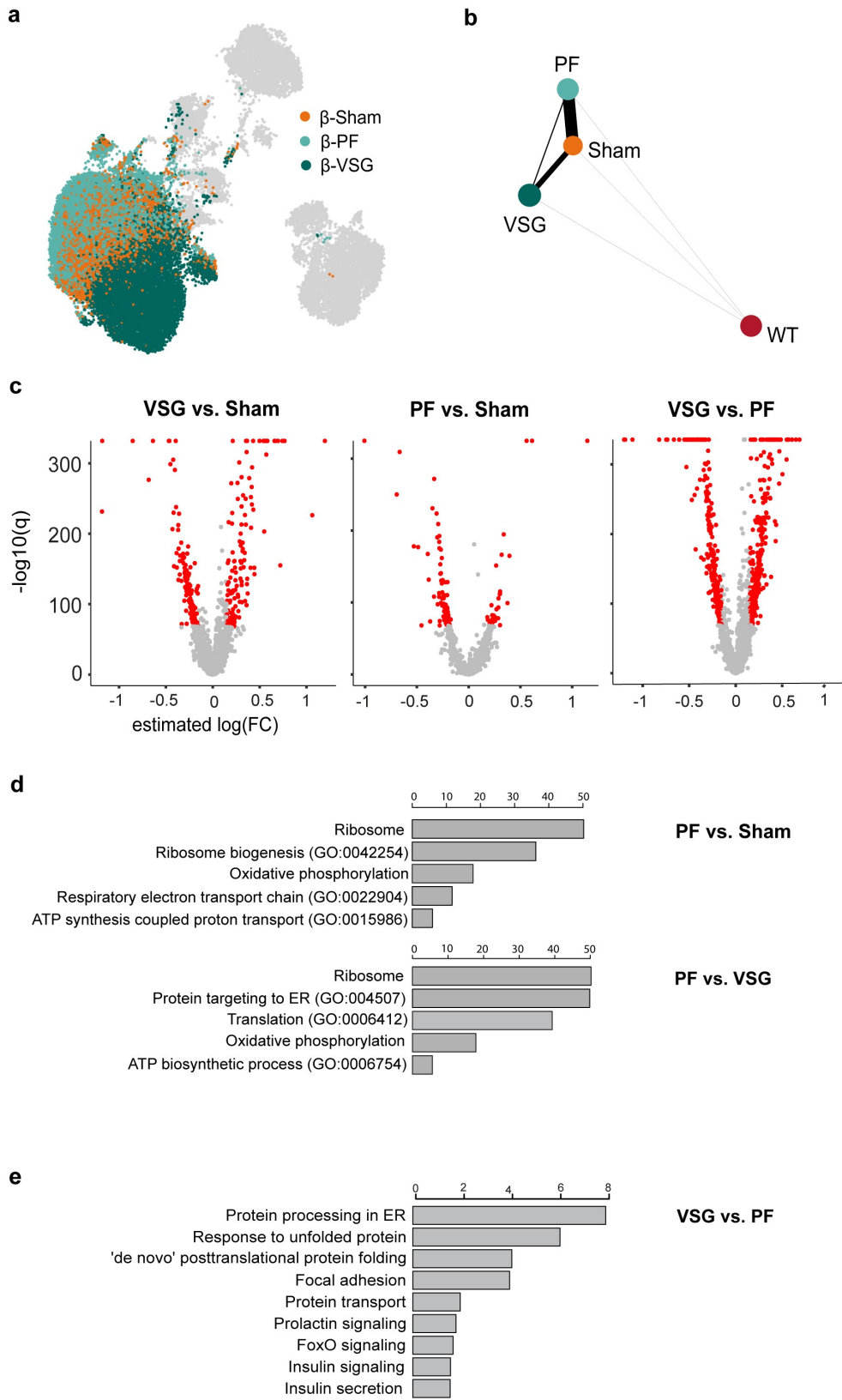


**Figure 17: The transcriptome of  $\alpha$ -,  $\delta$ -, and PP-cells is unchanged after VSG.** (a) Plot of 35,941 pancreatic endocrine cells from Sham (n=2), VSG (n=2) and PF (n=1) groups in a UMAP distribution showing five main endocrine cell types. (b) Volcano plots showing differentially expressed genes between VSG and Sham in  $\alpha$ -,  $\delta$ -, and PP-cells (threshold: absolute estimated  $\log(\text{FC}) > 0.15$ ,  $B > 150$  and adjusted  $p < 0.01$ ). Analysis and interpretation of scRNA-seq data in collaboration with Subarna Palit (Institute of Computational Biology). Figures from Oppenländer et al., in revision at Molecular Metabolism.

While VSG did not impact the transcriptome of  $\alpha$ -,  $\delta$ -, and PP-cells, we observed that  $\beta$ -cells of VSG mice presented a distinct transcriptional profile compared to  $\beta$ -cells of Sham and PF controls. In particular, VSG-derived  $\beta$ -cells clustered apart from Sham- and PF- derived  $\beta$ -cells in a UMAP space suggestive for divergent transcriptional effects of VSG (Fig. 18a). Furthermore, Partition-based graph abstraction (PAGA), a method that measures the connectivity and relatedness of single-cell clusters<sup>154</sup>, corroborated this observation (Fig. 18b). The VSG-derived  $\beta$ -cell cluster was only weakly connected to that Sham and PF, while Sham and PF revealed a strong connectivity. This implies that VSG induces intrinsic transcriptional changes in  $\beta$ -cells, while PF does not greatly alter the  $\beta$ -cell transcriptome but shares the transcriptional profiles of Sham-derived  $\beta$ -cells. In order to gain insights into the transcriptional mechanisms that might govern the fast recovery of  $\beta$ -cells upon VSG, we performed differential gene expression and pathway analyses. In line with our previous findings,  $\beta$ -cells of VSG presented a large number of differential genes compared to Sham and PF controls, while PF induced only a low number compared to Sham (Fig. 18c). Further, the few upregulated genes specific to PF, identified by comparing PF-derived  $\beta$ -cells to those of Sham and VSG, solely related to ribosomal and mitochondrial ontologies and pathways (Fig. 18d). In contrast, upregulated genes of VSG-derived  $\beta$ -cells related to diverse mechanisms including ontologies and pathways such as translation, protein processing, the response to unfolded protein, prolactin signaling, insulin signaling, and secretion (Fig. 18e). This suggests that VSG enhances insulin synthesis and pathways that ensure proper folding of insulin. In summary, we show that VSG induces intrinsic changes in the  $\beta$ -cell transcriptome mirroring potential mechanisms of  $\beta$ -cell recovery after VSG, whereas PF did not improve metabolic control in severely diabetic *db/db* mice and hence did not modulate the  $\beta$ -cell transcriptome.



Caption on next page.

**Figure 18: VSG and PF differently affect the  $\beta$ -cell transcriptome.** (a) UMAP plot of pancreatic endocrine cells of VSG, Sham and PF mice distinguishing group-specific  $\beta$ -cell populations. (b) Abstracted graph of cluster connectivity assessing transcriptomic similarity between VSG-, PF-, Sham- and WT- derived  $\beta$ -cells inferred using PAGA. PAGA is based on a statistical method that measures relatedness between single-cell clusters with edge weights indicating link significance. (c) Differentially expressed genes of  $\beta$ -cells between VSG and control groups and Sham and PF (Threshold: absolute estimated  $\log(\text{FC}) > 0.15$  and  $B > 150$ ). (d-e) GO term and KEGG pathway enrichment of upregulated genes in  $\beta$ -cells (estimated  $\log(\text{FC}) > 0.15$  and  $B > 150$ ) comparing (d) PF vs. Sham and VSG and (e) VSG vs. PF using EnrichR webtool. X-axes indicate  $-\log_{10}(\text{adjusted p-value})$ . Analysis and interpretation of scRNA-seq data in collaboration with Subarna Palit (Institute of Computational Biology). Figures from Oppenländer et al., in revision at Molecular Metabolism.

### 3.3.4 VSG Restores $\beta$ -Cell Identity and Function

To delineate mechanisms of  $\beta$ -cell recovery upon VSG, we analyzed expression changes in genes crucial for the identity and functionality of  $\beta$ -cells. We found that VSG rapidly increased the expression of several  $\beta$ -cell maturation and functionality markers and markedly decreased  $\beta$ -cell dedifferentiation markers within only two weeks of intervention. In particular, VSG increased the expression of  $\beta$ -cell identity markers, such as *Ins1*, *Mafa*, *Pdx1*, *Isl1*, or *Neurod1* and decreased the expression of dedifferentiation markers, *Aldh1a3*, *Cd81*, *Rbp4*, *Slc5a10*, *Gast*, *Gc*, and *Cck* (Fig. 19a). Of note, the expression of the maturation marker *Ucn3* was not altered suggesting that long-term intervention is required. Furthermore, VSG significantly enhanced the expression of various  $\beta$ -cell functionality genes, such as genes involved in glucose sensing (Glucokinase (*Gck*), *Trpm5*, Calcium voltage gated channel subunit alpha 1A (*Cacna1a*), and Free fatty acid receptor 1 (*Ffar1*)), insulin processing (Protein convertase 1 (*Pcsk1*), *Pcsk2*, Carboxypeptidase E (*Cpe*)), and insulin exocytosis (Chromogranin B (*Chgb*)<sup>155</sup>, Synaptotagmin 7<sup>156</sup> (*Syt7*), Synaptosomal-associated protein 25 kDa<sup>157</sup> (*Snap25*)) (Fig. 19b). Immunohistochemical analyses of MafA, Insulin, *Aldh1a3*, *Slc5a10*, and *Pcsk1* validated the changes seen on mRNA-level (Fig. 19c-g). Of note, the major glucose sensor in  $\beta$ -cells, *Slc2a2*, was found to be partly restored by VSG as shown by immunofluorescent stainings but was not mirrored at mRNA-level, potentially owing to dietary regulation of *Slc2a2* protein levels<sup>158,159</sup> (Fig. 19d). In order to delineate the extent to which VSG improved  $\beta$ -cell identity and function, we charted genes that were gradually expressed between Sham, VSG and healthy WT  $\beta$ -cells. In particular,  $\beta$ -cells were ordered using diffusion pseudotime<sup>160</sup> (DPT) and grouped according to Sham, VSG and WT and the expression of gradually expressed genes was reconstructed along PAGA paths (see Methods). In fact, VSG-derived  $\beta$ -cells revealed a variety of markers that inched to approach WT-levels, including *Ins1*, *Mafa*, *Neurod1*, *Cck*, *Gast*, *Cltn*, *Aldh1a3*, *Gc*, and *Cd81* (Fig. 19h). In summary, our findings reveal that VSG is capable of rapidly inducing dynamic changes in the  $\beta$ -cell transcriptome that trend towards a healthy  $\beta$ -cell identity and restore  $\beta$ -cell function.



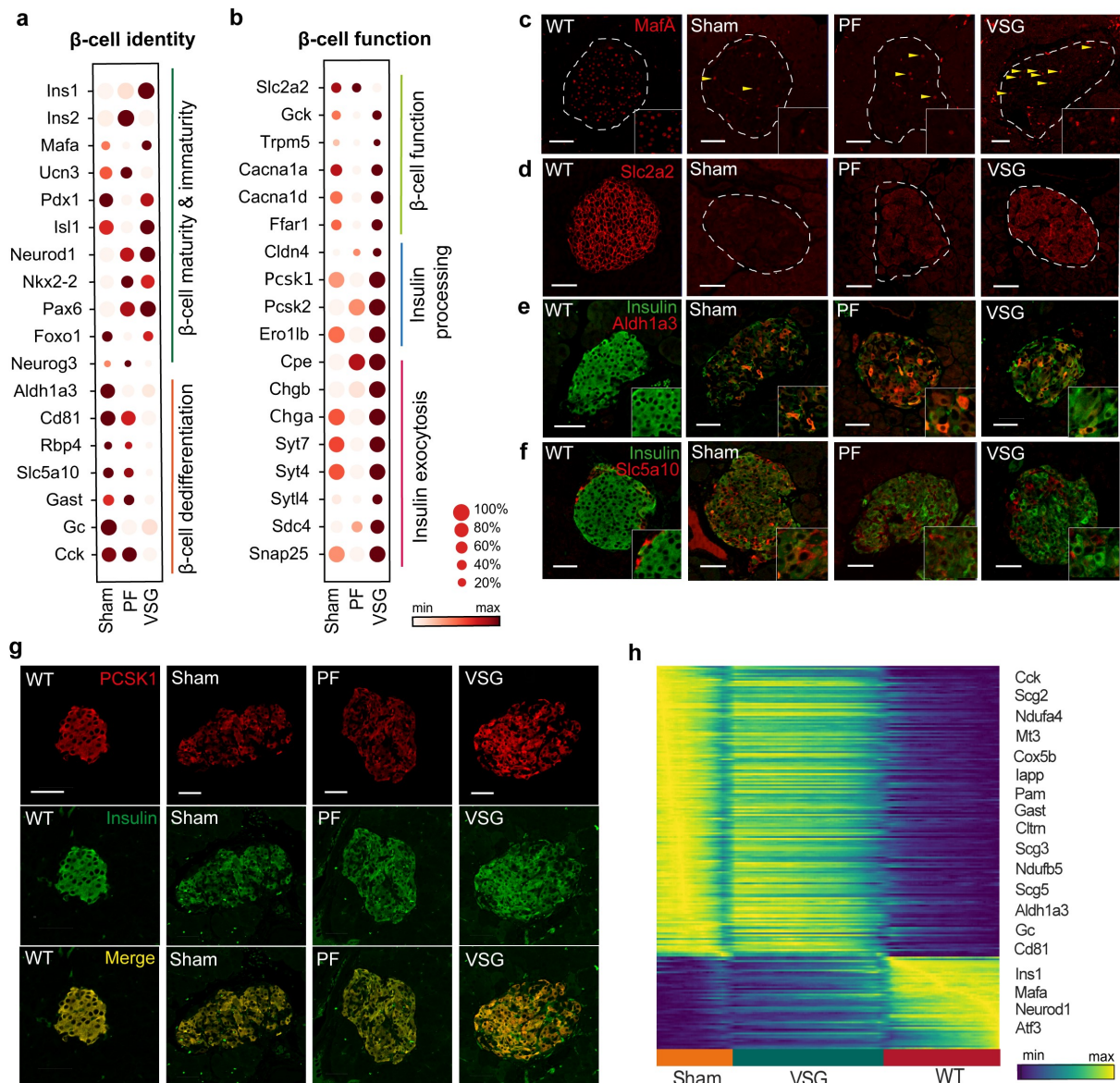


**Figure 19: VSG but not PF improves β-cell identity and function. (a,b)** Expression changes of genes involved in (a) β-cell identity and (b) function. Color intensity shows normalized mean expression; dot size indicates the percentage of cells in a cluster expressing that gene. Expression is scaled per gene. **(c-g)** Immunohistochemical analysis of MafA, Slc2a2, Insulin, Aldh1a3, Slc5a10 and Pcsk1 in β-cells of WT, Sham, PF and VSG mice at study end. Scale is 50 μm. **(h)** Heatmap showing gradually expressed genes across Sham, VSG and WT β-cells. Cells were ordered using diffusion pseudotime (DPT) with a root cell within dedifferentiated β-cells and grouped according to Sham, VSG and WT. Y-axis shows normalized gene expression scaled to the maximum observed level per gene. Analysis and interpretation of scRNA-seq data in collaboration with Subarna Palit (Institute of Computational Biology). Figures from Oppenländer et al., in revision at Molecular Metabolism.

Our previous results show that VSG restored  $\beta$ -cell function and remarkably enhanced fasting and postprandial insulin secretion. Concomitantly, pathway analyses of upregulated genes presented ontologies related to translation, protein processing, and the unfolded protein response (UPR) (Fig. 18e) that likely reflect processes paralleling the enhanced insulin secretion observed in VSG mice. Therefore, we reasoned there must be additional  $\beta$ -cell intrinsic compensatory mechanisms that help  $\beta$ -cells cope with increased endoplasmic reticulum stress (ER-stress) accompanying insulin secretion. To this end, we tested whether the two essential cellular adaptive response mechanisms to ER-stress, the UPR and ER-associated protein degradation (ERAD), are specifically being activated upon VSG. The UPR senses ER-stress, serves to restore cell homeostasis and, when exceeding manageable levels, contributes to loss of  $\beta$ -cell mass in T1D and T2D<sup>161,162</sup>. Here, we observed that VSG increased the overall score of the UPR in  $\beta$ -cells compared to WT, Sham and PF using canonical UPR genes (see Methods) (Fig. 20a). The major ER chaperone and upstream regulator of the UPR, Heat shock protein family A member 5 (*Hspa5*, also known as 78-kDa glucose-regulated protein, GRP78)<sup>163</sup>, was found to be explicitly activated upon VSG both, on mRNA- and protein-levels (Fig. 20b,c). Other members of the UPR, such as Wolframsyndrome 1 (*Wfs1*), Eukaryotic translation initiation factor 2 alpha kinase 3 (*Eif2ak3*, also known as Perk), and activating transcription factor 3 (*Atf3*), which play a role in  $\beta$ -cell homeostasis and survival<sup>164,165</sup>, and insulin processing<sup>166</sup> were found to be highly expressed upon VSG (Fig. 20b).

ERAD serves to resolve ER-stress by degrading misfolded proteins and is crucially involved in maintaining  $\beta$ -cell identity and function<sup>167,168</sup>. Here, we discovered that VSG increases the overall score of canonical ERAD genes (see Methods) in  $\beta$ -cells compared to controls (Fig. 20d). Especially, SEL1L adaptor subunit of ERAD E3 ubiquitin ligase (*Sel1l*), which forms the major ERAD complex together with Synoviolin 1 (*Syvn1* also known as Hrd1)<sup>169</sup> was found upregulated in  $\beta$ -cells of VSG mice on both, mRNA- and protein-level (Fig. 20e,f). Furthermore, VSG increased the expression of other ERAD genes, for instance DnaJ Heat Shock Protein Family (*Hsp40*) Member B2 (*Dnajb2*), *Dnajb4*, ER lipid raft associated 1 (*Erlin1*), Homocysteine-responsive endoplasmic reticulum-resident ubiquitin-like domain member 1 protein (*Herpud1*), or Osteosarcoma amplified 9 (*Os9*) in  $\beta$ -cells (Fig. 20e). Collectively, our results reveal enhanced adaptive-response mechanisms to ER-stress that likely parallel the extreme insulin secretion upon VSG and imply a VSG-specific supportive role of ERAD during ER-stress in  $\beta$ -cells.

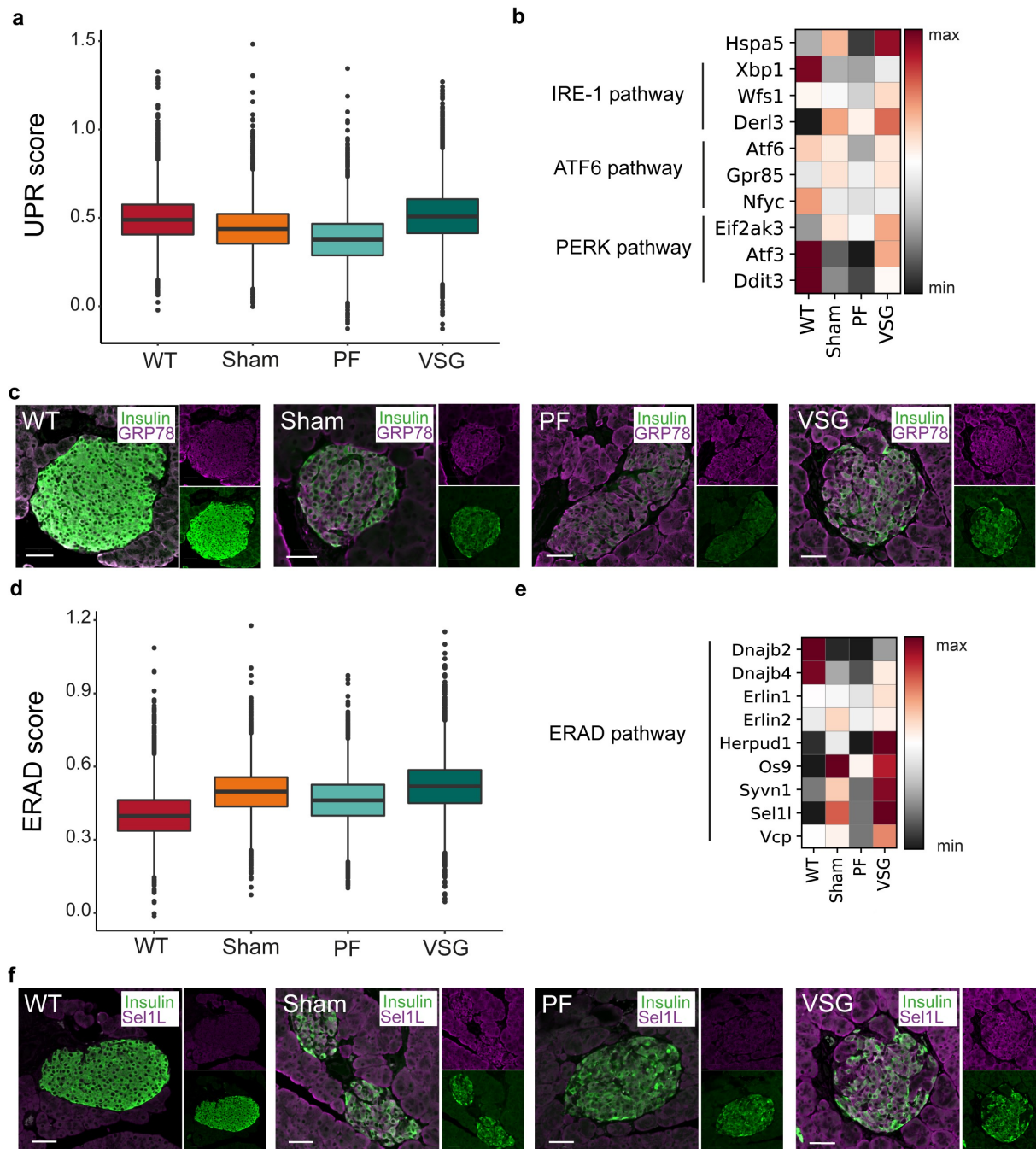


**Figure 20: VSG enhances the UPR and ERAD to counteract ER-stress in  $\beta$ -cells.** (a) UPR scores per group, calculated using canonical UPR markers. Box plots show median (WT=0.489, Sham=0.437, PF=0.376, VSG=0.508), quartile and whisker values. VSG revealed increased UPR score compared to WT ( $p<0.0001$ ), Sham ( $p<0.0001$ ), and PF ( $p<0.0001$ ) using Welch-Test (one way) with Bonferroni correction. (b) Expression levels of selected genes involved in the three branches of the UPR. Color gradient indicates mean z-score scaled gene expression. (c) Immunohistochemical analysis of GRP78 (Hspa5 gene) in  $\beta$ -cells of WT, Sham, PF and VSG mice at study end. Scale is 50  $\mu$ m. (d) ERAD scores per group, calculated using canonical ERAD genes. Box plots show median (WT=0.398, Sham=0.497, PF=0.461, VSG=0.519), quartile and whisker values. VSG revealed a higher ERAD score compared to WT ( $p<0.0001$ ), Sham ( $p<0.0001$ ), PF ( $p<0.0001$ ) using Welch-Test (one way) with Bonferroni correction. (e)

Expression levels of selected genes involved in ERAD. Color gradient indicates mean z-score scaled gene expression. **(f)** Immunohistochemical analysis of Sel1L in  $\beta$ -cells of WT, Sham, PF and VSG mice at study end. Scale is 50  $\mu$ m. Analysis and interpretation of scRNA-seq data in collaboration with Subarna Palit (Institute of Computational Biology). Figures from Oppenländer et al., in revision at Molecular Metabolism.

### 3.3.5 Mechanisms of $\beta$ -Cell Regeneration upon VSG

The opportunity of scRNA-seq to resolve the transcriptional profile of large amounts of single cells has greatly advanced the understanding of  $\beta$ -cell heterogeneity. While specific  $\beta$ -cell identities have well been described in health<sup>68,170–172</sup>, human diabetes<sup>173,174</sup> and some diabetes mouse models<sup>68,175</sup>, such as STZ-induced diabetes, a single-cell based transcriptional characterization of  $\beta$ -cells derived from the *db/db* diabetes mouse model has not been dealt with so far. Here, we resolved distinct  $\beta$ -cell subclusters in WT and *db/db* mice originating from Sham, PF and VSG mice and identified 4 different populations: mature, immature, dedifferentiated, and extreme  $\beta$ -cells (Fig. 21a,b). Mature  $\beta$ -cells irrespective of group presented high expression levels of  $\beta$ -cell maturation markers (*Mafa*, *Pdx1*, *Neurod1*, *Nkx6-1*) and functionality markers (*Ins1*, Forkhead box protein O1 (*Foxo1*), *Trpm5*) (Fig. 21c,d). Immature  $\beta$ -cells have only rarely been described in literature so far and have been defined in scRNA-seq datasets based on low expression levels of the maturity marker *Mafa* and high expression of *Cltn*, *Cd81*, and *Gpx3*<sup>68,72</sup>. In our datasets, only the WT mice presented a clearly distinguishable immature subset (2% of all  $\beta$ -cells), while there was no such immature cluster identifiable in *db/db*-derived  $\beta$ -cells. A fraction of  $\beta$ -cells originating from *db/db* mice displayed characteristic features of dedifferentiation while being absent in WT mice (Fig. 21c,d). Recently, another specific population termed as extreme  $\beta$ -cells has been discovered<sup>176</sup>. Extreme  $\beta$ -cells display explicitly high expression profiles of *Ins2* and crucial  $\beta$ -cell function genes (e.g. *Pcsk1*, *Chga*, *Abcc8*, *Kcnj11*) while presenting normal to low levels of mature insulin<sup>176,177</sup>. Thus, extreme  $\beta$ -cells have been suggested a specialized role in constant basal insulin secretion instead of regulated postprandial insulin secretory functions. Here, extreme  $\beta$ -cells were identified in both, WT and *db/db* mice, based on their reported high expression of genes such as *Ins2*, *Pcsk1*, *Pcsk2*, *Chga*, *Chgb*, *Abcc8*, and *Kcnj11* (Fig. 21c,d). Whether VSG differently affects the transcriptional profile and composition of mature, dedifferentiated, and extreme  $\beta$ -cells represent valuable questions that will be addressed in the following.

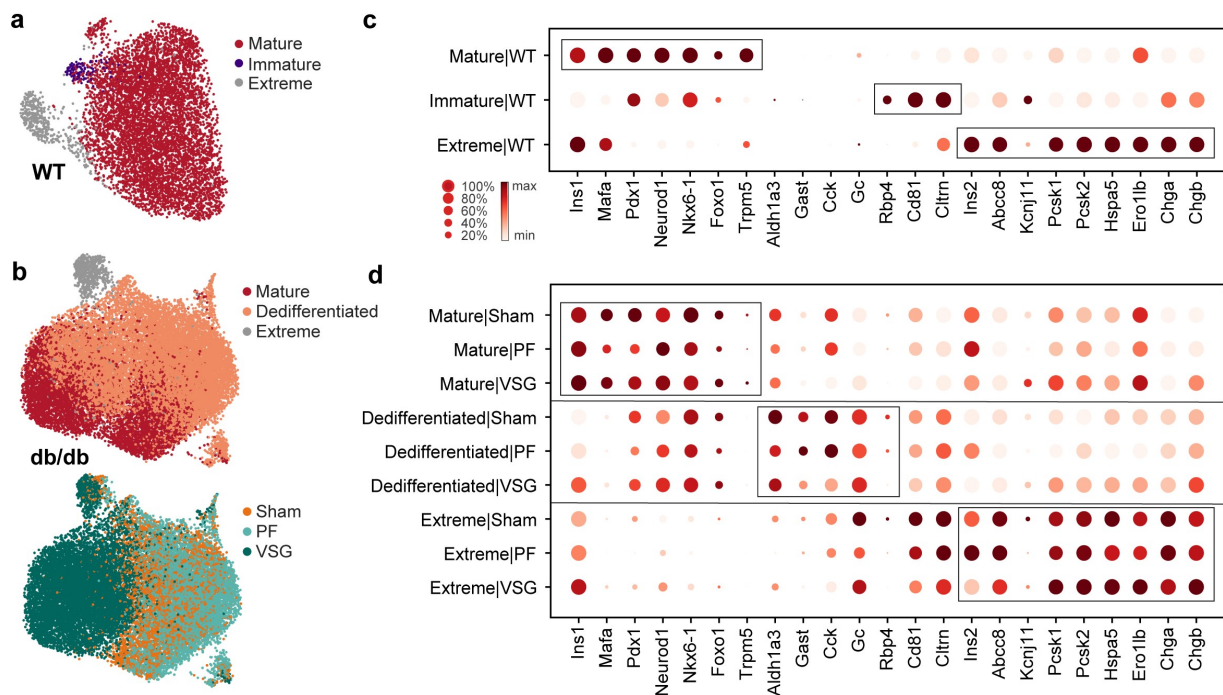


**Figure 21: *db/db* mice present heterogeneous  $\beta$ -cell states.** (a,b) Refined clustering of (a) 7183  $\beta$ -cells from WT and (b) 21,047  $\beta$ -cells from *db/db* (VSG+PF+Sham) identified four main  $\beta$ -cell subpopulations (mature, immature, dedifferentiated, extreme  $\beta$ -cells). (c,d) Expression changes of characteristic genes of  $\beta$ -cell maturity, immaturity, dedifferentiation, extreme  $\beta$ -cells in (c) WT  $\beta$ -cell subclusters and (d) *db/db* (VSG+PF+Sham)  $\beta$ -cell subclusters. Color intensity shows normalized mean expression in a cell cluster; dot size indicates the percentage of cells expressing that gene. Expression is scaled per gene. Analysis and interpretation of scRNA-seq data in collaboration with Subarna Palit (Institute of Computational Biology). Figures from Oppenländer et al., in revision at Molecular Metabolism.

We next investigated whether VSG distinctly affects the transcriptome of mature and dedifferentiated  $\beta$ -cells. To this end, we performed differential gene analyses within mature and dedifferentiated  $\beta$ -cells. Interestingly, we found that VSG increased  $\beta$ -cell identity and function genes in both, mature (*Pcsk1*, *Pcsk2*, *Cpe*, *Chgb*) and dedifferentiated  $\beta$ -cells (*Ins1*, *Neurod1*, *Cpe*, *Pcsk1*, *Pcsk2*, Adrenoreceptor alpha A69 (*Adra2a*), Claudin 470 (*Cldn4*), *Chgb*), compared to Sham controls (Fig. 22a,b). Furthermore, dedifferentiated  $\beta$ -cells from VSG groups revealed reduced expression levels of dedifferentiation markers, such as *Aldh1a3*, *Gast*, *Cck*, and *Rbp4* (Fig. 22a,b). Collectively, this data shows that VSG impacts mature and dedifferentiated  $\beta$ -cells by boosting the function of mature  $\beta$ -cells and concomitantly ameliorating the transcriptional profile of dedifferentiated  $\beta$ -cells.

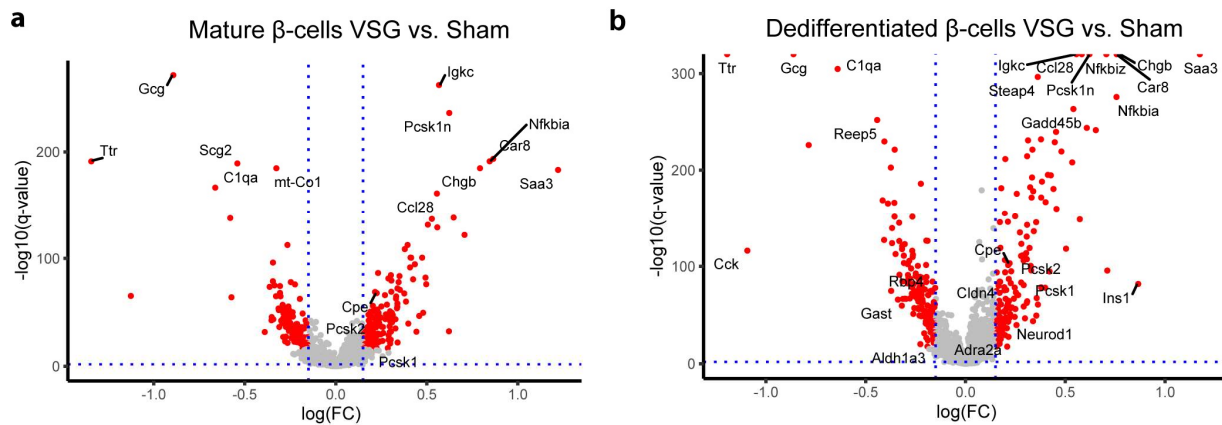


**Figure 22: VSG improves transcriptional signature of mature and dedifferentiated  $\beta$ -cells. (a,b)** Volcano plots showing differentially expressed genes in (a) mature  $\beta$ -cells and (b) dedifferentiated  $\beta$ -cells in VSG vs. Sham using a threshold of estimated  $\log FC > 0.15$ ,  $B > 30$ ,  $p(\text{adj}) < 0.01$ . Analysis and interpretation of scRNA-seq data in collaboration with Subarna Palit (Institute of Computational Biology). Figures from Oppenländer et al., in revision at Molecular Metabolism.

Our previous results showed that *db/db* mice display an overt diabetes phenotype involving  $\beta$ -cell dedifferentiation and that VSG is able to remarkably enhance  $\beta$ -cell function in these mice. Furthermore, we demonstrated that VSG explicitly upregulates genes associated with  $\beta$ -cell identity, insulin synthesis, and secretion paralleling the increased insulin secretion observed in vivo. Thus, we next reasoned whether VSG reverts dysfunctional  $\beta$ -cells to a functional state through mechanisms of redifferentiation. To this end, we assessed the percentage composition of  $\beta$ -cell subclusters per group, and performed RNA-velocity, a computational analysis predicting cell dynamics. In particular, Sham and PF groups presented reduced fractions of mature  $\beta$ -cells (23% and 19%) compared to WT (91%), while VSG increased the proportions of mature  $\beta$ -cells (37%) (Fig. 23a). The great majority of *db/db*-derived  $\beta$ -cells revealed features of dedifferentiation. Sham and PF presented the highest portion (74% and 80%) and VSG displayed lower fractions (57%). Thus, we suggest that VSG induces redifferentiation, a shift from dedifferentiated to mature  $\beta$ -cell states. In order to further corroborate these findings, we performed an RNA-velocity analysis to predict transitions of mature and dedifferentiated  $\beta$ -cells in Sham groups and after VSG (Fig. 23b). In particular, we observed that  $\beta$ -cells of Sham mice transitioned from the mature to the dedifferentiated state, while  $\beta$ -cells of VSG mice were directed towards the mature state clearly indicating redifferentiation processes upon VSG (exemplary maturity (*Mafa*, *G6pc2*) and dedifferentiation markers (*Aldh1a3*, *Cck*) displayed in lower panel) (Fig. 23b). Additionally, we computed metrics with regard to velocity length and confidence to gain insights into the extent of cell transitions (velocity length) and confidence of the results. Dedifferentiated  $\beta$ -cells from VSG revealed a faster pace of transition and a higher RNA-velocity

confidence value compared to Sham, indicating more active transcriptional cell changes after VSG (Fig. 23c,d). Collectively, our results reveal that VSG promotes mechanisms of redifferentiation for  $\beta$ -cell recovery.

Besides the compositional changes in mature and dedifferentiated  $\beta$ -cells after VSG, we observed group-specific changes in extreme  $\beta$ -cells (Fig. 23a). Notably, early diabetic *db/db* mice (14 weeks) have recently been shown to display increased proportions of extreme  $\beta$ -cells and have thus been speculated to exert compensatory functions in counteracting hyperglycaemia in early diabetes<sup>176</sup>. In contrast, our data revealed lower levels of extreme  $\beta$ -cells in late stage diabetic Sham (3%) and PF (2%) groups (18-20 weeks) compared to WT (7%) suggesting that the extreme  $\beta$ -cell state might be favored in early compensatory stages of diabetes but may be compromised in late stages of the disease eventually contributing to T2D progression. Surprisingly, VSG increased the portions of extreme  $\beta$ -cells to WT-level (6%) (Fig. 23a). In order to confirm these findings, we performed an in-situ hybridization of the marker gene *Ins2* in islets of all groups. Extreme  $\beta$ -cells have been reported to reveal a strong apical cell polarization of *Ins2* mRNA<sup>176</sup>. Similar to the initial study on extreme  $\beta$ -cells<sup>176</sup>, we analyzed the polarization of *Ins2* per group by calculating the skewness per cell and confirmed a stronger *Ins2* mRNA polarization in  $\beta$ -cells of VSG suggestive of increased numbers of extreme  $\beta$ -cells (Fig. 23e). Collectively, these findings indicate that the extreme  $\beta$ -cell state can be recovered by VSG and might play a mechanistic role. The definite contribution of extreme  $\beta$ -cells in glucose regulation and in how far these play a role during the recovery of  $\beta$ -cell function after VSG remains to be investigated in mechanistic studies.

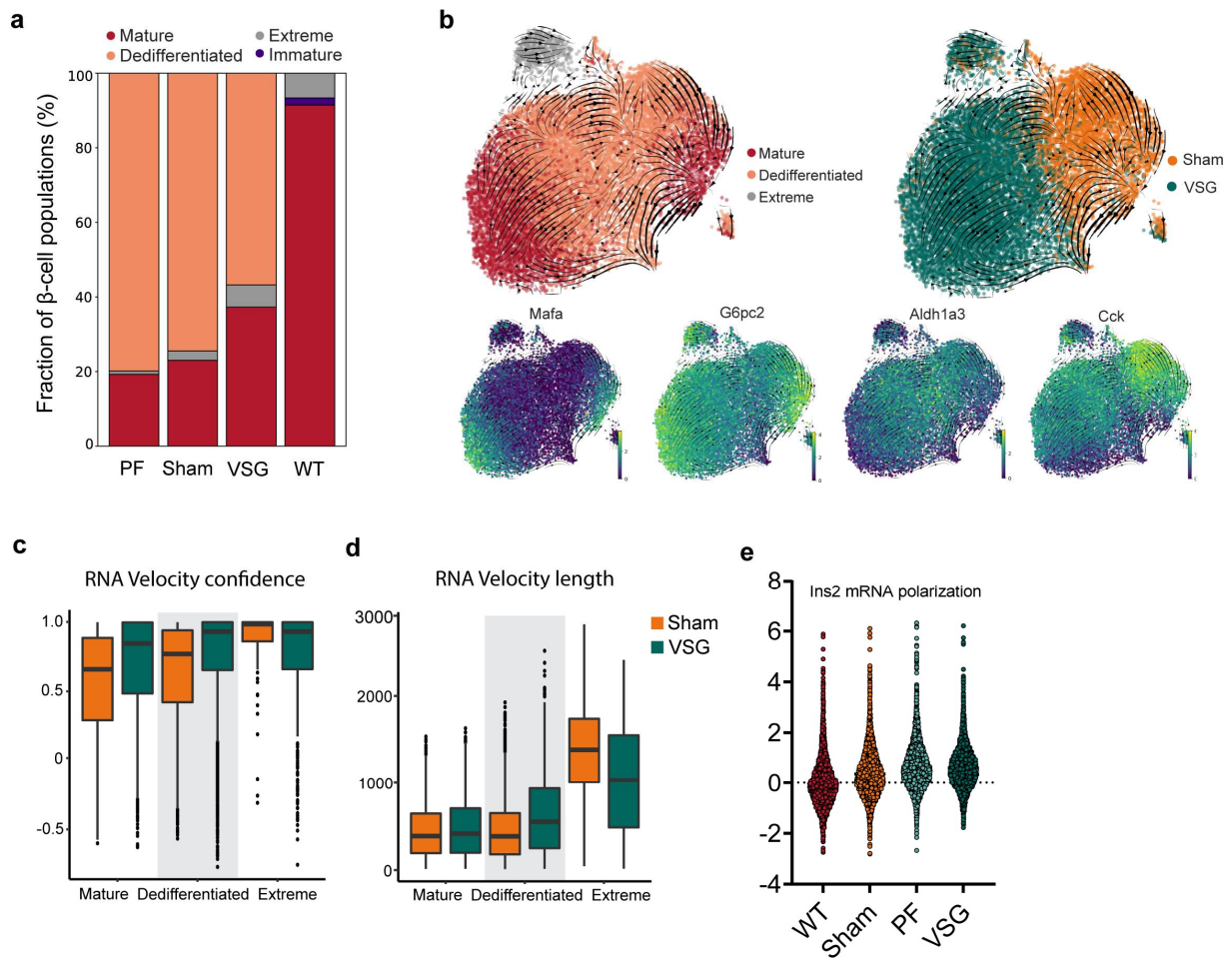


**Figure 23: VSG induces  $\beta$ -cell redifferentiation and shifts towards extreme  $\beta$ -cell states.** (a) Percentage of  $\beta$ -cell subclusters per group shows increase in mature and extreme  $\beta$ -cells after VSG. (b) Estimated cell-transitions (arrows) calculated by RNA-velocity in Sham and VSG groups shows dedifferentiation in Sham-derived  $\beta$ -cells and redifferentiation in VSG-derived  $\beta$ -cells (top panel). Umap plots show expression of characteristic genes to distinguish between mature (Mafa, G6pc2) and dedifferentiated  $\beta$ -cells (Aldh1a3, Cck). (c) Velocity confidence calculated per group and subclusters. Box plots show median (Sham(dediff)=0.768, VSG(dediff)=0.931), quartile and whisker values of velocity confidence. VSG revealed a significantly higher velocity confidence compared to Sham ( $p < 0.0001$ , Welch-Test (One-Way) with Bonferroni post-hoc test). (d) Velocity length as a measure of speed of differentiation calculated per group and subcluster. Box plots show median (Sham(dediff)=385.41, VSG(dediff)=552.51), quartile and whisker values of velocity length. VSG revealed a significantly higher velocity length compared to Sham ( $p < 0.0001$ , Welch-Test (One-Way) with Bonferroni post-hoc test). (e) Cellular Ins2 mRNA polarization visualized by cellular Ins2 intensity skewness obtained from in situ hybridization. In situ quantification of extreme  $\beta$ -cells performed in collaboration with Dr. Annette Feuchtinger (Institute of Analytical Pathology). Analysis and interpretation of scRNA-seq data in collaboration with Subarna Palit (Institute of Computational Biology). Figures from Oppenländer et al., in revision at Molecular Metabolism.

In order to better understand the function of extreme  $\beta$ -cells in health and disease, we compared uniquely upregulated genes of extreme  $\beta$ -cells versus non-extreme  $\beta$ -cells (mature, dedifferentiated, immature subclusters) of WT mice to those of *db/db* mice. In fact, the great majority of genes specific



to extreme  $\beta$ -cells in WT were also upregulated in *db/db*-derived extreme  $\beta$ -cells (97%) (Fig. 24a). Notably, *db/db*-derived extreme  $\beta$ -cells revealed a higher number of upregulated genes than those of WT potentially owing to a more heterogeneous pool of non-extreme  $\beta$ -cells in the *db/db* group (Fig. 24a). With the purpose of better understanding the general function of extreme  $\beta$ -cells, we enriched the unique, upregulated genes of extreme  $\beta$ -cells that were common in WT and *db/db* groups for gene ontologies and biological pathways. In line with the previous two studies on extreme  $\beta$ -cells, we found terms related to protein processing and secretion upregulated in extreme  $\beta$ -cells. These findings confirm previous studies claiming a functional role of constant insulin secretion<sup>176,177</sup>. We next asked what distinguishes healthy WT extreme  $\beta$ -cells from those of diabetic *db/db* mice. To this end, we explored 425 uniquely upregulated genes originating from the *db/db* group and discovered novel genes specific to extreme  $\beta$ -cells (Fig. 24c). Those comprised genes coding for insulin processing, secretory, and ER-located proteins, as well as long non-coding RNA (lncRNA) Mouse maternal expressed gene 3 (*Meg3*) known to regulate *Mafa* expression and insulin synthesis<sup>178</sup> and lncRNA Small nucleolar host gene 11 (*Snhg11*), a gene upregulated in reprogrammed pancreatic duct cells<sup>179</sup>. Further, extreme  $\beta$ -cells downregulated the expression of antioxidant genes Metallothionein 1 (*Mt1*) and *Gpx1* (Fig. 24c). Overall, our findings support a role of extreme  $\beta$ -cells in basal insulin secretion by revealing a remarkable enrichment of genes related to insulin biosynthesis and secretion and provide novel genes that could be the basis for better defining extreme  $\beta$ -cells and for targeting these in diabetes.

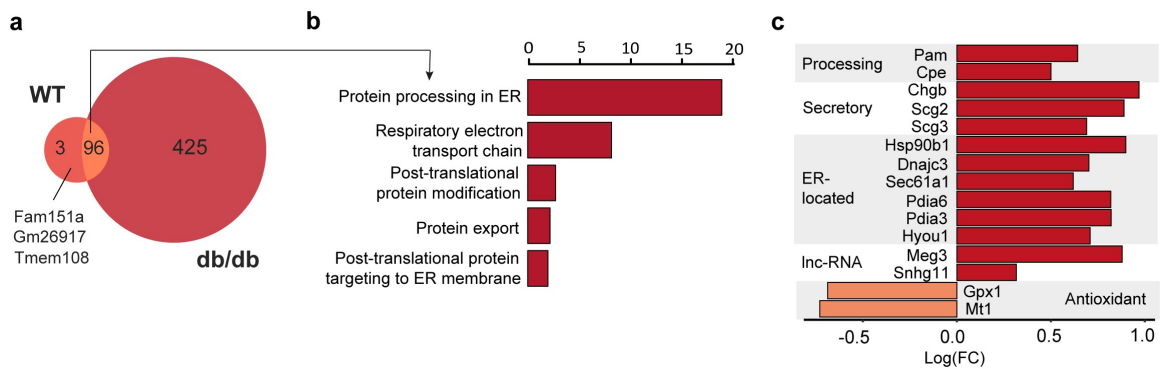


**Figure 24: Extreme  $\beta$ -cells show a characteristic profile marked by high expression of insulin machinery genes.** (a) Venn diagram showing the overlap of enriched genes of WT- and *db/db*-derived (Sham, PF, VSG) extreme  $\beta$ -cells. Limma method was used to find differentially expressed genes at threshold of absolute estimated  $\log(\text{FC}) > 0.15$  and  $B > 100$ . (b) GO and KEGG pathway analysis of commonly upregulated genes of WT and *db/db* extreme  $\beta$ -cells. X-axis indicates  $-\log_{10}(\text{adjusted p-value})$ . (c) Bar plot showing estimated  $\log(\text{FC})$  of selected significantly regulated genes in *db/db*-derived (Sham, PF, VSG) extreme  $\beta$ -cells. Analysis and interpretation of scRNA-seq data in collaboration with Subarna Palit (Institute of Computational Biology). Figures from Oppenländer et al., in revision at Molecular Metabolism.

Our previous results show that VSG induces various functional adaptive mechanisms to enhance  $\beta$ -cell function. However, besides these functional improvements, increased  $\beta$ -cell mass might represent an additional source of increased insulin levels upon VSG. To test this hypothesis, we quantitatively assessed  $\beta$ -cell mass. Here, VSG was able to rapidly increase  $\beta$ -cell area within only two weeks of intervention compared to controls (Fig. 25a). We then reasoned this increase to not only originate from active redifferentiation processes upon VSG, but additionally from proliferative mechanisms. In fact, VSG increased the rate of  $\beta$ -cell proliferation compared to WT and modestly, albeit not statistically significant, when compared to Sham and PF controls (Fig. 25b,c). Here, it is important to note the possibility that the major  $\beta$ -cell replication might have occurred already during the first days after VSG, as we captured proliferating cells solely during the last 72h before sacrifice. In support of our histological quantification, we observed similar effects in our scRNA-seq dataset. VSG showed the highest fraction of cycling  $\beta$ -cells expressing key cell-cycle markers, such as *Mki67*, *Top2a*, and *Cdk1* (54/9252, 0.6%), compared with Sham (14/4491, 0.31%) and PF controls (17/7389, 0.23%) (Fig. 25d). Moreover, VSG-derived  $\beta$ -cells over-expressed genes relating to cell-cycle GO terms such as positive regulation of cell cycle or negative regulation of apoptosis (Fig. 25e). Specifically, non-cycling  $\beta$ -cells of VSG showed an upregulation of genes promoting proliferation. In particular, VSG significantly increased the expression of Cyclin D2 (*Ccnd2*), the key cell-cycle progression gene in adult  $\beta$ -cells<sup>180</sup>. Furthermore, VSG upregulated the expression of SRY-box transcription factor 4 (*Sox4*) and concomitantly downregulated Cyclin dependent kinase inhibitor 1A (*Cdkn1a*) in non-cycling  $\beta$ -cells, which has been reported to allow adult  $\beta$ -cell replication<sup>181</sup> (Fig. 25f). Collectively, these findings indicate that VSG triggers a proliferation-competent  $\beta$ -cell state. We then asked whether VSG triggers proliferation in mature or dedifferentiated  $\beta$ -cells. In fact, cycling  $\beta$ -cells from VSG mainly displayed a gene profile of dedifferentiation marked by high expression of *Aldh1a3*, *Cck*, *Gc*, and low expression of  $\beta$ -cell maturity markers, *Ins1*, *Mafa*, and *Pdx1* (Fig. 25g). These findings show that dedifferentiated  $\beta$ -cells are more likely to enter cell-cycle. In summary, our data reveals combined mechanisms of  $\beta$ -cell redifferentiation and enhanced proliferation in recovering functional  $\beta$ -cell mass after VSG.

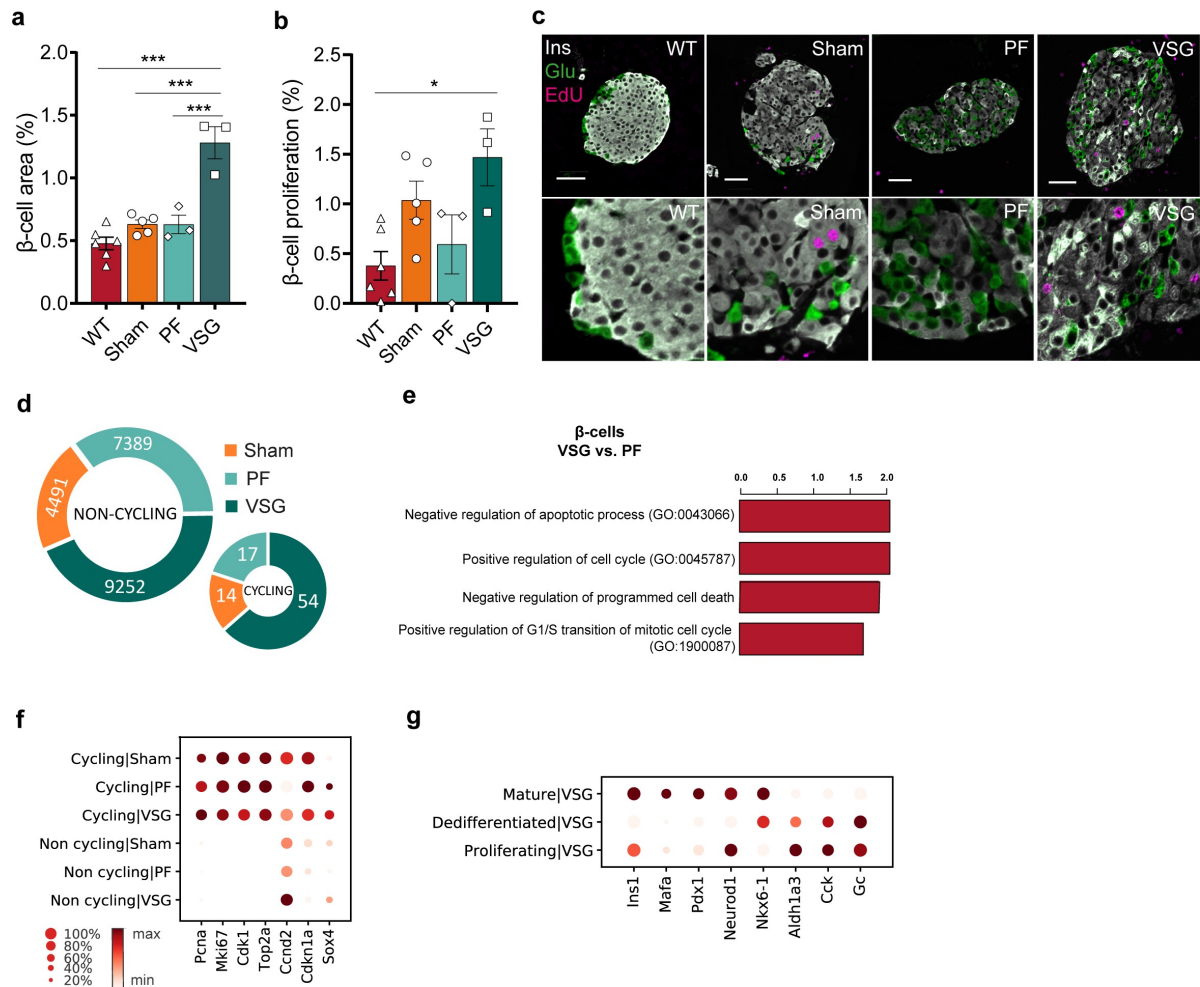


**Figure 25: VSG expands β-cell mass.** (a) Postsurgical percentage β-cell area. VSG increased β-cell area compared to controls ( $n_{WT}=6$ ,  $n_{Sham}=5$ ,  $n_{PF}=3$ ,  $n_{VSG}=3$ , One-way ANOVA with Bonferroni post hoc test; VSG vs. WT,  $p<0.0001$ ; VSG vs. Sham,  $p<0.0001$ ; VSG vs. PF,  $p=0.0003$ ). (b) Postsurgical percentage β-cell proliferation ( $n_{WT}=6$ ,  $n_{Sham}=5$ ,  $n_{PF}=3$ ,  $n_{VSG}=3$ ). VSG enhanced β-cell proliferation compared to WT (One-way ANOVA with Bonferroni post hoc test; VSG vs. WT,  $p=0.019$ ). (c) Representative confocal microscopy images of proliferating β-cells (EdU+ cells) per group. Scale is 50 μm. (d) Fractions of cycling and non-cycling β-cells from the scRNA-seq dataset resolved per group (VSG-54/9252, PF-17/7389, Sham-14/4491). (e) VSG-specific proliferation-related GO terms and KEGG pathways obtained from upregulated genes in β-cells of VSG vs. PF with threshold at  $\log_{2}FC>0.15$ ,  $B>150$ ,  $\text{adj}(p)<0.01$ . X-axis indicates  $-\log_{10}(\text{adjusted } p\text{-value})$ . (f) Dotplot showing expression of cell cycle-related genes in cycling vs. non-cycling cells per group. Expression is scaled per gene. (g) Dotplot comparing the identity of proliferating *db/db* β-cells (Sham, PF, VSG) with dedifferentiated and mature β-cells of *db/db* mice. Statistical testing was performed using One-way-ANOVA and Bonferroni correction. Data is presented as mean  $\pm$  s.e.m. Morphological analysis performed in collaboration with Dr. Annette Feuchtinger (Institute of Analytical Pathology). Analysis and interpretation of scRNA-seq data in collaboration with Subarna Palit (Institute of Computational Biology). Figures from Oppenländer et al., in revision at Molecular Metabolism.

In order to identify genes that are uniquely modulated by VSG and that could drive the  $\beta$ -cell specific gluco-regulatory effects of VSG, we screened 418 upregulated genes in VSG (Fig. 26a). Surprisingly, the top upregulated genes by VSG involved genes associated with immune function and pregnancy (Fig. 26b-d). Pregnancy involves profound adaptive functional and proliferative mechanisms in  $\beta$ -cells<sup>182</sup>. Here, we found key genes that are induced in islets during pregnancy, such as *Sftpd*, coding for Surfactant-associated protein D (*SP-D*), Carbonic anhydrase 8 (*Car8*), *Tnfrsf11b*, coding for Osteoprotegerin (OPG), and *Chgb* (Fig. 26d). OPG (*Tnfrsf11b*) represents a decoy receptor of TNFR superfamily known to be induced by lactogens. OPG has been reported to act as a  $\beta$ -cell mitogen by preventing the interaction of Receptor activator of NFkB Ligand (RANKL) and RANK. Further, OPG robustly promotes  $\beta$ -cell proliferation under different conditions, for instance during pregnancy, in young, aged, and diabetic STZ-treated mice<sup>183,184</sup>. Here, we introduce OPG for the first time as a possible driver of  $\beta$ -cell replication in the context of VSG. In order to obtain a full picture of genes upregulated by VSG that are associated with pregnancy, we compared genes from our  $\beta$ -cell dataset with those derived from islets of pregnant mice<sup>185-187</sup>. We identified 32 common genes induced by VSG and pregnancy involving crucial pregnancy-associated genes (*Sftpd*, *Tnfrsf11b*, *Car8*, *Socs2*), immune-modulatory genes (*Il13ra1*, *Ifngr2*), and  $\beta$ -cell identity and function genes (*Mafa*, *Pdx1*, *Ins1*, *Chgb*) (Fig. 26e). These may reflect the compensatory functional and proliferative mechanisms during pregnancy and may be induced by VSG to exert similar adaptive functions in  $\beta$ -cells to enhance insulin secretion. Mechanistic studies will be required to address the relevance of pregnancy-associated factors upon VSG and their potential as novel therapeutic targets for diabetes therapy.

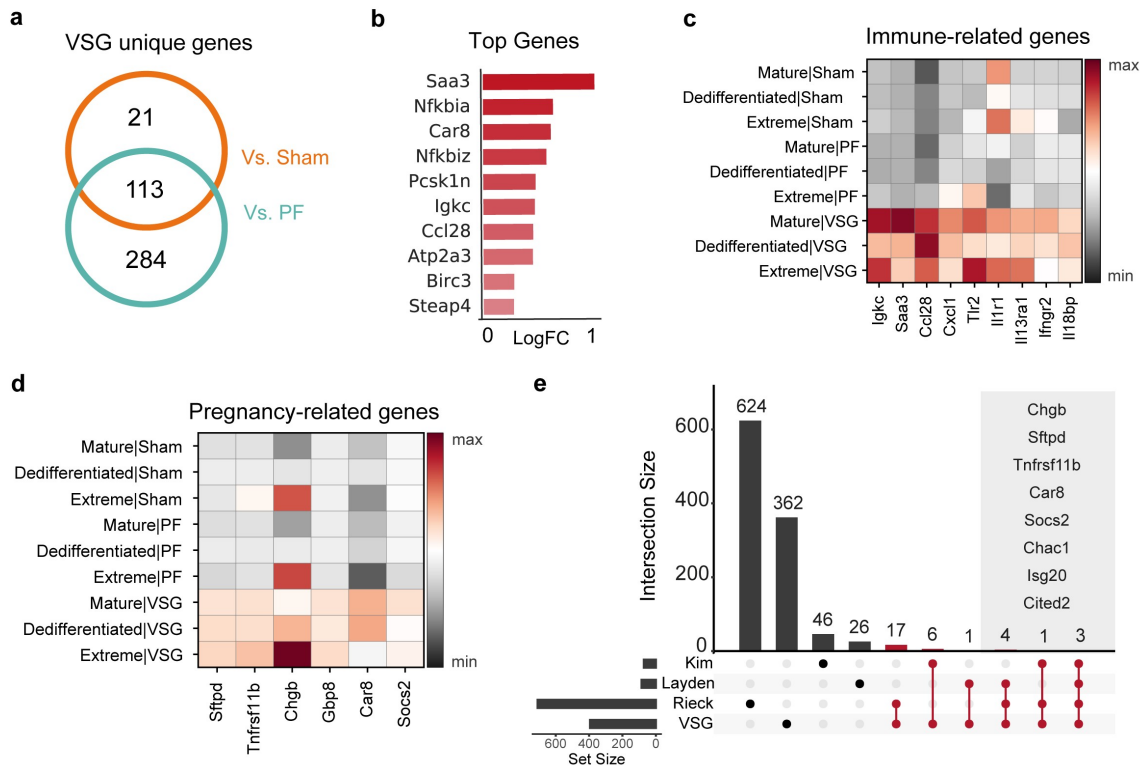


**Figure 26: The  $\beta$ -cell transcriptome reveals unique targets of VSG.** (a) Venn diagram showing uniquely upregulated genes in  $\beta$ -cells of VSG vs. control groups. (b) Top 10 unique VSG genes (plotted for VSG vs. Sham, estimated  $\log(\text{FC}) > 0.25$ ,  $B > 150$ ). (c,d) Expression of genes related to (c) immune-response and (d) pregnancy in  $\beta$ -cells resolved per group and subcluster. Color gradient indicates mean z-score scaled gene expression. (e) Overlap between VSG-specific genes derived from our study and literature curated genes that are differentially expressed in islets during pregnancy (Layden et al. 2010, Rieck et al. 2009, Kim et al. 2010). Upset plot is used to visualize intersection of sets. Horizontal bars on the left indicate total number of genes per set. Vertical bars indicate the intersection size between datasets. The bars highlighted in red refer to the genes uniquely shared among VSG and the participating sets. Limma method was used to extract differentially expressed genes for VSG vs. Sham and VSG vs. PF at absolute estimated  $\log(\text{FC}) > 0.15$  and  $B > 150$ . Venn diagrams aided in identifying the VSG regulated genes. Analysis and interpretation of scRNA-seq data in collaboration with Subarna Palit (Institute of Computational Biology). Figures from Oppenländer et al., in revision at Molecular Metabolism.

In conclusion, we show that VSG is a powerful surgical intervention capable of rapidly reversing extreme conditions of diabetes in *db/db* mice. We believe that the effects of VSG are not only of systemic origin but involve  $\beta$ -cell intrinsic mechanisms as well. Precisely, our findings demonstrate that VSG triggers additive mechanisms involving functional improvements and the recovery of  $\beta$ -cell mass through redifferentiation and replication. Further, our data suggests immune- and pregnancy-associated factors to mediate these local effects in  $\beta$ -cells and, thus, suggests functional verification of these novel, potential drug targets in future studies.

## 4. Discussion

This thesis aimed at advancing the mechanistic understanding of the remarkable gluco-regulatory effects induced by VSG to fuel the progress of diabetes therapies. As a basis of this, we characterized different DIO and genetic obesity-linked diabetes mouse models with special regard to the severity of the T2D phenotype (**Chapter 4.1**). Further, we explored mechanisms underlying diabetes remission by VSG in conditions of pre-diabetes with the goal to unravel morphological adaptations that may counteract early diabetes progression (**Chapter 4.2**), as well as in stages of prolonged, severe diabetes promising the discovery of novel paths involved in the restoration of dysfunctional  $\beta$ -cells (**Chapter 4.3**).

### 4.1 Modeling Pre-Diabetes and Diabetes in Mice

Although interventions in both diabetes and obesity at early and late stages improve long-term prognoses, classic pharmacological and life-style related therapies are not sufficiently effective stopping  $\beta$ -cell failure, potent surgical approaches including VSG are limited especially due to their invasiveness. Hence, the discovery of novel pharmacological entry points is of utmost importance for the progress in diabetes therapy. To this end, mouse models are popular means to study disease pathogenic mechanisms, and are required for testing targets and novel compounds before entering clinical phases. It is well known that different diet-, chemical-induced or monogenic diabetes and obesity models present distinct patho-physiological phenotypes. In addition, these phenotypes can vary depending on the mouse strain, age, gender, as well as laboratory conditions<sup>138,139,188</sup>. Therefore, we characterized the physiological phenotypes of HFD-induced obesity-diabetes models in B6J and B6N mouse strains and compared these to the genetic diabetes *db/db* mouse model. Principally, *db/db* mice display defects in Leptin-receptor signaling caused by a spontaneous mutation in the *Lepr* gene<sup>143</sup>. This causes hyperphagia due to defective satiety signaling by Leptin, which promotes the development of extreme diabetes, obesity, and co-morbidities with age and premature death<sup>144,145</sup>. Hence, both DIO and *db/db* models are able to mimic chronic over-nutrition and recapitulate large parts of obesity-linked diabetes in human. While previous studies reported robust diabetic phenotypes for the *db/db* model<sup>144,145</sup>, studies on DIO models generated conflicting results and revealed variable diabetes outcomes ranging from modest pre-diabetes to severe diabetes<sup>138,141,189-193</sup>. Similarly, our physiological analyses showed that all models including HFD-fed

B6J- and B6N mice as well as *db/db* mice developed robust obesity, while the severity of the diabetes phenotypes between strains varied significantly. B6J and B6N mice in the DIO model developed different pre-diabetic characteristics. B6J mice presented modest postprandial hyperglycaemia and hyperinsulinaemia on a HFD, whereas B6N mice responded by remarkably enhanced insulin secretion with no effects on glycaemia. These results were similar to a report showing that chronic HFD-feeding in B6N mice resulted in progressive and strong elevations of insulin levels without deteriorating hyperglycaemia but maintaining steady, mildly increased glucose levels<sup>192</sup>. Consequently, we propose that B6J DIO models are more suitable to induce pre-diabetes, while B6N mice represent the better model to study the  $\beta$ -cell insulin-compensatory mechanisms in diabetes as these counteract overnutrition by extreme hyperinsulinaemia. By contrast, the *db/db* model displayed late-stage overt diabetes phenotypes at the age of 16-18 weeks involving extreme hyperglycaemia. Collectively, our results indicate that DIO and *db/db* mouse models resemble different stages and characteristics of human diabetes, therefore are suitable for a range of different preclinical research questions tackling early and late stage diabetes interventions.

## **4.2 Counteracting Pre-Diabetes through VSG intervention**

At present, VSG is the most commonly performed bariatric surgical procedure<sup>96</sup> and the only treatment promising stable body weight reduction and diabetes remission<sup>94</sup>. Due to its invasiveness VSG is solely clinically-indicated for patients displaying severe obesity and diabetes. Nonetheless, VSG may as well be an effective preventative treatment for developing diabetes as reported in two preclinical studies<sup>148,194</sup>. In order to make the remarkable metabolic effects of VSG applicable to a broader spectrum of patients, the underlying mechanisms of VSG have been extensively explored during the past decade with the aim to generate pharmacotherapies mimicking bariatric surgery. Despite the effort, single targets could not explain the multitude of beneficial metabolic effects upon VSG but led to a basic understanding of VSG to induce a variety of systemic and tissue specific metabolic effects that act in concert to counteract diabetes and obesity. Further, we believe that VSG might have effects with distinct mechanisms in different stages of diabetes. Thus, we explored the effects of VSG in pre-diabetes in preventing the progression or reversing pre-diabetic and obese conditions.

### **4.2.1 Similar Physiological Outcomes of VSG and Calorie-Restriction in Obesity-Linked Pre-Diabetes**

A plethora of studies have proven the efficacy of VSG in normalizing body weight and glycaemia in HFD-induced (pre-)diabetes phenotypes in mice on a B6J background<sup>103,118,195-202</sup>. While the beneficial physiological effects of VSG certainly involve the contribution of lowered body weight, recent reports indicate additional effects that are independent of body weight. This was based on the observations that glucose regulation is normalized shortly after surgery prior to the major weight loss<sup>118,203-205</sup> and that VSG improved glycaemia in hyperphagic db/db mice without affecting body weight<sup>117</sup>. Whether acute post-surgical reduction in food intake plays a role in the early gluco-regulatory effects is not fully understood yet. A study in human reported similar early effects of very low-calorie diet and RYGB on insulin sensitivity and  $\beta$ -cell function<sup>115</sup>. Studies involving VSG and calorie-matched PF interventions in DIO mice provided slightly different results. In some studies VSG and PF yielded equal effects<sup>198,206</sup>, while two other reports showed that VSG was more efficient than PF in lowering body weight and glucose levels<sup>118,200</sup>. In our study, VSG and PF achieved equal improvements with respect to body weight and blood glycaemia in diet-induced obese, pre-diabetic B6J mice 4 weeks after intervention. Discrepancies between studies likely arise from differences in the baseline diabetes phenotype. In our study, pre-diabetes with only modest hyperglycaemia and



insulin dysregulation, a condition that might be easier to reverse. In addition to the shared effects of VSG and PF, many studies including ours consistently reported a VSG-specific augmentation in postprandial insulin secretion that was not present after PF<sup>118,200,206</sup>. This strongly suggests that VSG and PF are equally efficient in normalizing glycaemia and lowering body weight, whereas only VSG is able to significantly enhance  $\beta$ -cell function and thus indicates that VSG and PF involve different mechanisms. In fact, a recent study has shown islet intrinsic, persistent functional changes that are specific to VSG<sup>118</sup>, while calorie restriction might majorly involve peripheral mechanisms. Further, although VSG and calorie restriction partly result in similar metabolic outcomes, VSG shows more durable long-term benefits. Contrary to caloric deficits induced by food restriction which lead to relapses in eating behavior and body weight regain, the weight loss after VSG has been shown to involve central mechanisms that might explain one part of the superiority of VSG in its long-term success<sup>99,207</sup>.

So far, the effects of VSG have never been addressed in pre-diabetic models with extreme  $\beta$ -cell compensation. Such models would give the opportunity to assess interventional effects in very early pre-diabetic stages in which hyperglycaemia is not yet manifested, whereas  $\beta$ -cells are already tuned towards massive compensatory insulin secretion. Here, we present a DIO model involving B6N mice that show extreme compensatory insulin secretion and normal glycaemia upon 12 weeks of HFD-feeding. VSG and PF induced similar reductions in body weight, but VSG did not affect glycaemia. These findings seem plausible as B6N HFD-fed mice do not show hyperglycaemia. PF reduced postprandial glycaemia to levels below those of WT mice, an observation which could be explained by the fact that these have been starved for a longer time prior the MMTT because they were not fed ad libitum, but received restricted amounts of chow once a day. Surprisingly, albeit B6N HFD-fed mice displayed already extremely high insulin levels compared to all models tested in this study, VSG further increased the postprandial insulin response. Thus, our data indicates that VSG robustly enhances  $\beta$ -cell secretory function even above levels naturally occurring upon dietary challenges of long-term over-nutrition.

In summary, we show that VSG and calorie restriction are able to potently reverse early obesity-linked pre-diabetes, however, only VSG enhanced  $\beta$ -cell function. This effect might likely be governed by specific mechanisms of VSG that are superior to those of PF and might contribute to the more sustainable metabolic effects of VSG compared to calorie restriction. Understanding the driving mechanisms, systemically and in specific tissues that are unique to VSG in pre-diabetes will fuel the development of pharmacotherapies aiming at stopping and reversing pre-diabetes.

#### 4.2.2 Morphological Adaptations are Dispensable for VSG Outcomes in Obesity-Linked Pre-Diabetes

The intestinal epithelium and pancreatic islets are capable of adapting to metabolic challenges from chronic overnutrition to meet metabolic demand<sup>32,36,192,208</sup>. In particular, many studies reported hyperproliferation of the intestinal epithelium and an imbalance in intestinal lineages upon chronic HFD-feeding in mice<sup>29,31,34,35</sup>. The hyperproliferation was mainly observed in absorptive enterocytes and serves to increase the nutrient uptake and thus favor energy surplus<sup>31</sup>, while the misbalance in EEC lineages and intestinal hormones are believed to fuel obesity-linked diabetes<sup>31,40</sup>. By its direct influence via the altered transit of food, we believe VSG has the potential to alter intestinal morphology to counteract these dietary-driven mal-adaptation and alleviate conditions of obesity and diabetes. So far, reports on intestinal adaptations after VSG in rodent DIO models are rare and show contradictory results. While these studies consistently showed a higher density in GLP-1 expressing EECs after VSG<sup>122,123</sup>, findings with respect to small intestinal epithelial size were opposing, with an increase in villus size 2 weeks after surgery<sup>122</sup> or no change in villus size assessed 8 weeks after VSG<sup>123</sup>. The results from our study in HFD-fed B6J mice confirmed the expansion of the small intestine upon chronic HFD, however, did not uncover changes in small intestinal morphology, proliferation or the frequency of GLP-1 expressing EECs upon VSG intervention. Thus, in our model, the metabolic improvements observed after VSG did not rely on adaptive morphological mechanisms of the small intestine. Further, although we did not observe increases in the frequency of GLP-1 expressing EECs, the potentiated postprandial GLP-1 responses induced by VSG can well be explained by an enhanced stimulation of distal EECs as previously reported<sup>120</sup>. Due to the pronounced effects of VSG on *intestinal* GLP-1 secretion, great attention was initially drawn to GLP-1 in mediating the beneficial effects of VSG<sup>103,209,210</sup> and is still subject to controversial discussions<sup>211</sup>. In fact, rather than *intestinal* GLP-1<sup>125,127</sup>, studies were arguing for a role of *α-cell derived* GLP-1<sup>125-128,212</sup> or recently even *gastric* GLP-1 in glucose regulation<sup>124</sup>. Nonetheless, the postprandial increase in *intestinal* GLP-1 remains a robust biomarker for successful surgery.

β-cells display a remarkable repertoire of compensation in terms of insulin secretion and mass in response to a chronic energy surplus. Various factors have been shown to expand or protect β-cell mass including mild ER-stress<sup>208</sup>, autophagy<sup>213</sup>, neural<sup>214</sup>, or hepatic signals<sup>215</sup>. Although the actual mechanisms of adult β-cell expansion, namely proliferation, transdifferentiation from α-cells to β-cells, or neogenesis from pancreatic epithelial precursors are not completely resolved yet, there is ample evidence supporting hyperplasia as the principal mechanism<sup>216-218</sup>. Studies addressing the

possibility of bariatric surgery to enhance insulin secretion through expansion of  $\beta$ -cell mass are rare and have led to opposing results. RYGB increased  $\beta$ -cell mass in healthy pigs<sup>219</sup>, but did not affect  $\beta$ -cell mass in diabetic, non-obese Goto-Kakizaki rats<sup>220</sup>. Interestingly, VSG differentially affected  $\beta$ -cell mass depending on the stage of disease progression. While VSG lowered  $\beta$ -cell proliferation and mass in stages where insulin secretory compensation takes place, namely in early diabetic *db/db*<sup>117</sup> and HFD-fed mice<sup>132</sup>, VSG increased the  $\beta$ -cell mass in severely diabetic Goto-Kakizaki rats<sup>221</sup>. In our study, we intended to investigate whether morphological changes in the islet including  $\beta$ -cell mass contribute to the insulin hypersecretion observed after VSG in both our models, a DIO pre-diabetic model (B6J) and a strong  $\beta$ -cell compensatory model (B6N). We show that VSG did not alter islet morphology,  $\beta$ -cell or  $\alpha$ -cell proliferation and mass, suggesting that morphological alterations in islets are dispensable for the beneficial metabolic effects of VSG in our models but instead suggest that functional adaptations might play a role. Further, the variation in results regarding  $\beta$ -cell mass and proliferation after bariatric surgery not only emphasize that different procedures govern distinct mechanisms but also show that specific parameters such as the stage of diabetes, the model and species used, as well as the interventional time point and duration are critical to study outcomes.

### 4.3 Reversing Clinically-Overt Diabetes through VSG intervention

A multitude of studies has evidenced that VSG is a potent therapeutic intervention to reverse obesity-linked pre-diabetes and early stages of diabetes in DIO<sup>103,118,200</sup>, *db/db*<sup>117</sup> and Goto-Kakizaki<sup>220</sup> models. However, in clinics, VSG is only carried out in patients with morbid obesity linked to varying stages of diabetes resulting in complete or partial remission. Recent attempts to correlate VSG outcomes with preoperative markers have been challenging but raised concerns on the efficacy of VSG after long-term diabetes<sup>222,223</sup>. Hence, in this study, we chose a clinically-relevant model of late-stage diabetic, 16-18 weeks old *db/db* mice and tested the ability of VSG to reverse far-progressed diabetes. We studied the metabolic outcomes of VSG 14 days after surgery to unravel the early metabolic events. As the exact molecular complement of diabetes remission after VSG is still elusive, we resolved VSG-specific transcriptional programs in pancreatic islets for the first time using scRNA-seq. This approach enabled us to describe dynamic transcriptional changes in the heterogeneous pool of islet cells after VSG intervention, providing a fundamental understanding of VSG's islet-specific effects which is necessary to drive scientific progress in the field of bariatric surgery.

#### 4.3.1 Pathomechanisms of Clinically-Overt Diabetes

The *db/db* mouse model is a useful tool to study morbid obesity and modest to severe diabetes phenotypes, depending on age<sup>143,144</sup>. It has been shown that the diabetic features in *db/db* mice resembles a better clinical diabetes phenotype than DIO models<sup>224</sup>. Similar to human diabetes progression<sup>64</sup>, some studies have proven  $\beta$ -cell dedifferentiation as pathomechanism in *db/db* mice including downregulated levels of  $\beta$ -cell functional genes (*Mafa*, *Ucn3*, *Neurod1*, *Nkx6-1*, *Slc2a2*, *Pcsk1*) and upregulated dedifferentiation markers (*Gc*, *Aldh1a3*) in islets of *db/db* mice<sup>117,150</sup>. However, a detailed analysis of the *db/db* islet transcriptome on single-cell resolution is still missing in the field. Using scRNA-seq we show that among islet cells,  $\beta$ -cells are most impacted by the hostile diabetic conditions in *db/db* mice and should therefore primarily be addressed when investigating diabetes pathogenesis and entry-points for diabetes therapy. In 2016, the Accili laboratory has discovered the first unique marker for  $\beta$ -cell dedifferentiation, *Aldh1a3*<sup>69</sup>. In our study, the great majority of *db/db*-derived  $\beta$ -cells revealed high expression levels of *Aldh1a3* and other recently described dedifferentiation markers including *Gast*, *Cck*, or *Gc*, while only a small fraction of  $\beta$ -cells still presented a mature identity expressing *Mafa*. Furthermore, based on RNA-velocity, we were able

to trace the process of  $\beta$ -cell dedifferentiation within a continuum of mature to highly dedifferentiated  $\beta$ -cells in the *db/db* model. Hence, in support of prevailing literature, our results emphasize the clinical-relevant diabetes phenotype and the possibility of the *db/db* model in studying redifferentiation and to discover novel entry points for regenerative diabetes therapy.

#### **4.3.2 Restoring Glucose Regulation through VSG**

VSG is superior to medical diabetes therapy in achieving high diabetes remission rates in humans<sup>94</sup> and animal models of early and modest diabetes<sup>117,118,200</sup>. However, clinical reports recently indicated that VSG might be less efficacious after prolonged diabetes<sup>222,223</sup> urging for complementation studies in animal models. In this study, we show for the first time that VSG is indeed able to effectively reverse advanced, extreme stages of diabetes in *db/db* mice and, thus, allows investigating the underlying gluco-regulatory mechanisms of VSG in clinically-overt diabetes. Principally, VSG has been shown to exert its gluco-regulatory effects through peripheral mechanisms including improving insulin sensitivity in liver and muscle<sup>117</sup>, as well as functional improvements intrinsic to islets<sup>118</sup>. Further, gluco-regulatory effects of VSG were proven independent of body weight as these effects preceded the major body weight loss in DIO models, and were even present in hyperphagic *db/db* mice regaining body weight after VSG<sup>117</sup>, as well as in absence of body-weight changes in diabetic but non-obese Goto-Kakizaki rats<sup>220</sup>. Similarly, our results demonstrate that VSG was able to rapidly reverse advanced diabetes within only two weeks of intervention without changes in body weight. In particular, VSG restored normo-glycaemia and markedly potentiated insulin secretion in *db/db* mice. Thus, we indicate that VSG commonly enhances the insulin secretory response in early as well as late stages of diabetes suggesting VSG intrinsically modulates  $\beta$ -cell function. Likewise, a study by Douros et al. pointed out that VSG not only enhanced insulin secretion in vivo but also that the secretory phenotype induced by VSG persisted ex vivo in islet cultures<sup>118</sup>.

Further, our data proves the superiority of VSG over PF in restoring glycaemia in late stages of diabetes. We and others have shown that PF is able to similarly improve glycaemia in early diabetes compared to VSG<sup>118,198</sup>, although likely driven by distinct mechanism than VSG. In contrast, prolonged severe diabetes in *db/db* mice (16-18 weeks old) could not be reversed by modest calorie restriction of 10% applied to the PF group. Supporting our data, a study by Abu-Gazala and colleagues using modestly diabetic *db/db* mice (8-10 weeks old) showed that VSG effectively restored glycaemic regulation without affecting body weight, while a PF intervention of one week was unable to reduce body weight and glycaemia<sup>117</sup>. Another study in *db/db* mice, showed that a 50% food restriction in diabetic *db/db* mice (12 weeks old) for 4 weeks improved glycaemia in only half of the mice, while

the rest did not respond<sup>151</sup>. In opposite, strong, long-term calorie restriction of 60-70% in diabetic *db/db* mice (12 weeks age) for 12 weeks restored normo-glycaemia<sup>148</sup>. In summary, we suggest 1) that VSG performs better in normalizing glycaemia than VSG-matched PF in advanced stages of diabetes and 2) that counteracting diabetes by calorie restriction becomes less efficient as the disease progresses and requires extreme, long-term food restriction to take effect at all. Considering the drawback of calorie restrictive interventions to easily trigger relapses including regaining initial body weight and deteriorating glycaemia, VSG represents a more sustainable intervention involving fundamental beneficial metabolic adaptations.

#### **4.3.3 Recovering $\beta$ -Cell Identity and Function through VSG**

The molecular complement underlying the remarkable gluco-regulatory effects of VSG is largely unknown. While a recent study by Douros and colleagues firstly showed that VSG enhances  $\beta$ -cell function paralleled by a significant modulation of the islet transcriptome<sup>118</sup>, a deep, cell type specific analysis of islets after VSG intervention is still missing. To this end, we performed a comprehensive scRNA-seq analysis of islets derived from our VSG cohort in advanced diabetic *db/db* mice. Based on the severe disease phenotype in our *db/db* model and the marked metabolic improvements we observed after VSG, we expected to detect the underlying transcriptional paths intrinsic to specific islet cell types upon VSG enabling us to advance the mechanistic understanding of glucose regulation after VSG. Our analyses for the first time showed that VSG majorly modulated the  $\beta$ -cell transcriptome but not that of  $\alpha$ -,  $\delta$ -, or PP-cells indicating a superior mechanistic role of  $\beta$ -cells in the recovery of glycaemic regulation upon VSG.

Further, we demonstrate that the  $\beta$ -cell transcriptome from VSG mice was extensively modulated and distinct to that of Sham and PF groups. VSG-derived  $\beta$ -cells approached closest to WT  $\beta$ -cells, Sham- and PF- derived  $\beta$ -cells were strongly connected and majorly shared transcriptional signatures. Hence, these findings nicely mirror the inability of PF to improve glycaemia and insulin secretion on a molecular level in our model. In accordance with these results, Douros and colleagues recently showed that only VSG but not PF altered the islet transcriptome<sup>118</sup> once more suggesting that calorie restriction and VSG govern distinct gluco-regulatory mechanisms. Discerning the molecular paths of VSG and PF, we reveal that PF regulated only a few ribosomal and mitochondrial genes compared to Sham controls, while VSG regulated a larger number of genes relevant to diverse cell functions. Despite no reports on mitochondrial and ribosomal function after calorie restriction in  $\beta$ -cells, PF possibly enhanced mitochondrial function as described in muscle cells, hepatocytes and HeLa cells after prolonged calorie restriction, which might play a role in cellular ageing<sup>225,226</sup>. In

contrast, VSG upregulated a multitude of genes related to cellular functions of healthy  $\beta$ -cells including protein processing, folding, transport, and insulin secretion. In fact, we reveal that a short-term VSG intervention of 2 weeks already ameliorated the identity and function of  $\beta$ -cells. In particular, VSG increased the expression of two master transcription factors, *Mafa* and *Neurod1*, critical for mature  $\beta$ -cells<sup>227-229</sup>. Further VSG enhanced the expression of other crucial  $\beta$ -cell identity and function genes including *Isl1*<sup>230</sup>, *Pax6*<sup>231,232</sup>, and *Nkx2-2*<sup>233</sup>. The fact that the expression of other genes with known functions in  $\beta$ -cells including *Pdx1*<sup>234</sup> and *Foxo1*<sup>235</sup> was unchanged after VSG implies that the recovery of  $\beta$ -cell function does not necessarily require a full restoration of all factors regulating  $\beta$ -cell identity and function. Further, VSG did not recover the expression of the maturation marker *Ucn3* indicating that UCN3 is not functionally required to recover  $\beta$ -cell function, similar as recently reported<sup>236</sup>. Nevertheless, we speculate that prolonged VSG intervention might likely recover the expression of additional key  $\beta$ -cell identity genes and further enhance their expression. In support of this hypothesis, the Ben-Zvi laboratory showed that UCN3 levels progressively improved between one week and one month after VSG in early diabetic *db/db* mice<sup>117</sup>.

VSG remarkably enhanced the expression of a multitude of genes involved in  $\beta$ -cell function. These genes involve a broad range of insulin-related processes including glucose sensing (*Gck*, *Trpm5*, *Cacna1a*, *Cacna1d*, *Ffar1*), insulin processing (*Pcsk1*, *Pcsk2*, *Cpe*, *Ero1lb*), and insulin exocytosis (*Chga*, *Chgb*, *Syt4*, *Syt7*, *Syt14*, *Snap25*), which mirror the enhanced insulin secretory phenotype observed after VSG on a molecular level. This is the first report extensively describing transcriptional changes in the insulin synthesis and release processes. Furthermore, our scRNA-seq analysis of  $\beta$ -cells for the first time demonstrate that the UPR parallels the insulin synthesis machinery accompanying the high insulin secretion after VSG. The UPR as an adaptive response to ER-stress in many tissues including  $\beta$ -cells has been shown to maintain cellular homeostasis<sup>164,237</sup>, adaptive proliferation<sup>208</sup>, and insulin processing<sup>166</sup> particularly in  $\beta$ -cells. Further, our data shows a specific induction of ERAD by VSG, a process serving to mitigate ER-stress and has recently by attributed a crucial role in maintaining  $\beta$ -cell identity and function<sup>167,168</sup>. Hence, the UPR and ERAD might be a beneficial adaptation to protect and help  $\beta$ -cells cope with the increased insulin demand occurring after VSG.

#### 4.3.4 Mechanisms of Expanded $\beta$ -Cell Mass upon VSG

Principally,  $\beta$ -cell mass and its functionality determine overall insulin secretory capacity. While we have demonstrated that VSG significantly enhances  $\beta$ -cell function, we sought to further explore the possibility of VSG to increase  $\beta$ -cell mass in our late-stage diabetes model. As reviewed in chapter 4.2.2, findings on  $\beta$ -cell mass after bariatric surgery were controversial<sup>117,132,219-221</sup> likely driven by differences in diabetes phenotypes and procedures. In our study, VSG markedly increased overall  $\beta$ -cell area compared to PF and Sham controls. Two mechanisms were likely to account for the expanded  $\beta$ -cell area: redifferentiation and/or proliferation of existing  $\beta$ -cells. Among the approaches for diabetes therapy, regeneration of functional  $\beta$ -cell mass from dedifferentiated  $\beta$ -cells is one of the most promising and elegant ones. Studying targets to induce redifferentiation provides the basis for novel pharmacotherapies. So far, only few therapeutic interventions have been proven to induce redifferentiation including long-term, pronounced calorie restriction<sup>238</sup> and GLP-1/Estrogen conjugates<sup>68</sup>, while common anti-diabetic drugs such as the SGLT1/2 inhibitor Phloridzin and the insulin sensitizer Rosiglitazone were unable to induce redifferentiation<sup>151</sup>. Here, we demonstrate for the first time that VSG is capable of inducing  $\beta$ -cell redifferentiation as shown by the decreased dedifferentiation markers (*Aldh1a3*, *Gc*, *Gast*, *Cck*, *Cd81*) in the VSG  $\beta$ -cells from our scRNA-seq dataset, suggesting a shift towards more mature and less dedifferentiated  $\beta$ -cells in our scRNA-seq dataset. This was further corroborated by computational modeling of cell transition based on RNA-velocity. While the driving factors mediating gluco-regulatory actions of VSG are still unresolved, we believe that the rapid relief of metabolic stress in combination with the VSG-specific adaptations of metabolic tissues including their central control and the release of humoral factors might synergistically act on pancreatic  $\beta$ -cells to enhance function and induce redifferentiation.

Based on the massive increase in  $\beta$ -cell area we suspected that there could be additional proliferative mechanisms. In fact, VSG induced a slight but not statistically significant increase in  $\beta$ -cell proliferation between 11-14 days after surgery. Therefore, it is plausible that the major proliferation might have taken place already during the first days after VSG. However, more importantly, our scRNA-seq dataset showed that VSG induced a proliferation-competent state in non-cycling  $\beta$ -cells. This comprised a specific upregulation of the major cell-cycle progression gene in  $\beta$ -cells *Ccnd2*<sup>180</sup>, as well as *Sox4*, and a specific downregulation of the cell-cycle inhibitor *Cdkn1a* in VSG-derived  $\beta$ -cells. Notably, *Sox4* has been shown to repress *Cdkn1a* thereby allowing adult  $\beta$ -cell replication<sup>181</sup>. Thus, VSG might have induced similar expression patterns to facilitate  $\beta$ -cell proliferation. Moreover, our scRNA-seq data revealed that VSG mice present the highest number of cycling  $\beta$ -cells and that these



display a rather dedifferentiated signature involving high expression of *Aldh1a3*, *Cck*, and *Gc*. These findings suggest that dedifferentiated  $\beta$ -cells are more likely to undergo proliferation than mature  $\beta$ -cells and support previous reports in rodent and human studies. While replication of mature  $\beta$ -cells in adult seems to be negligible in human compared to rodent adult  $\beta$ -cells<sup>239–241</sup>, a recent study showed that switching to a less functional and immature state of  $\beta$ -cells enables proliferation in adult<sup>242</sup>. Similarly, our dataset showed that dedifferentiated  $\beta$ -cells at the same time resemble features of immaturity including high expression of *Cd81*<sup>72</sup> and showed high proliferation scores suggesting that dedifferentiated  $\beta$ -cells present the capacity to proliferate.

Collectively, our data indicates that VSG induces additive mechanisms of  $\beta$ -cell redifferentiation and proliferation to expand  $\beta$ -cell mass to adapt the insulin demand post VSG.

#### **4.3.5 Novel VSG Target Genes in $\beta$ -Cells**

To date, only a few targets have been discovered that might explain VSG's body-weight lowering and glycaemic benefits. These include the bile acid receptors FXR and TGR5<sup>137,199</sup> and circulating PYY<sup>243</sup>. However,  $\beta$ -cell intrinsic targets of VSG that provide a basis for the development of novel glucose-regulating drugs are still elusive. To this end, we screened the  $\beta$ -cell transcriptome after VSG to discover genes that might be causally linked to the metabolic benefits observed after VSG. We detected a multitude of genes unique to VSG that relate to immune functions (*Igkc*, *Saa3*, *Ccl28*, *Cxcl1*, *Tlr2*, *Il13ra1*, *Ifngr2*) as well as genes associated with the adaptive response in  $\beta$ -cells during pregnancy (*Sftpd*, *Tnfrsf11b*, *Chgb*, *Gbp8*, *Car8*, *Socs2*).

Low-grade chronic tissue inflammation plays a mechanistic role in obesity and diabetes pathogenesis<sup>244,245</sup>. While the effect of bariatric surgical interventions on systemic immune functions and immune responses in adipose tissue and liver have extensively been studied, adaptive immune responses intrinsic to  $\beta$ -cells have never been addressed before. Bariatric surgery has been shown to improve systemic inflammation<sup>246–248</sup>, to shift immune-cells from a pro-inflammatory to an anti-inflammatory phenotype<sup>245</sup>, as well as to modulate tissue-specific immune-responses in liver, intestine, and adipose tissue<sup>201,249–251</sup>. Lowered post-surgical meta-inflammation has been correlated with improved conditions of obesity and diabetes<sup>252</sup>, however, tissue specific immune-responses after bariatric surgery and their consequences on metabolic outcomes are not yet fully understood.

In  $\beta$ -cells, anti-inflammatory cytokines may play a protective role<sup>253</sup>. One of them is interleukin-13 exerting survival functions in  $\beta$ -cells<sup>254</sup>. In our study, we found *Il13ra1* upregulated in VSG, which codes for the receptor binding interleukin-13, suggesting that enhanced interleukin-13 signaling

might contribute to  $\beta$ -cell protection after VSG. Furthermore, we found the interferon- $\gamma$  receptor *Ifngr2* upregulated in  $\beta$ -cells upon VSG. While interferon- $\gamma$  signaling is known to be pro-inflammatory and to contribute to  $\beta$ -cell dysfunction<sup>255</sup>, there is a study reporting that enhanced interferon- $\gamma$  secretion from mesenteric lymph nodes occurring after VSG induced an increase in liver and intestinal FXR<sup>256</sup>. Similarly, increased interferon- $\gamma$  signaling in  $\beta$ -cells after VSG might equally increase  $\beta$ -cell FXR expression and contribute to enhanced insulin secretion as previously reported for FXR<sup>257,258</sup>. In our dataset, mRNA-levels of FXR were not changed after VSG (data not shown), however, yet the protein level of FXR still need to be assessed. Further, mechanistic studies are required to order to explore the possibility of enhanced interferon- $\gamma$  signaling, FXR expression and beneficial consequences on  $\beta$ -cell function. Another implication of increased postsurgical pro-inflammatory cytokine levels in the pancreas could be the neogenesis of  $\beta$ -cells. A study by the Kulkarni laboratory showed that intra-ductal injections of interferon- $\gamma$ , TNF- $\alpha$ , and interleukin-1 $\beta$  triggered ductal-to-endocrine reprogramming<sup>259</sup> suggesting a potential role of  $\beta$ -cell derived cytokines in increasing  $\beta$ -cell mass after VSG. Moreover, VSG increased the expression of *Saa3* in  $\beta$ -cells, a gene coding for an acute-phase protein of the serum amyloid A (SAA) family. While the SAA family is a hallmark of inflammation<sup>260</sup>, it is not clear whether it promotes or counteracts inflammation and what the exact functions of each SAA variant are. Genetic deletion of *Saa3* in mice has shown that it is required for normal growth and immune-metabolic function<sup>261</sup>, however, the consequence of increased *Saa3* expression in  $\beta$ -cells is unknown. In a mouse model of colitis, *Saa3* exerts protective functions: *Saa3* binds to its neutrophil receptor Tlr2 in order to induce the expression of interleukin-22, which has been attributed a beneficial role in the inflamed colon<sup>260</sup>, as well as in pancreatic islets<sup>243</sup>. In the latter study, stimulation of islets with interleukin-22 positively regulated the release of PYY from islets, which in turn exerted gluco-regulatory effects in islets *ex vivo*<sup>243</sup> (Guida 2019). Thus, we speculate that *Saa3*-Tlr2 signaling between islets and neutrophils might exert protective effects and might indirectly contribute to the improved glucose regulation after VSG via the interleukin-22-PYY axis as demonstrated by Guida and colleagues. Overall, we describe an altered immune-profile of  $\beta$ -cells after VSG with increased levels of pro- and anti-inflammatory cytokines as well as immune-regulatory factors that might present a shift towards beneficial immune responses. These findings open up a multitude of hypotheses to explain the gluco-regulatory benefits of VSG that warrant future mechanistic investigations.

In addition to the immune-factors, we report for the first time that VSG induces the expression of genes that are specifically upregulated in islets during pregnancy (*Sftpd*, *Tnfrsf11b*, *Chgb*, *Gbp8*, *Car8*, *Socs2*). In pregnancy, the hormones prolactin and placental lactogen trigger a collection of distinct

compensatory processes in maternal  $\beta$ -cells including proliferative and functional adaptations to maintain euglycaemia<sup>182,183,185,187,262-264</sup>. Principally, these effects can also be induced in islets from males as shown in a study, in which prolactin induced a pregnancy-like mRNA signature in islets derived from male mice<sup>265</sup>. Moreover, a recent study in VSG patients revealed that surgical intervention increases blood prolactin levels<sup>266</sup> indicating a possible link of VSG and the upregulation of pregnancy-associated genes reported by our study, which needs to be conclusively proven by mechanistic experiments.

Despite belonging to the top upregulated genes in islets during pregnancy, the functions of *Sftpd* and *Car8* in islets are largely unknown<sup>185-187</sup>. SP-D, the protein encoded by *Sftpd*, is an anti-microbial collectin implicated in the innate immune response, which is expressed by pulmonary and non-pulmonary epithelial cells and was originally discovered in pulmonary surfactant<sup>267</sup>. SP-D defects are linked to pulmonary, cardiovascular and metabolic diseases including obesity likely because they commonly underlie inflammation and can occur as comorbidities<sup>267,268</sup>. Furthermore, SP-D has been shown to be overexpressed in islets during pregnancy as well as in newly formed  $\beta$ -cells during the perinatal period and to exert anti-inflammatory functions in adult  $\beta$ -cells<sup>186,269</sup>. Thus, SP-D might be upregulated after VSG to exert protective, immune-regulatory actions in  $\beta$ -cells after VSG. *Car8* codes for Carbonic Anhydrase 8, a protein named according to its similarity to carbonic anhydrases, however, lacks catalytic activity. Car8's function has mainly been described in brain where its deficiency has been linked to various neuropathological disorders because of its role in modulating intracellular  $\text{Ca}^{2+}$ -signaling by inhibiting the inositol-trisphosphate receptor-1 (ITPR1)<sup>270</sup>. In adult  $\beta$ -cells, *Car8* expression is weak but gets upregulated during pregnancy<sup>187,271</sup> suggesting specific adaptive functions during conditions of high insulin demand such as pregnancy. Similarly, we found *Car8* highly expressed in  $\beta$ -cells after VSG suggesting that Car8 might contribute to the enhanced insulin secretion after VSG eventually by modulating  $\text{Ca}^{2+}$ -signaling and stimulus-secretion coupling in  $\beta$ -cells. Future functional experiments will have to conclusively prove the relevance of the targets identified by our scRNA-seq screening to the gluco-regulatory functions of VSG and may serve as novel pharmacological entry points.

OPG is a naturally-occurring  $\beta$ -cell mitogen during pregnancy and equally stimulates  $\beta$ -cell proliferation in human and mouse when pharmacologically administered<sup>183</sup>. Mechanistically, OPG prevents the binding of Receptor activator of NF $\kappa$ B Ligand (RANKL) to RANK thereby modulating downstream programs to activate proliferation including cyclins and cyclin-dependent kinases<sup>183,184</sup>. Our study for the first time reveals that VSG is able to intrinsically upregulate *Tnfrsf11b* (OPG) expression in  $\beta$ -cells after VSG. This finding indicates that, similar to pregnancy, VSG might induce

OPG expression upon post-surgical high insulin demand to expand  $\beta$ -cell mass. The exact mechanisms through which OPG-levels get upregulated during pregnancy are not fully understood but involve the enhanced actions of prolactin<sup>183</sup>. Similarly, VSG has recently been reported to increase prolactin levels in human patients<sup>266</sup>. Thus, this study provides a possible mediator of VSG and increased OPG expression, which might in turn stimulate  $\beta$ -cell replication and expansion of  $\beta$ -cell mass observed after VSG. Nevertheless, possible upstream driving factors that mediate the metabolic and especially glycaemic benefits remain poorly understood and require thorough mechanistic investigation.

In summary, we discovered novel,  $\beta$ -cell intrinsic targets in a model of VSG-induced remission of severe T2D. These targets may be causally-linked to the beneficial gluco-regulatory effects of VSG and potentially represent novel pharmacological entry points for the treatment of late-stage T2D. Thus, future research will need to mechanistically test our proposed VSG candidates and explore their potential to restore  $\beta$ -cell function or to trigger  $\beta$ -cell redifferentiation and proliferation in T2D.

#### **4.3.6 Role of Extreme $\beta$ -Cells in Diabetes and after VSG**

Current research in the field of islet biology aims at resolving the heterogeneous states of  $\beta$ -cells in order to better explain the intra-islet interplay of  $\beta$ -cells for regulated insulin secretion. In the process, specific  $\beta$ -cell subpopulations including hub-cells<sup>272</sup> and virgin  $\beta$ -cells<sup>273</sup> have recently been identified. Hub-cells present an immature but metabolically active phenotype and functionally dictate synchronized insulin secretion, while virgin  $\beta$ -cells refer to a niche of immature but insulin expressing  $\beta$ -cells residing at the edge of islets that originate from  $\alpha$ -cells and may provide a source for new  $\beta$ -cells<sup>272,273</sup>. Additionally, the Itzkovitz laboratory discovered another small subset termed extreme  $\beta$ -cells using single-molecule transcript imaging, which are molecularly distinct from hub and virgin  $\beta$ -cells<sup>176,274</sup>. Based on their explicitly high expression of *Ins2* and other insulin secretion-related genes and simultaneously low insulin protein levels, extreme  $\beta$ -cells have been suggested a specialized function in basal insulin secretion. Unlike phasic postprandial insulin secretion, basal low insulin secretion is required throughout the day for the constant energy supply. In line with the study by Farack et al., another scRNA-seq-based study by the Johnson laboratory reported a subpopulation of  $\beta$ -cells that highly express *Ins2* and a multitude of insulin-related genes<sup>177</sup>. The extreme  $\beta$ -cell population we discovered in our scRNA-seq dataset shows a high consistency to the markers reported by the two studies and likely represents the same specification of  $\beta$ -cells. Our study for the first time reveals a full transcriptional characterization of extreme  $\beta$ -cells not only in WT but also in late-stage diabetic *db/db* mice. We show that the transcriptional signature of WT- and *db/db*-derived

extreme  $\beta$ -cells was similar but the proportions differed in healthy and diabetic conditions. The study by Farack et al. revealed that the numbers of extreme  $\beta$ -cells increase in early diabetic stages likely reflecting compensatory adaptations. In turn, we show that the fractions of extreme  $\beta$ -cells are lowered upon prolonged, severe T2D. Together, these findings indicate that extreme  $\beta$ -cells may play a compensatory role in counteracting hyperglycaemia in early T2D, while the extreme state of  $\beta$ -cells is compromised in late stages of T2D and might eventually contribute to T2D progression. Interestingly, VSG in turn rescued the levels of extreme  $\beta$ -cells either suggesting a role of extreme  $\beta$ -cells in the recovery of  $\beta$ -cell function after VSG or that the extreme  $\beta$ -cell state recovers upon glycaemic normalization. Whether the numbers of extreme  $\beta$ -cells change due to altered rates of proliferation or through transitions between extreme and non-extreme states is still unknown. However, the rapid increase in extreme  $\beta$ -cells upon short-term VSG intervention rather suggests dynamic state-specific changes. Finally, the fact that extreme  $\beta$ -cells are modulated in number along the progression of T2D and upon VSG intervention warrants further investigation aiming at assessing the actual function and contribution of extreme  $\beta$ -cells in T2D progression and remission upon VSG. Future research will show whether pharmacological modulation of the extreme  $\beta$ -cell state might be of therapeutic value.

## 4.4 Conclusions

This thesis revealed the potent metabolic effects and the ability of VSG to rescue pre-diabetes as well as far-progressed T2D, and advances the understanding of  $\beta$ -cell intrinsic gluco-regulatory mechanisms induced by VSG.

In DIO models of pre-diabetes, we showed that VSG and PF similarly reduce body weight and glycaemia, however, only VSG enhances  $\beta$ -cell function. Thus, our findings indicate that calorie restriction is a suitable intervention for early stages of T2D as well, although underlying different metabolic mechanisms than VSG. By contrast, only VSG was capable of reversing late-stage T2D, while PF failed to improve glycaemia revealing the superiority of VSG over calorie-restrictive interventions to treat far-progressed, severe T2D in our model. Albeit VSG represents a remarkably potent therapy for T2D, VSG is limited to a narrow range of patients due to its invasiveness. Therefore, current research investigates underlying mechanisms of the diverse metabolic effects including T2D remission in order to develop novel pharmaceuticals that mimic bariatric surgery. Our study showed that morphological and cellular adaptations in intestinal epithelial and pancreatic endocrine tissues are dispensable for the metabolic effects of VSG in prediabetes DIO models suggesting more downstream effects independent of morphological adaptations. Future research will be required to resolve molecular paths of VSG intrinsic to intestinal epithelial and islet cells that underlie VSG-mediated T2D remission in pre-diabetes.

In far-progressed T2D, the present study deciphered intrinsic transcriptional adaptations in  $\beta$ -cells including genes of the insulin synthesis and secretion machinery that paralleled the rapid T2D remission induced by VSG. Our data revealed that VSG restores insulin secretion by synergistic effects of increased  $\beta$ -cell mass and enhanced  $\beta$ -cell function. Mechanistically, we propose that VSG expands  $\beta$ -cell mass by additive effects of  $\beta$ -cell proliferation and redifferentiation to a more mature identity and functional state. Finally, our study identified unique VSG target genes in the  $\beta$ -cell transcriptome that potentially drive local gluco-regulatory benefits of VSG. Future functional experiments will show if these candidates can be used to generate novel pharmacotherapies to treat far-progressed T2D.

## 5. Materials and Methods

### 5.1 Materials

#### 5.1.1 Mouse Lines and Animal Diets

Mouse line	Experimental group name	Background	Source
FoxA2-Venus-Fusion (FVF)	B6J	C57/BL/6J	Burtscher, Barkey & Lickert 2013
Wildtype	B6N	C57/BL/6N	Charles River, Germany
<i>db/db</i>	<i>db/db</i>	C57BKSCg-Dock7m+/+Leprdb/J	The Jackson Laboratory, US

Diet	Source	Order Number
High-fat high-sugar diet (HFD) (58 % kcal from fat, 25 % kcal from carbohydrates, 17% kcal from protein)	Research Diets Inc.	D12331
Control diet (11 % kcal from fat, 64 % kcal from carbohydrates, 25 % kcal from protein)	Ssniff	E15051-047
Liquid diet Osmolite HiCal	Abbott	N/A
Liquid diet Osmolite HiCal supplemented with 10% D- glucose (for MMTT)	Abbott	N/A
Hydrogel	Clear H2O	70-01-5022

### 5.1.2 Equipment

AxioScan.Z1 digital slide scanner	Zeiss
Centrifuge 5430 R	Eppendorf
Counting chambers	Neubauer, Laboroptik
Clamp Straight 35 mm	Fine Science Tools
Confocal Microscope LSM 880	Zeiss
Confocal Microscope TCS SP5	Leica Microsystems
Chromium Controller	10×Genomics
Cryostat CM 1860	Leica
EchoMRI	LLC. USA
Feeding needle (Gavage) 18060-20	Fine Science Tools
Fluorescence Plate Reader Varioskan LUX	Thermo Fisher Scientific
Forceps Dumount Inox, 11251-, 11252-20	Fine Science Tools
Glassware	Schott
Glucometer Freestyle freedom lite	Abbot Diabetes Care Oxon
Microtome RM 2255	Leica
Paraffin embedding station EG1160	Leica Microsystems
pH meter	Mettler Toledo
Pipette Controller Accu-jet® pro	Brand
Scissors 14088-10	Fine Science Tools
Waterbath Memmert SWB25	Thermo Fisher Scientific
Water purification system Millipore Q-POD	Merck

### 5.1.3 Consumables

Cannula Sterican 20 G	Braun
Cell strainer 70µm nylon 70 µm	Falcon, Fisher Scientific
Cover slips	VWR International
Cryo embedding medium OCT	Leica
Cryotubes	Sarstedt



DNA Lo Bind tubes 1.5ml	Eppendorf
Embedding molds	Sigma Aldrich
Glass slides Menzel superfrost plus	Thermo Scientific
Glucose strips	Abbott Diabetes Care Oxon
Microvette CB300 K2 EDTA	Sarstedt
S-Monovette K2 EDTA	Sarstedt
S-Monovetten cannula 21G	Sarstedt
Syringe 3 ml	Omnifix
Syringe 3 ml Luer lock	BD Becton and Dickinson
Petri dish 10 cm	Thermo Scientific
Pipettes 1000 µl / 100 µl / 10 µl	Eppendorf
Pipettes 25 ml / 10 ml / 5 ml	Greiner
Insulin Syringe Ultra-Fine Needle 8 mm	BD Becton and Dickinson
Tubes 50 ml/ 15 ml	BD Becton and Dickinson
Tubes Safe-lock, 2 ml/ 1.5 ml / 0.2 ml	Eppendorf

#### 5.1.4 Chemicals

Chemicals were purchased from Carl Roth GmbH & Co. KG (Karlsruhe), Merck KGaA (Darmstadt) or Sigma-Aldrich GmbH (Hamburg) if not stated otherwise.

Aprotinin	Sigma, #A-1153
Bovine Serum Albumine (BSA)	
DAPI	Life technologies
Diprotin	Abcam, #145599
Ethylene-diamine-tetra-acetic acid (EDTA)	
5-Ethynyl-2-deoxyuridine (EdU)	Life Technologies, #A10044
Ethanol	
Fetal Bovine Serum (FBS)	PAN-Seratech, #ST40-37500
Neutrally buffered formalin	
Glucose (D+)	
Glycine	

KCl	
NaCl	
Na <sub>2</sub> HPO <sub>4</sub>	
Paraffin Wax Paraplast	Leica
Paraformaldehyde (PFA)	
Sodium chloride (NaCl)	
Triton X-100	
Trypan Blue 0.4 %	Gibco, Thermo Fisher Scientific
Tween-20	

### 5.1.5 Kits and Assays

Glucose Assay	CrystalChem, #81692
Mouse Insulin ELISA	CrystalChem, #90080
Mouse GLP-1 ELISA	CrystalChem, #81508
Click-IT EDU Alexa Fluor 647	Life Technologies, #C10340
Chromium™ Single cell 3' library and gel bead kit v2	10X Genomics, #120237

### 5.1.6 Buffers and Solutions

#### Surgical Interventions and Blood Measurements

Buprenorphin, Buprenovet	Bayer
Isoflurane CP	CP-Pharma
Heparin Sodium 5000 U/ml	Braun
Saline 0.9 %	Braun
Antiproteolytic cocktail	250 µg Diprotin A, 50 mg Aprotinin in 2 ml saline, 6 ml 0.5M EDTA, 2 ml 5000 U/ml Heparin
Meloxicam, Metacam Suspension	Böhringer Ingelheim

### **Islet Isolation and Single-Cell Preparation**

Collagenase P (1 mg/ml) solution	Collagenase P (Roche) in G-solution
G-Solution	HBSS (Lonza Verviers) supplemented with 1x Penicillin/Streptomycin (100x Gibco, Invitrogen) and 1% BSA (Sigma)
Gradient medium	5 ml G-solution, 30 µl 1M HEPES (Life Technologies), 970µl DPBS (Lonza Verviers), 2 ml Optiprep density gradient medium (Sigma, # D1556-250ML)
RPMI 1640 medium	RPMI 1640 medium (Invitrogen, #21875091) supplemented with 10% FCS (Gibco) and 1% penicillin-streptomycin (Life Technologies, #15140122)
DPBS without Mg <sup>2+</sup> /Ca <sup>2+</sup>	Gibco, Invitrogen

### **Single-cell preparation and scRNA-seq**

FACS buffer	1×DPBS, 1% FBS, 0.1mM EDTA
TrypLE	Life technologies, #12605

### **Immunohistochemistry**

10x PBS (pH 7.4)	1.37M NaCl, 26.8mM KCl, 0.1M Na <sub>2</sub> HPO <sub>4</sub> , 13.8mM KH <sub>2</sub> PO <sub>4</sub>
PBS-T	1×PBS, 0.1% Tween20, pH7.4
Permeabilisation	0.25 % TritonX-100, 100mM glycine in dH2O
Rodent Decloaker 10X	Biocare Medical, #RD913
Blocking Buffer	10% FCS, 3% serum (donkey) in PBST, 1% BSA
ProLong Diamond antifade mountant	Thermo Fisher Scientific, #P36961
Vecta Shield Hard Set mountant	Vector Laboratories #VEC-H-1400

### 5.1.7 Antibodies

Polyclonal rabbit anti-Aldh1a3	LSBio, #LS-C498339-100	1:300
Polyclonal goat anti-Chromogranin A	Santa Cruz, #sc-1488	1:200
Polyclonal rabbit anti-GLP-1	Abcam, #ab22625	1:200
Polyclonal guinea pig anti-glucagon	Takara, #M182	1:2500
Monoclonal mouse anti-GRP78	BD Bioscience, #610979	1:200
Monoclonal rabbit anti-insulin	Cell Signaling, #3014	1:400
Polyclonal guinea pig anti-insulin	Thermo Scientific, #PA1-26938	1:200
Polyclonal rabbit anti-MafA	Aviva systems biology, #ARP47760_P050	1:200
Monoclonal mouse anti-Pcsk1	Santa Cruz, #sc-100578	1:200
Polyclonal goat anti-Sel1L	Novus Biologicals, #NB100-93463	1:200
Polyclonal goat anti-Slc2a2	Abcam, #ab111117	1:300
Polyclonal rabbit anti-Slc5a10	Abcam, #ab167156	1:300
Polyclonal rabbit anti-UCN3	Phoenix Pharmaceuticals, #H-019-29	1:500
Donkey anti-rabbit IgG 488	Invitrogen, #A21206	1:800
Donkey anti-guinea pig Alexa 488	Dianova, #706-545-148	1:800
Donkey anti-rabbit IgG 555	Invitrogen, #A31572	1:800
Donkey anti-mouse IgG 555	Invitrogen, #A31570	1:800
Donkey anti-goat IgG 555	Invitrogen, #A21432	1:800
AlexaFluor750 goat anti-rabbit	Invitrogen, #A21039	1:2500
Biotinylated goat anti-guinea pig	Vector, #BA7000	1:100
Cy3-conjugated streptavidin	Invitrogen, #SA1010	1:100

### 5.1.6 RNA Scope Probes

Ins2 mRNA Probe	ACD Biotechne, # 497811-C2	1:200
Dye Opal 520	Akoya Biosciences, #FP1487001KT	1:800

## 5.2 Methods

### 5.2.1 Animal Handling, Mouse Models and Dietary Interventions

Animals were maintained at the central facilities at Helmholtz Zentrum München, German Research Center of Environmental Health under standard controlled conditions.

For diet-induced obesity-diabetes mouse models, male B6J-Foxa2-Venus-Fusion (FVF) and B6N mice were introduced to a high-fat high-sugar diet (HFD) at the age of 8-12 weeks for a period of 12-14 weeks until surgery intervention. Regular chow diet-fed B6N mice and control chow diet (CD)-fed B6J-FVF mice served as controls for the respective HFD groups. FVF-B6J mice present a fluorescent label of nuclear FoxA2 protein and reveal a normal B6J WT phenotype. FVF-B6J (hereafter referred to as B6J) mice were initially chosen for comparability reasons in order to directly link to a previous HFD-study from our laboratory<sup>31</sup> and to allow the opportunity for possible fluorescent-activated cell sorting experiments.

In the genetic obese-diabetic mouse model (*db/db*), male *Lepr*-deficient *db/db* and WT mice were fed a regular rodent chow until surgery intervention at the age of 15-18 weeks. *db/db* mice exhibit an innate hyperphagic drive resulting in progressive increase in body weight and T2D manifestation<sup>143</sup>. Body weight was regularly measured to track obesity progression. Mice were single-housed one week prior to surgery. Housing of WT mice was continued in groups of 2-4 per cage.

All animal experiments were carried out in compliance with the German Animal Protection Act and with the approved guidelines of the Society of Laboratory Animals (GV-SOLAS) and of the Federation of Laboratory Animal Science Associations (FELASA). This study was approved by the Animal Use and Care Committee of Bavaria, Germany.

### 5.2.2 Surgical and Animal Experimental Procedures

Preoperatively, mice were matched for body weight and metabolic parameters and assigned to VSG, Sham and pair-fed (PF) groups. VSG and sham surgeries were conducted as described previously<sup>100</sup>. Briefly, VSG surgery included the lateral excision of 70% of the stomach generating a tubular gastric remnant in continuity with the esophagus superiorly and the pyloric sphincter and duodenum inferiorly. For Sham surgery groups (Sham), the abdomen was opened and slight pressure was

applied to the stomach by using blunt forceps along the line starting from the esophagus to the duodenum. Before surgery, mice were fasted for 12h. Surgery was performed under isoflurane anaesthesia and administration of Buprenorphin (0.1mg/kg body weight). In the *db/db* model, WT mice were considered as a healthy control group and did not undergo surgery.

### **5.2.3 Postoperative Care and Dietary Regimen**

Postoperatively, all surgical groups were subcutaneously injected Meloxicam (1mg/kg body weight, daily for 2-3 days), and warm saline (1 ml, daily for 2-3 days). Mice received ad libitum Osmolite HiCal liquid diet (Abbott) and hydrogel for 3 days after surgery before being returned to a solid diet on day 4. Henceforth, VSG and sham mice had access to ad libitum HFD (B6J, B6N) or chow (*db/db*). A subgroup of sham mice was pair-fed (PF) in order to match the food intake of VSG mice. To this end, PF mice received weighed amounts of HFD or chow once daily calculated based on the average food consumption of the VSG group during the previous 24h.

### **5.2.4 Mixed-Meal Tolerance Test, Insulin Secretion Test and GLP-1 Measurements**

Mixed-meal tolerance tests (MMTTs) were performed 14 days prior and 13 days post-surgery. Mice were fasted for 6 h and blood from the tail vein was collected for basal blood glucose and insulin measurements. Mice were gavaged with 200  $\mu$ l of Osmolite HiCal liquid diet (+20% D-Glucose). Tail vein blood was collected using tubes containing anti-proteolytic cocktail (250  $\mu$ g Diprotin A, 50 mg Aprotinin in 2 ml saline, 6 ml 0.5M EDTA, 2 ml 5000 U/ml Heparin) at different time points to assess postprandial GLP-1 levels at 12 min and glucose and insulin levels at 15, 30, 60, and 120 during the MMTT. Blood glucose was assessed in plasma using mouse glucose assay kit (CrystalChem, #81692). Levels of circulating insulin and GLP-1 were assayed in plasma using mouse-specific ELISA kits (CrystalChem, #90080, #81508).

### **5.2.5 Adiposity Index**

The Adiposity index was calculated by dividing fat through lean mass obtained from nuclear magnetic resonance (NMR) spectroscopy.

### **5.2.6 NMR Spectroscopy**

Lean and fat mass of mice was measured by NMR technology (EchoMRI, Houston, TX, USA).

### **5.2.7 EdU Administration**

To label proliferative cells, mice were intraperitoneally injected 10 mg/g body weight 5-ethynyl-2'-deoxyuridine (EdU, Thermo Fisher, #E-10187) 4h before the end of the experiment for intestinal proliferation or once a day on 3 consecutive to assess pancreatic proliferation.

### **5.2.8 Immunohistochemistry and EdU Assay**

Pancreata of B6J (FVF) mice were fixed in 4 % paraformaldehyde/PBS for a minimum of 12h, intestines of B6J (FVF) mice were fixed in 4 % paraformaldehyde/PBS for 4h. Organs were cryo-preserved using sucrose gradients of 7.5, 15, and 30% sucrose in PBS, and were subsequently embedded using OCT and frozen. Sections of 12  $\mu$ m thickness were cut.

Pancreata of B6N and *db/db* mice were fixed in 4 % neutrally buffered formalin for a minimum of 12h and sectioned into 3-5 parallel, equidistant slices. Subsequently, the tissue slices were vertically embedded in paraffin to ensure coverage of all regions of the pancreas including head, neck, body and tail. Sections of 3  $\mu$ m thickness were cut.

EdU staining was performed as per manufacturer's protocol (Click-IT EdU Alexa Fluor 647 Imaging Kit, Thermo Fisher Scientific). Slides were stained using primary and secondary antibodies (see list of antibodies) and nuclei were labelled with Hoechst33342 (H1399, Thermo Fischer) or 4', 6-diamidino-2-phenylindole (DAPI; Life Technologies, 1:500). Slides were mounted with Vecta Shield and imaged using confocal microscopy (Zeiss LSM or Leica SP5).

### **5.2.9 Pancreas Morphometric Quantification**

Per animal, 6 pancreatic sections were analyzed. The stained sections were scanned with an AxioScan.Z1 digital slide scanner (Zeiss, Jena, Germany) with a 40x magnification objective. Islets were automatically detected (100 islets/animal) and insulin, glucagon, and EdU positive cells were quantified with help of the image analysis software Definiens Developer XD2 (Definiens AG, Germany).  $\beta$ -cell and  $\alpha$ -cell area were detected based on Insulin+ or Glucagon+ area, respectively, over pancreatic tissue area. To evaluate  $\alpha$ - and  $\beta$ -cell replication, the respective ratio of glucagon/EdU/Hoechst or insulin/EdU/Hoechst co-positive cells over the total glucagon or insulin positive cells were quantified.

### **5.2.10 In Situ Hybridization**

In situ hybridization (ISH) was performed using RNAscope® 2.0 Assay according to the manufacturer's protocol (Wang 2012). Dilution of *Ins2* probe (acdbio) was 1:200 and 1:800 for the subsequent fluorophore Opal 520 (Akoya Biosciences). Microscopy images of three mice per group (WT, Sham, PF, VSG) with 3 technical replicates each were captured using AxioScan.Z1 digital slide scanner (Zeiss, Jena, Germany) equipped with a 40x magnification objective. Islets of Langerhans were manually annotated and cytoplasmic *Ins2* ISH pixel intensity was measured using image analysis software Definiens Developer XD2 (Definiens AG, Germany). Subsequently, *Ins2* mRNA skewness of a minimum of 4000 *Ins2*-positive cells per group was calculated.

### **5.2.11 Statistical Analysis of Metabolic Data**

Results are expressed as mean  $\pm$ s.e.m. (Standard Error Mean). Two-way ANOVA corrected by Bonferroni's multiple comparison test was used for statistically comparing longitudinal data. Remaining data was compared using one-way ANOVA corrected by Bonferroni's multiple comparison test or student's t-test. A value of  $p < 0.05$  % was considered statistically significant. Analyses were performed using the GraphPad Prism 8 Software (GraphPad Software, USA). Statistical significance is displayed by asterisks: \*  $p < 0.05$ , \*\*  $p < 0.01$ , \*\*\*  $p < 0.001$ , \*\*\*\*  $p < 0.0001$ .



### **5.2.12 Islet Isolation and Single-Cell Preparation**

Pancreata were excised and digested using collagenase P followed by centrifugation using OptiPrep™ density gradient medium. Isolated islets were selected under a stereomicroscope and subsequently cultured in RPMI 1640 medium supplemented with 10% FCS and 1% penicillin-streptomycin for 1h at 37 °C. In order to generate single cells, islets were dissociated by incubating with TrypLE for 12-15 min at 37 °C and gentle repeated pipetting. Number of dead cells were measured by staining a fraction of each sample with Trypan Blue and counting dead cells using Neubauer Counting Chambers. Cells were washed twice with FACS buffer before continuing with library generation for single-cell RNA sequencing.

### **5.2.13 Single-cell RNA Sequencing: RNA Preparation, Library Generation and Sequencing**

Single-cell libraries were generated using the Chromium™ Single cell 3' library and gel bead kit v2 (10x Genomics, #120237) according to the manufacturer's instructions. 16,000 cells per sample were applied to a channel of the 10x chip to generate Gel Bead-in-Emulsions (GEMs) to obtain 10,000 cells per sample. This was followed by reverse transcription to barcode RNA, cleanup, and cDNA amplification. Subsequently, enzymatic fragmentation was performed and 5' adaptor and sample indexes were attached. Libraries were sequenced using NovaSeq6000 (Illumina) with 150 bp paired-end sequencing.

### **5.2.14 Preprocessing of 10x scRNA-seq Data**

Preprocessing of the 10x scRNA-seq data was performed as described in detail in Oppenländer et al., submitted to Molecular Metabolism. Briefly, the CellRanger (v3.1.0) software was used to demultiplex the binary bas cell (BCL) files, to align and filter reads, and count barcodes and unique molecular identifier (UMI) in order to generate a digital gene expression matrix (DGE). Further downstream analyses were performed using Python 3.7.7 from the Scanpy package (v1.4.6)<sup>275</sup>. Cell-by-gene count matrices for each sample were concatenated for one merged dataset. Standard preprocessing method and quality control measures were applied to filter cells and genes from the raw data. Non-endocrine cells expressing Krt19 (ductal cells), Prss2 (acinar cells), Plvap (endothelial cells), Col1a2 (stellate cells), and Cd74 (immune cells) were excluded from the analysis. Scrublet pipeline (v0.2.1) was used to identify potential cell doublets or technical artifacts. Subsequently, we

obtained 19,878 endocrine cells from WT and Sham (median number of transcripts per cell of 3962 and a mean of 33,206 counts per cell). In Sham, PF, and VSG groups, we obtained 35,941 endocrine cells (median number of transcripts per cell of approximately 3621 and a mean of 30,251 counts per cell). Highly variable genes (HVGs) were used for dimensionality reduction. HVGs were identified using the function *pp.highly\_variable\_genes* from Scanpy. 4000 top HVGs were used to run principal component analysis (PCA). Cells were clustered and visualized via Uniform Manifold Approximation and Projection (UMAP).

### **5.2.15 Dimensionality Reduction, Clustering and Cell Type Annotation**

Dimensionality reduction, clustering and cell type annotation of the 10x scRNA-seq data was performed as described in detail in Oppenländer et al., submitted to Molecular Metabolism. Briefly, principal component analysis (PCA) was performed using 4000 HVGs, a k-nearest-neighborhood (KNN) graph was computed using *pp.neighbors* from scanpy, and data was analyzed for transcriptomic similarity in a two-dimensional embedding. Next, UMAP embedding (v0.4.0, scanpy function *tl.umap*) and Louvain clustering (v0.6.1, scanpy function *tl.louvain*, igraph: v0.8.0) was performed. We assigned 5 endocrine clusters based on the expression of known canonical markers: *Ins1* ( $\beta$ -cells), *Gcg* ( $\alpha$ -cells), *Sst* ( $\delta$ -cells) and *Ppy* (PP-cells), and a combination of these (polyhormonal cells). In order to further resolve  $\beta$ -cell subclusters, we computed another KNN graph and performed Louvain clustering based on gene sets from literature or gene ontologies from EnrichR. Differential gene expression analyses between clusters irrespective of treatment groups was performed using a variance-overestimated t-test, implemented through scanpy using *tl.rank\_genes\_groups* and helped with assigning  $\beta$ -cell subclusters.

### **5.2.16 Differential Expression Analyses between Treatment Interventions and Subpopulations**

Differential gene expression was performed as described in detail in Oppenländer et al., submitted to Molecular Metabolism. Briefly, analyses were performed on log-normalized counts using limma-trend (v3.42.2) and edgeR (v3.28.1). Genes with an FDR of <0.01 were included for downstream analyses. Linear models were fit to the expression of each gene using *lmFit* function. Genes were then ranked by using an empirical Bayes method (*eBayes*) in order to detect expression changes between

groups and subpopulations. Using the Benjamini Hochberg method, top ranked genes were corrected for FDR and multiple testing. The obtained differentially expressed genes were analyzed for GO terms and KEGG pathways using EnrichR.

### **5.2.17 Pseudotime, Cluster Connectivity and Cell Transitions**

Pseudotime, cluster connectivity, and cell transition analyses were performed as described in detail in Oppenländer et al., submitted to Molecular Metabolism.

Partition-based graph abstraction (PAGA), a measure for cluster connectivity, was used to assess transcriptomic similarities of  $\beta$ -cells between treatment groups.

In order to investigate the pseudotime of  $\beta$ -cell dedifferentiation upon different treatment, cells were ordered along a trajectory by applying diffusion pseudotime (DPT) using *tl.dpt* function in scanpy. Herein, a root-cell was randomly assigned within the cluster of dedifferentiated  $\beta$ -cells. The root cell served as starting point for computing potential cell transitions along a trajectory. Prior, all  $\beta$ -cells were corrected for batches using BBKNN (v1.4.1) from Scanpy. Extreme  $\beta$ -cells were removed from this analysis because they were not part of a linear trajectory. Remaining  $\beta$ -cells were visualized according to Sham, VSG and WT by plotting genes that were significantly and gradually regulated along the cell trajectory.

In order to investigate possible transitions within  $\beta$ -cells in Sham and transitions induced by VSG, we used the stochastic model of RNA velocity (scVelo python package (v0.2.2)). Filtered, top 2000 genes were used to compute first and second order moments for every cell using 30 principal components and 30 nearest neighbors. To validate the extent of cell transitions in Sham- and VSG-derived  $\beta$ -cells, we computed the confidence and length of velocity. Confidence refers to the coherence of RNA velocities, while length indicates the pace of transitions.

### **5.2.18 Scoring ERAD and UPR Markers**

In order to calculate ERAD and UPR scores per cell, we extracted canonical genes implicated in ERAD and UPR. These included the following genes for ERAD: Bag6, Der11, Der12, Der13, Dnajb2, Dnajb4, Dnajb9, Edem1, Edem2, Edem3, Erlin1, Erlin2, Fbxo2, Fbxo6, Herpud1, Hspa5, Hsp90b1, Man1b1, Os9, Sec61b, Nrros, Selenos, Sgta, Sgtb, Svip, Syvn1, Sel1l, Vcp, Usp19, Usp14, Ubqln1, Ubqln2, Yod1, and the following for UPR: Hspa5, Ern1, Xbp1, Edem2, Pdia3, Wfs1, Der11, Der13, Atf6, Gpr85, Nfyc,

Eif2ak3, Eif2a, Atf4, Atf3, Ddit3, Trib3, Herpud1, Aatf, Asns. Based on these genes, scores were then computed using the *tl.score\_genes* function in scanpy for each of the groups: WT, Sham, PF and VSG. Statistical differences of the cell scores among the four groups were further assessed using Welch's Heteroscedastic F Test using Bonferroni correction to adjust the significance level for pairwise comparisons (p value < 0.01, *welch.test* from R package onewaytests (v2.4)).

### **5.2.19 Comparing VSG-Specific $\beta$ -cell Genes with Pregnancy-Specific Genes in Pancreatic Islets**

To assess similarities between VSG- and pregnancy-specific  $\beta$ -cell adaptations, we compared published islet transcriptome datasets from pregnant vs. non-pregnant mice<sup>185-187</sup> with our VSG dataset. To obtain genes unique to VSG, we compared genes from all groups vs. control groups, Sham and PF respectively, using limma-trend as mentioned above, thresholded with an absolute estimated log (fold change) > 0.15 and B > 150. Venn diagrams helped to identify the VSG unique intersection including the overlapping VSG/WT intersection (representing genes with expression levels restored to WT) for up- and down-regulated genes, separately. The list of genes obtained from this analysis was subsequently compared to differentially expressed genes reported in islets during pregnancy (*Rieck et al., Layden et al., and Kim et al.*) and the intersection was visualized using an upset plot. The set size bar plot indicates the total number of genes in each set. The intersection size bar plot shows the total number of genes overlapping between two or more sets.

### **5.2.20 Generation of Graphs and Figures**

Graphs were generated using GraphPad Prism 9, and Adobe Illustrator (2021), R, and Python 3.7.7. Figures from introduction (Figure 1-5) were generated using biorender.com. Graphs presenting scRNA-seq data were generated in collaboration with Subarna Palit (ICB).

### **5.2.21 Data and Code Availability**

The single-cell RNA sequencing dataset generated in this study will be made available at the National Center for Biotechnology Information Gene Expression Omnibus (GEO) upon publication of the manuscript at Molecular Metabolism along with the code and custom scripts for analyzing scRNA-seq data generated in this study by Prof. Dr. Dr. Fabian Theis and Subarna Palit (ICB).



## References

1. O'Neill, S. & O'Driscoll, L. Metabolic syndrome: A closer look at the growing epidemic and its associated pathologies. *Obes. Rev.* **16**, 1–12 (2015).
2. Eizirik, D., Pasquali, L. & Cnop, M. Pancreatic  $\beta$ -cells in type 1 and type 2 diabetes mellitus different pathways to failure. *Nat. Rev. Endocrinol.* **16**, 349–362 (2020).
3. Brugmann, S. A. & Wells, J. M. Building additional complexity to in vitro-derived intestinal tissues. *Stem cell Res. Ther.* **4**, 1–5 (2013).
4. Kiela, P. & Ghishan, F. Physiology of Intestinal Absorption and Secretion. *Best Pract. Res. Clin. Gastroenterol.* **30**, 145–159 (2016).
5. Anderle, P. *et al.* Changes in the transcriptional profile of transporters in the intestine along the anterior-posterior and crypt-villus axes. *BMC Genomics* **6**, 1–17 (2005).
6. Comelli, E. M. *et al.* Biomarkers of human gastrointestinal tract regions. *Mamm. Genome* **20**, 516–527 (2009).
7. Haber, A. L. *et al.* A single-cell survey of the small intestinal epithelium. *Nature* **551**, 333–339 (2017).
8. Middendorp, S. *et al.* Adult Stem Cells in the Small Intestine Are Intrinsically Programmed with Their Location-Specific Function. *Stem Cells* **32**, 1083–1091 (2014).
9. Beumer, J. & Clevers, H. Cell fate specification and differentiation in the adult mammalian intestine. *Nat. Rev. Mol. Cell Biol.* **22**, 39–53 (2021).
10. Barker, N. *et al.* Identification of stem cells in small intestine and colon by marker gene Lgr5. *Nature* **449**, 1003–1007 (2007).
11. Salzman, N. H. *et al.* Enteric defensins are essential regulators of intestinal microbial ecology. *Nat Immunol* **11**, 76–83 (2010).
12. Sato, T. *et al.* Paneth cells constitute the niche for Lgr5 stem cells in intestinal crypts. *Nature* **469**, 415–418 (2011).
13. Ting, H.-A. & von Moltke, J. The Immune Function of Tuft Cells at Gut Mucosal Surfaces and Beyond. *J. Immunol.* **202**, 1321–1329 (2019).
14. Dillon, A. & Lo, D. D. M cells: Intelligent engineering of mucosal immune surveillance. *Front. Immunol.* **10**, 1–13 (2019).
15. Beumer, J. *et al.* Enteroendocrine cells switch hormone expression along the crypt-to-villus BMP signalling gradient. *Nat. Cell Biol.* **20**, 909–916 (2018).
16. Drucker, D. J. The role of gut hormones in glucose homeostasis. *J. Clin. Invest.* **117**, 24–32 (2007).
17. Gribble, F. M. & Reimann, F. Function and mechanisms of enteroendocrine cells and gut hormones in metabolism. *Nat. Rev. Endocrinol.* **15**, 226–237 (2019).
18. Worthington, J. J., Reimann, F. & Gribble, F. M. Enteroendocrine cells-sensory sentinels of the intestinal environment and orchestrators of mucosal immunity. *Mucosal Immunol.* **11**, 3–20 (2018).
19. Billing, L. J. *et al.* Single cell transcriptomic profiling of large intestinal enteroendocrine cells in mice – Identification of selective stimuli for insulin-like peptide-5 and glucagon-like peptide-1 co-expressing cells. *Mol. Metab.* **29**, 158–169 (2019).

20. Grün, D. *et al.* Single-cell messenger RNA sequencing reveals rare intestinal cell types. *Nature* **525**, 251–255 (2015).
21. Habib, A. M. *et al.* Overlap of endocrine hormone expression in the mouse intestine revealed by transcriptional profiling and flow cytometry. *Endocrinology* **153**, 3054–3065 (2012).
22. Steinert, R. E. *et al.* Ghrelin, CCK, GLP-1, and PYY(3-36): Secretory controls and physiological roles in eating and glycemia in health, obesity, and after RYGB. *Physiol. Rev.* **97**, 411–463 (2017).
23. Svendsen, B. *et al.* An analysis of cosecretion and coexpression of gut hormones from male rat proximal and distal small intestine. *Endocrinology* **156**, 847–857 (2015).
24. Cummings, D. *et al.* A Preprandial Rise in Plasma Ghrelin Levels Suggests a Role in Meal Initiation in Humans. *Diabetes* **50**, 1714–1718 (2002).
25. Gibbons, C. *et al.* Comparison of postprandial profiles of ghrelin, active GLP-1, and total PYY to meals varying in fat and carbohydrate and their association with hunger and the phases of satiety. *J. Clin. Endocrinol. Metab.* **98**, 847–855 (2013).
26. Schubert, M. L. & Peura, D. A. Control of Gastric Acid Secretion in Health and Disease. *Gastroenterology* **134**, 1842–1860 (2008).
27. Steinert, R. E. *et al.* Bile acids and gut peptide secretion after bariatric surgery: A 1-year prospective randomized pilot trial. *Obesity* **21**, (2013).
28. Baggio, L. L. & Drucker, D. J. Biology of Incretins: GLP-1 and GIP. *Gastroenterology* **132**, 2131–2157 (2007).
29. Le Gall, M. *et al.* Intestinal plasticity in response to nutrition and gastrointestinal surgery. *Nutr. Rev.* **77**, 129–143 (2019).
30. Beumer, J. & Clevers, H. Regulation and plasticity of intestinal stem cells during homeostasis and regeneration. *Dev.* **143**, 3639–3649 (2016).
31. Aliluev, A. *et al.* Diet-induced alterations in ISC function underlies obesity and pre-diabetes. *Nat. Metab. Revis.* (2021).
32. Beyaz, S. *et al.* High fat diet enhances stemness and tumorigenicity of intestinal progenitors. *Nature* **531**, 53–58 (2016).
33. Yilmaz, Ö. *et al.* mTORC1 in the Paneth cell niche couples intestinal stem cell function to calorie intake. *Nature* **486**, 490–495 (2012).
34. Verdam, F. J. *et al.* Small intestinal alterations in severely obese hyperglycemic subjects. *J. Clin. Endocrinol. Metab.* **96**, 379–383 (2011).
35. Dailey, M. Nutrient-induced intestinal adaption and its effect in obesity. *Physiol. Behav.* 74–78 (2014).
36. Baldassano, S., Amato, A., Cappello, F., Rappa, F. & Mulè, F. Glucagon-like peptide-2 and mouse intestinal adaptation to a high-fat diet. *J. Endocrinol.* **217**, 11–20 (2013).
37. Mao, J. *et al.* Overnutrition stimulates intestinal epithelium proliferation through  $\beta$ -catenin signaling in obese mice. *Diabetes* **62**, 3736–3746 (2013).
38. Mah, A. T., Landeghem, L. Van, Gavin, H. E., Magness, S. T. & Lund, P. K. Impact of diet-induced obesity on intestinal stem cells: Hyperproliferation but impaired intrinsic function that requires insulin/IGF1. *Endocrinology* **155**, 3302–3314 (2014).
39. Lean, M. E. J. & Malkova, D. Altered gut and adipose tissue hormones in overweight and obese individuals: Cause or consequence. *Int. J. Obes.* **40**, 622–632 (2016).



40. Wölnerhanssen, B. K. *et al.* Deregulation of transcription factors controlling intestinal epithelial cell differentiation; A predisposing factor for reduced enteroendocrine cell number in morbidly obese individuals. *Sci. Rep.* **7**, 1–13 (2017).
41. Zhou, W., Davis, E. A., Li, K., Nowak, R. A. & Dailey, M. J. Sex differences influence intestinal epithelial stem cell proliferation independent of obesity. *Physiol. Rep.* **6**, (2018).
42. Richards, P. *et al.* High fat diet impairs the function of glucagon-like peptide-1 producing L-cells. *Peptides* **77**, 21–27 (2016).
43. Aranas, T. *et al.* Lipid-rich diet enhances L-cell density in obese subjects and in mice through improved L-cell differentiation. *J. Nutr. Sci.* **4**, 1–11 (2015).
44. Dusaulcy, R. *et al.* Functional and molecular adaptations of enteroendocrine L-cells in male obese mice are associated with preservation of pancreatic  $\alpha$ -cell function and prevention of hyperglycemia. *Endocrinology* **157**, 3832–3843 (2016).
45. Röder, P. V., Wu, B., Liu, Y. & Han, W. Pancreatic regulation of glucose homeostasis. *Exp. Mol. Med.* **48**, e219 (2016).
46. Brissova, M. *et al.* Assessment of human pancreatic islet architecture and composition by laser scanning confocal microscopy. *J. Histochem. Cytochem.* **53**, 1087–1097 (2005).
47. Wierup, N., Svenson, H., Mulder, H. & Sundler, M. The ghrelin cell: a novel developmentally regulated islet cell in the human pancreas. *Regul. Pept.* **107**, 63–69 (2002).
48. Katsuura, G., Asakawa, A. & Inui, A. Roles of pancreatic polypeptide in regulation of food intake. *Peptides* **23**, 323–329 (2002).
49. Rorsman, P. & Braun, M. Regulation of insulin secretion in human pancreatic islets. *Annu. Rev. Physiol.* **75**, 155–179 (2012).
50. MacDonald, P. E., Joseph, J. W. & Rorsman, P. Glucose-sensing mechanisms in pancreatic  $\beta$ -cells. *Philos. Trans. R. Soc. B Biol. Sci.* **360**, 2211–2225 (2005).
51. Henquin, J. C. Triggering and amplifying pathways of regulation of insulin secretion by glucose. *Diabetes* **49**, 1751–1760 (2000).
52. Porte, D. & Pupo, A. A. Insulin responses to glucose: evidence for a two pool system in man. *J. Clin. Invest.* **48**, 2309–2319 (1969).
53. Birnbaum, M. Identification of a novel gene encoding an insulin-responsive glucose transporter protein. *Cell* **57**, 305–315 (1989).
54. Charron, M. J., Brosius, F. C., Alper, S. L. & Lodish, H. F. A glucose transport protein expressed predominately in insulin-responsive tissues. *Proc. Natl. Acad. Sci. U. S. A.* **86**, 2535–2539 (1989).
55. Leney, S. E. & Tavaré, J. M. The molecular basis of insulin-stimulated glucose uptake: Signalling, trafficking and potential drug targets. *J. Endocrinol.* **203**, 1–18 (2009).
56. Miller, T. B. & Larner, J. Mechanism of control of hepatic glycogenesis by insulin. *J. Biol. Chem.* **248**, 3483–3488 (1973).
57. Freychet, L. *et al.* Effect of intranasal glucagon on blood glucose levels in healthy subjects and hypoglycaemic patients with insulin-dependent diabetes. *Lancet* **1**, 1364–1366 (1988).
58. Nolan, C. J. & Prentki, M. Insulin resistance and insulin hypersecretion in the metabolic syndrome and type 2 diabetes: Time for a conceptual framework shift. *Diabetes Vasc. Dis. Res.* **16**, 118–127 (2019).
59. Hudish, L. I., Reusch, J. E. B. & Sussel, L.  $\beta$  Cell dysfunction during progression of metabolic syndrome to type 2 diabetes. *J. Clin. Invest.* **129**, 4001–4008 (2019).

60. Bensellam, M., Jonas, J.-C. & Laybutt, D. Mechanisms of  $\beta$ -cell dedifferentiation in diabetes: recent findings and future research directions. *J. Endocrinol.* **236**, (2018).
61. Talchai, C., Xuan, S., Lin, H. V., Sussel, L. & Accili, D. Pancreatic  $\beta$  cell dedifferentiation as a mechanism of diabetic  $\beta$  cell failure. *Cell* **150**, 1223–1234 (2012).
62. Halban, P. *et al.* Beta-Cell Failure in Type 2 Diabetes: Postulated Mechanisms and Prospects for Prevention and Treatment. *Diabetes Care* **37**, 1751–1758 (2014).
63. Wang, Z., York, N. W., Nichols, C. G. & Remedi, M. S. Pancreatic  $\beta$ -cell Dedifferentiation in Diabetes and Redifferentiation following Insulin Therapy. *Cell Metab.* **19**, 872–882 (2015).
64. Cinti, F. *et al.* Evidence of  $\beta$ -cell dedifferentiation in human type 2 diabetes. *J. Clin. Endocrinol. Metab.* **101**, 1044–1054 (2016).
65. Blum, B. *et al.* Functional beta-cell maturation is marked by an increased glucose threshold and by expression of urocortin 3. *Nat. Biotechnol.* **30**, 261–264 (2012).
66. van der Meulen, T. *et al.* Urocortin 3 Marks Mature Human Primary and Embryonic Stem Cell-Derived Pancreatic Alpha and Beta Cells. *PLoS One* **7**, 1–12 (2012).
67. Kuo, T. *et al.* Induction of  $\alpha$  cell-restricted Gc in dedifferentiating  $\beta$  cells contributes to stress-induced  $\beta$ -cell dysfunction. *JCI Insight* **4**, (2019).
68. Sachs, S. *et al.* Targeted pharmacological therapy restores  $\beta$ -cell function for diabetes remission. *Nat. Metab.* **2**, 192–209 (2020).
69. Kim-Muller, J. Y. *et al.* Aldehyde dehydrogenase 1a3 defines a subset of failing pancreatic  $\beta$  cells in diabetic mice. *Nat. Commun.* **7**, 2016 (2016).
70. Dahan, T. *et al.* Pancreatic  $\beta$ -Cells Express the Fetal Islet Hormone Gastrin in Rodent and Human Diabetes. *Islet Stud.* **66**, 426–436 (2017).
71. Camunas-Soler, J. *et al.* Patch-Seq Links Single-Cell Transcriptomes to Human Islet Dysfunction in Diabetes. *Cell Metab.* **31**, 1017–1031 (2020).
72. Salinno, C. *et al.* CD81 marks immature and dedifferentiated pancreatic  $\beta$ -cells. *Mol. Metab.* **49**, (2021).
73. Magkos, F., Hjorth, M. F. & Astrup, A. Diet and exercise in the prevention and treatment of type 2 diabetes mellitus. *Nat. Rev. Endocrinol.* **16**, 545–555 (2020).
74. Colberg, S. R. *et al.* Physical activity/exercise and diabetes: A position statement of the American Diabetes Association. *Diabetes Care* **39**, 2065–2079 (2016).
75. Lin, X. *et al.* Effects of exercise training on cardiorespiratory fitness and biomarkers of cardiometabolic health: A systematic review and meta-analysis of randomized controlled trials. *J. Am. Heart Assoc.* **4**, 1–28 (2015).
76. Schellenberg, E., Drydon, D., Vandermeer, B., Ha, V. & Korownyk, C. Lifestyle Interventions for Patients With and at Risk for Type 2 Diabetes. *Ann. Intern. Med.* (2013).
77. Intervention, L. & Metformin, O. R. Reduction of the incidence of type 2 diabetes with lifestyle intervention or metformin. *Int. Urol. Nephrol.* **34**, 162–163 (2002).
78. Weickert, M. O. Nutritional Modulation of Insulin Resistance. *Scientifica (Cairo)*. **2012**, 1–15 (2012).
79. Dela, F., Von Linstow, M. E., Mikines, K. J. & Galbo, H. Physical training may enhance  $\beta$ -cell function in type 2 diabetes. *Am. J. Physiol. - Endocrinol. Metab.* **287**, 1024–1031 (2004).
80. Solomon, T. P. J. *et al.* Improved pancreatic  $\beta$ -cell function in type 2 diabetic patients after lifestyle-induced weight loss is related to glucose-dependent insulinotropic polypeptide. *Diabetes Care* vol. 33

- 1561–1566 (2010).
81. Hjorth, M. F. *et al.* Pretreatment fasting plasma glucose and insulin modify dietary weight loss success: Results from 3 randomized clinical trials. *Am. J. Clin. Nutr.* **106**, 499–505 (2017).
  82. Greenway, F. L. Physiological adaptations to weight loss and factors favouring weight regain. *Int. J. Obes.* **39**, 1188–1196 (2015).
  83. Martins, C., Dutton, G. R., Hunter, G. R. & Gower, B. A. Revisiting the Compensatory Theory as an explanatory model for relapse in obesity management. *Am. J. Clin. Nutr.* **112**, 1170–1179 (2020).
  84. Campbell, J. & Drucker, D. J. Islet  $\alpha$  cells and glucagon--critical regulators of energy homeostasis. *Nat. Rev. Endocrinol.* 329–338 (2015).
  85. Tahrani, A. A., Barnett, A. H. & Bailey, C. J. Pharmacology and therapeutic implications of current drugs for type 2 diabetes mellitus. *Nat. Rev. Endocrinol.* **12**, 566–592 (2016).
  86. Deacon, C. F. Dipeptidyl peptidase 4 inhibitors in the treatment of type 2 diabetes mellitus. *Nat. Rev. Endocrinol.* **16**, 642–653 (2020).
  87. Clemmensen, C. *et al.* Emerging hormonal-based combination pharmacotherapies for the treatment of metabolic diseases. *Nat. Rev. Endocrinol.* **15**, 90–104 (2019).
  88. Alexiadou, K., Anyiam, O. & Tan, T. Cracking the combination: Gut hormones for the treatment of obesity and diabetes. *J. Neuroendocrinol.* **31**, 1–8 (2019).
  89. Finan, B. *et al.* Unimolecular dual incretins maximize metabolic benefits in rodents, monkeys, and humans. *Sci. Transl. Med.* **5**, (2013).
  90. Frias, J. P. *et al.* The Sustained Effects of a Dual GIP/GLP-1 Receptor Agonist, NNC0090-2746, in Patients with Type 2 Diabetes. *Cell Metab.* **26**, 343-352.e2 (2017).
  91. Sachs, S. *et al.* Plasma proteome profiles treatment efficacy of incretin dual agonism in diet-induced obese female and male mice. *Diabetes, Obes. Metab.* **23**, 195–207 (2021).
  92. Rubino, F. *et al.* Metabolic surgery in the treatment algorithm for type 2 diabetes: A joint statement by international diabetes organizations. *Diabetes Care* **39**, 861–877 (2016).
  93. Buchwald, H. *et al.* Weight and type 2 diabetes after bariatric surgery: systematic review and meta-analysis. *Am. J. Med.* **122**, (2009).
  94. Schauer, P. R. *et al.* Bariatric Surgery versus Intensive Medical Therapy for Diabetes — 5-Year Outcomes. *N. Engl. J. Med.* **376**, 641–651 (2017).
  95. Maciejewski, M. L. *et al.* Bariatric surgery and long-term durability of weight loss. *JAMA Surg.* **151**, 1046–1055 (2016).
  96. Welbourn, R. *et al.* Bariatric Surgery Worldwide: Baseline Demographic Description and One-Year Outcomes from the Fourth IFSO Global Registry Report 2018. *Obes. Surg.* **29**, 782–795 (2019).
  97. Seeley, R. J., Chambers, A. P. & Sandoval, D. A. The role of gut adaptation in the potent effects of multiple bariatric surgeries on obesity and diabetes. *Cell Metab.* **21**, 369–378 (2015).
  98. Evers, S. S., Sandoval, D. A. & Seeley, R. J. The Physiology and Molecular Underpinnings of the Effects of Bariatric Surgery on Obesity and Diabetes. *Annu. Rev. Physiol.* **79**, (2017).
  99. Clemmensen, C. *et al.* Gut-Brain Cross-Talk in Metabolic Control. *Cell* **168**, 758–774 (2017).
  100. Stefater, M. A. *et al.* Sleeve Gastrectomy Induces Loss of Weight and Fat Mass in Obese Rats, but Does Not Affect Leptin Sensitivity. *gastroent* **138**, 2426–2436 (2010).

101. Chambers, A. P. *et al.* The Effects of Vertical Sleeve Gastrectomy in Rodents Are Ghrelin Independent. *Gastroenterology* **144**, 50–52 (2013).
102. Mokadem, M., Zechner, J. F., Uchida, A. & Aguirre, V. Leptin is required for glucose homeostasis after roux-en-y gastric bypass in mice. *PLoS One* **10**, 1–17 (2015).
103. Wilson-Pérez, H. E. *et al.* Vertical sleeve gastrectomy is effective in two genetic mouse models of glucagon-like peptide 1 receptor deficiency. *Diabetes* **62**, 2380–2385 (2013).
104. Mokadem, M., Zechner, J. F., Margolskee, R. F., Drucker, D. J. & Aguirre, V. Effects of Roux-en-Y gastric bypass on energy and glucose homeostasis are preserved in two mouse models of functional glucagon-like peptide-1 deficiency. *Mol. Metab.* **3**, 191–201 (2014).
105. Boland, B. *et al.* The PYY/Y2R-deficient mouse responds normally to high-fat diet and gastric bypass surgery. *Nutrients* **11**, 1–15 (2019).
106. Patti, M.-E. *et al.* Serum Bile Acids Are Higher in Humans With Prior Gastric Bypass: Potential Contribution to Improved Glucose and Lipid Metabolism. *Obesity* **17**, 1671–1677 (2009).
107. Tremaroli, V. *et al.* Roux-en-Y Gastric Bypass and Vertical Banded Gastroplasty Induce Long-Term Changes on the Human Gut Microbiome Contributing to Fat Mass Regulation. *Cell Metab.* **22**, 228–238 (2015).
108. Ramirez-Perez, O., Cruz-Ramon, V., Chinchilla-Lopez, P. & Mendez-Sanchez, N. The Role of the Gut Microbiota in Bile Acid Metabolism. *Ann. Hepatol.* **16**, (2017).
109. Lozupone, C. A., Stombaugh, J. I., Gordon, J. I., Jansson, J. K. & Knight, R. Diversity, stability and resilience of the human gut microbiota. *Nature* **489**, 220–230 (2012).
110. Wahlström, A., Sayin, S. I., Marschall, H. U. & Bäckhed, F. Intestinal Crosstalk between Bile Acids and Microbiota and Its Impact on Host Metabolism. *Cell Metab.* **24**, 41–50 (2016).
111. Kurdi, P., Kawanishi, K., Mizutani, K. & Yokota, A. Mechanism of growth inhibition by free bile acids in lactobacilli and bifidobacteria. *J. Bacteriol.* **188**, 1979–1986 (2006).
112. Ridlon, J., Kang, D., Hylemon, P. & Bajaj, J. Bile Acids and the Gut Microbiome. *Curr. Opin. Gastroenterol.* **30**, 332–338 (2013).
113. Gutiérrez-Repiso, C., Moreno-Indias, I., Hollanda, A. De & Martín-Núñez, G. M. Gut microbiota specific signatures are related to the successful rate of bariatric surgery. *Am. J. Transl. Res.* **11**, 942–952 (2019).
114. Wang, M. *et al.* Role of Gut Microbiome and Microbial Metabolites in Alleviating Insulin Resistance After Bariatric Surgery. *Obes. Surg.* **31**, 327–336 (2021).
115. Jackness, C. *et al.* Very lowcalorie diet mimics the early beneficial effect of rouxen-Y gastric bypass on insulin sensitivity and  $\beta$ -cell function in type 2 diabetic patients. *Diabetes* **62**, 3027–3032 (2013).
116. Bradley, D. *et al.* Gastric bypass and banding equally improve insulin sensitivity and  $\beta$  cell function. *J. Clin. Invest.* **122**, 4667–4674 (2012).
117. Abu-Gazala, S. *et al.* Sleeve gastrectomy improves glycemia independent of weight loss by restoring hepatic insulin sensitivity. *Diabetes* **67**, 1079–1085 (2018).
118. Douros, J. D. *et al.* Sleeve gastrectomy rapidly enhances islet function independently of body weight. *JCI Insight* **4**, e126688 (2019).
119. Langer, F. B. *et al.* Sleeve gastrectomy and gastric banding: Effects on plasma ghrelin levels. *Obes. Surg.* **15**, 1024–1029 (2005).
120. Larraufie, P. *et al.* Important Role of the GLP-1 Axis for Glucose Homeostasis after Bariatric Surgery. *Cell Rep.* **26**, 1399-1408.e6 (2019).

121. Rollins, K. A. *et al.* The L cell transcriptome is unaffected by vertical sleeve gastrectomy but highly dependent upon position within the gastrointestinal tract. *Peptides* **113**, 22–34 (2019).
122. Cavin, J. B. *et al.* Differences in Alimentary Glucose Absorption and Intestinal Disposal of Blood Glucose after Roux-en-Y Gastric Bypass vs Sleeve Gastrectomy. *Gastroenterology* **150**, 454-464.e9 (2016).
123. Kim, K.-S. *et al.* Vertical Sleeve Gastrectomy Induces Enteroendocrine Cell Differentiation of Intestinal Stem Cells Through Farnesoid X Receptor Activation. *bioRxiv* 2021.04.22.440705 (2021).
124. Ribeiro-Parenti, L. *et al.* Bariatric surgery induces a new gastric mucosa phenotype with increased functional glucagon-like peptide-1 expressing cells. *Nat. Commun.* **12**, 1–11 (2021).
125. Kim, K. *et al.* Glycemic effect of pancreatic proglucagon in mouse sleeve gastrectomy Find the latest version : Glycemic effect of pancreatic proglucagon in mouse sleeve gastrectomy. *JCI Insight* **4**, (2019).
126. Garibay, D. *et al.*  $\beta$  Cell GLP-1R Signaling Alters  $\alpha$  Cell Proglucagon Processing after Vertical Sleeve Gastrectomy in Mice. *Cell Rep.* **23**, 967–973 (2018).
127. Chambers, A. P. *et al.* The Role of Pancreatic Preproglucagon in Glucose Homeostasis in Mice. *Cell Metab.* **25**, 927-934.e3 (2017).
128. Marchetti, P. *et al.* A local glucagon-like peptide 1 (GLP-1) system in human pancreatic islets. *Diabetologia* **55**, 3262–3272 (2012).
129. Víttek, L. & Haluzík, M. The role of bile acids in metabolic regulation. *J. Endocrinol.* **228**, R85–R96 (2016).
130. Brighton, C. A. *et al.* Bile acids trigger GLP-1 release predominantly by accessing basolaterally located G protein-coupled bile acid receptors. *Endocrinology* **156**, 3961–3970 (2015).
131. Kumar, D. P. *et al.* Activation of transmembrane bile acid receptor tgr5 modulates pancreatic islet - Cells to promote glucose homeostasis. *J. Biol. Chem.* **291**, 6626–6640 (2016).
132. McGavigan, A. K. *et al.* TGR5 contributes to glucoregulatory improvements after vertical sleeve gastrectomy in mice. *Gut* **66**, 226–234 (2017).
133. Teodoro, J., Rolo, A. & Palmera, C. Hepatic FXR: key regulator of whole-body energy metabolism. *Trends Endocrinol. Metab.* **22**, 458–466 (2011).
134. Yamagata, K. *et al.* Bile acids regulate gluconeogenic gene expression via small heterodimer partner-mediated repression of hepatocyte nuclear factor 4 and Foxo1. *J. Biol. Chem.* **279**, 23158–23165 (2004).
135. Ma, K., Saha, P. K., Chan, L. & Moore, D. D. Farnesoid X receptor is essential for normal glucose homeostasis. *J. Clin. Invest.* **116**, 1102–1109 (2006).
136. Düfer, M. *et al.* Bile Acids Acutely Stimulate Insulin Secretion of. *Diabetes* **61**, 1479–1489 (2012).
137. Ryan, K. K. *et al.* FXR is a molecular target for the effects of vertical sleeve gastrectomy. *Nature* **509**, 183–188 (2014).
138. Alonso, L. C. *et al.* Simultaneous measurement of insulin sensitivity, insulin secretion, and the disposition index in conscious unhandled mice. *Obesity* **20**, 1403–1412 (2012).
139. Montgomery, M. K. *et al.* Mouse strain-dependent variation in obesity and glucose homeostasis in response to high-fat feeding. *Diabetologia* **56**, 1129–1139 (2013).
140. Lang, P., Hasselwander, S., Li, H. & Xia, N. Effects of different diets used in diet-induced obesity models on insulin resistance and vascular dysfunction in C57BL/6 mice. *Sci. Rep.* **9**, 1–14 (2019).
141. Li, J., Wu, H., Liu, Y. & Yang, L. High fat diet induced obesity model using four strains of mice: kunming, c57bl/6, balb/c and icr. *Exp. Anim.* **69**, 326–335 (2020).

142. Siersbæk, M. S. *et al.* C57BL/6J substrain differences in response to high-fat diet intervention. *Sci. Rep.* **10**, 1–15 (2020).
143. Hummel, K. P., Dickie, M. M. & Coleman, D. L. Diabetes, a new mutation in the mouse. *Science (80-. )*. **153**, 1127–1128 (1966).
144. Dalbøge, L. S. *et al.* Characterisation of age-dependent beta cell dynamics in the male db/db mice. *PLoS One* **8**, 1–10 (2013).
145. Coleman, D. L. Obese and diabetes: Two mutant genes causing diabetes-obesity syndromes in mice. *Diabetologia* **14**, 141–148 (1978).
146. Sachdeva, M. M. & Stoffers, D. A. Minireview: Meeting the demand for insulin: Molecular mechanisms of adaptive postnatal  $\beta$ -cell mass expansion. *Mol. Endocrinol.* **23**, 747–758 (2009).
147. Pan, F. C. & Wright, C. Pancreas organogenesis: From bud to plexus to gland. *Dev. Dyn.* **240**, 530–565 (2011).
148. Li, F. *et al.* Preventative Sleeve Gastrectomy Contributes to Maintaining  $\beta$  Cell Function in db/db Diabetic Mouse. *Obes. Surg.* **26**, 2402–2410 (2016).
149. Kang, T. *et al.* Characterization of signaling pathways associated with pancreatic  $\beta$ -cell adaptive flexibility in compensation of obesity-linked diabetes in db-db mice. *Mol. Cell. Proteomics* **19**, 971–993 (2020).
150. Neelankal John, A., Ram, R. & Jiang, F. X. RNA-Seq Analysis of Islets to Characterise the Dedifferentiation in Type 2 Diabetes Model Mice db/db. *Endocr. Pathol.* **29**, 207–221 (2018).
151. Ishida, E., Kim-Muller, J. Y. & Accili, D. Pair feeding, but not insulin, phloridzin, or rosiglitazone treatment, curtails markers of  $\beta$ -cell dedifferentiation in db/db mice. *Diabetes* **66**, 2092–2101 (2017).
152. Oliver-Krasinski, J. M. & Stoffers, D. A. On the origin of the beta cell. *genes Dev.* 1998–2021 (2008).
153. Gittes, G. K., Rutter, W. J. & Debas, H. T. Initiation of gastrin expression during the development of the mouse pancreas. *Am. J. Surg.* **165**, 23–26 (1993).
154. Wolf, F. A. *et al.* PAGA: graph abstraction reconciles clustering with trajectory inference through a topology preserving map of single cells. *Genome Biol.* **20**, 1–9 (2019).
155. Bearrows, S. C. *et al.* Chromogranin B regulates early-stage insulin granule trafficking from the Golgi in pancreatic islet  $\beta$ -cells. *J. Cell Sci.* **132**, (2019).
156. Dolai, S. *et al.* Synaptotagmin-7 Functions to Replenish Insulin Granules for Exocytosis in Human Islet  $\beta$ -Cells. *Diabetes* **65**, 1962–1976 (2016).
157. Sadoul, K. *et al.* SNAP-25 is expressed in islets of Langerhans and is involved in insulin release. *J. Cell Biol.* **128**, 1019–1028 (1995).
158. Gremlich, S., Roduit, R. & Thorens, B. Dexamethasone induces posttranslational degradation of GLUT2 and inhibition of insulin secretion in isolated pancreatic  $\beta$  cells. Comparison with the effects of fatty acids. *J. Biol. Chem.* **272**, 3216–3222 (1997).
159. Ohtsubo, K. *et al.* Dietary and genetic control of glucose transporter 2 glycosylation promotes insulin secretion in suppressing diabetes. *Cell* **123**, 1307–1321 (2005).
160. Haghverdi, L., Büttner, M., Wolf, F. A., Büttner, F. & Theis, F. J. Diffusion pseudotime robustly reconstructs lineage branching. *Nat. Methods* **13**, 845–848 (2016).
161. Fonseca, S. G., Gromada, J. & Urano, F. Endoplasmic reticulum stress and pancreatic  $\beta$ -cell death. *Trends Endocrinol. Metab.* **22**, 266–274 (2011).

162. Bilekova, S., Sachs, S. & Lickert, H. Pharmacological Targeting of Endoplasmic Reticulum Stress in Pancreatic Beta Cells. *Trends Pharmacol. Sci.* **42**, 85–95 (2021).
163. Lee, A. S. The ER chaperone and signaling regulator GRP78/BiP as a monitor of endoplasmic reticulum stress. *Methods* **35**, 373–381 (2005).
164. Abreu, D. *et al.* Wolfram syndrome 1 gene regulates pathways maintaining beta-cell health and survival. *Lab. Investig.* **100**, 849–862 (2020).
165. Zmuda, E. J. *et al.* The Roles of ATF3, an Adaptive-Response Gene, in High-Fat-Diet-Induced Diabetes and Pancreatic  $\beta$ -Cell Dysfunction. *Mol. Endocrinol.* **24**, 1423–1433 (2019).
166. Sowers, C. R. *et al.* The protein kinase PERK/EIF2AK3 regulates proinsulin processing not via protein synthesis but by controlling endoplasmic reticulum chaperones. *J. Biol. Chem.* **293**, 5134–5149 (2018).
167. Shrestha, N. *et al.* Sel1L-Hrd1 ER-associated degradation maintains  $\beta$  cell identity via TGF- $\beta$  signaling. *J. Clin. Invest.* **130**, 3499–3510 (2020).
168. Hu, Y. *et al.* Endoplasmic reticulum-associated degradation (ERAD) has a critical role in supporting glucose-stimulated insulin secretion in pancreatic B-cells. *Diabetes* **68**, 733–746 (2019).
169. Christianson, J. C. *et al.* Defining human ERAD networks through an integrative mapping strategy. *Nat. Cell Biol.* **14**, 93–105 (2012).
170. Bader, E. *et al.* Identification of proliferative and mature  $\beta$ -cells in the islets of Langerhans. *Nature* **535**, 430–434 (2016).
171. Baron, M. *et al.* A Single-Cell Transcriptomic Map of the Human and Mouse Pancreas Reveals Inter- and Intra-cell Population Structure. *Cell Syst.* **3**, 346–360 (2016).
172. Xin, Y. *et al.* Pseudotime ordering of single human B-cells reveals states of insulin production and unfolded protein response. *Diabetes* vol. 67 1783–1794 (2018).
173. Segerstolpe, Å. *et al.* Single-Cell Transcriptome Profiling of Human Pancreatic Islets in Health and Type 2 Diabetes. *Cell Metab.* **24**, 593–607 (2016).
174. Fang, Z. *et al.* Single-Cell Heterogeneity Analysis and CRISPR Screen Identify Key  $\beta$ -Cell-Specific Disease Genes. *Cell Rep.* **26**, 3132–3144.e7 (2019).
175. Feng, Y. *et al.* Characterizing pancreatic  $\beta$ -cell heterogeneity in the streptozotocin model by single-cell transcriptomic analysis. *Mol. Metab.* **37**, (2020).
176. Farack, L. *et al.* Transcriptional Heterogeneity of Beta Cells in the Intact Pancreas. *Dev. Cell* **48**, 115–125 (2019).
177. Modi, H. *et al.* Ins2 gene bursting activity defines a mature  $\beta$ -cell state. *bioRxiv* (2019).
178. Wang, N., Zhua, Y., Yuanb, Q. & Dea, W. Long Noncoding RNA Meg3 Regulates Mafa Expression in Mouse Beta Cells by Inactivating Rad21, Smc3 or Sin3 $\alpha$ . *Cell. Physiol. Biochem.* 2031–2043 (2018).
179. Wang, Y. *et al.* Long-Term Correction of Diabetes in Mice by In Vivo Reprogramming of Pancreatic Ducts. *Mol. Ther.* **26**, 1327–1342 (2018).
180. Kushner, J. A. *et al.* Cyclins D2 and D1 Are Essential for Postnatal Pancreatic  $\beta$ -Cell Growth. *Mol. Cell. Biol.* **25**, 3752–3762 (2005).
181. Xu, E. E., Sasaki, S., Speckmann, T., Nian, C. & Lynn, F. C. SOX4 allows facultative  $\beta$ -cell proliferation through repression of cdkn1a. *Diabetes* **66**, 2213–2219 (2017).
182. Ernst, S., Demirci, C., Valle, S., Velazquez-Garcia, S. & Ocaña, A. G.-. Mechanisms in the adaptation of maternal  $\beta$ -cells during pregnancy. *Diabetes Manag.* **1**, 239–248 (2011).

183. Kondegowda, N. G. *et al.* Osteoprotegerin and Denosumab Stimulate Human Beta Cell Proliferation through Inhibition of the Receptor Activator of NF- $\kappa$ B Ligand Pathway. *Cell Metab.* **22**, 77–85 (2015).
184. Schmitz, F., Roscioni, S. & Lickert, H. Repurposing an Osteoporosis Drug for  $\beta$  Cell Regeneration in Diabetic Patients. *Cell Metab.* **22**, 58–59 (2015).
185. Rieck, S. *et al.* The transcriptional response of the islet to pregnancy in mice. *Mol. Endocrinol.* **23**, 1702–1712 (2009).
186. Layden, B. T. *et al.* Regulation of pancreatic islet gene expression in mouse islets by pregnancy. *J. Endocrinol.* **207**, 265–279 (2010).
187. Kim, H. *et al.* Serotonin regulates pancreatic beta cell mass during pregnancy. *Nat. Med.* **16**, (2010).
188. Kleinert, M. *et al.* Animal models of obesity and diabetes mellitus. *Nat. Rev. Endocrinol.* **14**, 140–162 (2018).
189. Shortreed, K. E. *et al.* Muscle-specific adaptations, impaired oxidative capacity and maintenance of contractile function characterize diet-induced obese mouse skeletal muscle. *PLoS One* **4**, (2009).
190. Nicholson, A. *et al.* Diet induced obesity in two C57BL/6 substrains with intact or mutant Nicotinamide Nucleotide Transhydrogenase (Nnt) gene. *Obesity* **18**, 1902–1905 (2010).
191. Hull, R. L. *et al.* High fat feeding unmasks variable insulin responses in male C57BL/6 mouse substrains. *J. Endocrinol.* **233**, 53–64 (2017).
192. Gupta, D. *et al.* Temporal characterization of  $\beta$  cell-adaptive and -maladaptive mechanisms during chronic high-fat feeding in C57BL/6NTac mice. *J. Biol. Chem.* **292**, 12449–12459 (2017).
193. Sinha, R. *et al.* Pre-diabetes increases tuberculosis disease severity while high body fat without impaired glucose tolerance is protective. *bioRxiv* (2021).
194. Mumphrey, M. B. *et al.* Gastric bypass surgery in lean adolescent mice prevents diet-induced obesity later in life. *Sci. Rep.* **9**, 1–14 (2019).
195. Mul, J. D. *et al.* MGAT2 deficiency and vertical sleeve gastrectomy have independent metabolic effects in the mouse. *Am. J. Physiol. - Endocrinol. Metab.* **307**, E1065–E1072 (2014).
196. Arble, D. M., Sandoval, D. A., Turek, F. W., Woods, S. C. & Seeley, R. J. Metabolic effects of bariatric surgery in mouse models of circadian disruption. *Int. J. Obes.* **39**, 1310–1318 (2015).
197. Pressler, J. W. *et al.* Vertical sleeve gastrectomy restores glucose homeostasis in apolipoprotein A-IV KO mice. *Diabetes* **64**, 498–507 (2015).
198. Arble, D. M., Schwartz, A. R., Polotsky, V. Y., Sandoval, D. A. & Seeley, R. J. Vertical sleeve gastrectomy improves ventilatory drive through a leptin-dependent mechanism. *JCI Insight* **4**, 1–11 (2019).
199. Ding, L. *et al.* Vertical sleeve gastrectomy activates GPBAR-1/TGR5 to sustain weight loss, improve fatty liver, and remit insulin resistance in mice. *Hepatology* **64**, 760–773 (2016).
200. Douros, J. *et al.* Enhanced glucose control following vertical sleeve gastrectomy does not require a  $\beta$ -cell GLP-1 R. *Diabetes* **67**, 1504–1511 (2018).
201. Griffin, C. *et al.* Inflammatory responses to dietary and surgical weight loss in male and female mice. *Biol. Sex Differ.* **10**, 1–16 (2019).
202. Bozadjieva Kramer, N. *et al.* The Role of Elevated Branched-Chain Amino Acids in the Effects of Vertical Sleeve Gastrectomy to Reduce Weight and Improve Glucose Regulation. *Cell Rep.* **33**, 108239 (2020).
203. Laferrère, B. *et al.* Effect of weight loss by gastric bypass surgery versus hypocaloric diet on glucose and incretin levels in patients with type 2 diabetes. *J. Clin. Endocrinol. Metab.* **93**, 2479–2485 (2008).



204. Jørgensen, N. B. *et al.* Acute and long-term effects of Roux-en-Y gastric bypass on glucose metabolism in subjects with Type 2 diabetes and normal glucose tolerance. *Am. J. Physiol. - Endocrinol. Metab.* **303**, 122–131 (2012).
205. Chambers, A. P. *et al.* Weight-Independent Changes in Blood Glucose Homeostasis after Gastric Bypass or Vertical Sleeve Gastrectomy in Rats. *Gastroenterology* **141**, 950–958 (2011).
206. Ahn, C. H. *et al.* Vertical sleeve gastrectomy induces distinctive transcriptomic responses in liver, fat and muscle. *Sci. Rep.* **11**, 1–11 (2021).
207. Grayson, B. E. *et al.* Weight loss by calorie restriction versus bariatric surgery differentially regulates the HPA axis in male rats. *Stress* **17**, 484–493 (2014).
208. Sharma, R. B. *et al.* Insulin demand regulates  $\beta$  cell number via the unfolded protein response. *J. Clin. Invest.* **125**, 3831–3846 (2015).
209. Jiménez, A. *et al.* GLP-1 and glucose tolerance after sleeve gastrectomy in morbidly obese subjects with type 2 diabetes. *Diabetes* **63**, 3372–3377 (2014).
210. Boland, B. B. *et al.* Combined loss of GLP-1R and Y2R does not alter progression of high-fat diet-induced obesity or response to RYGB surgery in mice. *Mol. Metab.* **25**, 64–72 (2019).
211. Hutch, C. R. & Sandoval, D. The role of GLP-1 in the metabolic success of bariatric surgery. *Endocrinology* **158**, 4139–4151 (2017).
212. de Souza, A. H. *et al.* Intra-islet GLP-1, but not CCK, is necessary for  $\beta$ -cell function in mouse and human islets. *Sci. Rep.* **10**, (2020).
213. Rivera, J. F., Costes, S., Gurlo, T., Glabe, C. G. & Butler, P. C. Autophagy defends pancreatic  $\beta$  cells from Human islet amyloid polypeptide-induced toxicity. *J. Clin. Invest.* **124**, 3489–3500 (2014).
214. Imai, J. *et al.* Regulation of pancreatic beta cell mass by neuronal signals from the liver. *Science (80-. ).* **322**, 1250–4 (2008).
215. El Ouaamari, A. *et al.* SerpinB1 Promotes Pancreatic  $\beta$  Cell Proliferation. *Cell Metab.* **23**, 194–205 (2016).
216. Stamateris, R. E., Sharma, R. B., Hollern, D. A. & Alonso, L. C. Adaptive  $\beta$ -cell proliferation increases early in high-fat feeding in mice, concurrent with metabolic changes, with induction of islet cyclin D2 expression. *Am. J. Physiol. - Endocrinol. Metab.* **305**, (2013).
217. Stewart, A. F. *et al.* Human  $\beta$ -Cell proliferation and intracellular signaling: Part 3. *Diabetes* vol. 64 1872–1885 (2015).
218. Mosser, R. E. *et al.* High-fat diet-induced  $\beta$ -cell proliferation occurs prior to insulin resistance in C57Bl/6J male mice. *Am. J. Physiol. - Endocrinol. Metab.* **308**, E573–E582 (2015).
219. Lindqvist, A. *et al.* Gastric bypass improves  $\beta$ -cell function and increases  $\beta$ -cell mass in a porcine model. *Diabetes* **63**, 1665–1671 (2014).
220. Miskelly, M. *et al.* GK-rats respond to gastric bypass surgery with improved glycemia despite unaffected insulin secretion and beta cell mass. *Peptides* **136**, 170445 (2021).
221. Grong, E. *et al.* Sleeve gastrectomy, but not duodenojejunostomy, preserves total beta-cell mass in Goto-Kakizaki rats evaluated by three-dimensional optical projection tomography. *Surg. Endosc.* **30**, 532–542 (2016).
222. Elgenaied, I. *et al.* Factors associated with complete and partial remission, improvement, or unchanged diabetes status of obese adults 1 year after sleeve gastrectomy. *Surg. Obes. Relat. Dis.* **16**, 1521–1530 (2020).
223. Luo, Y. *et al.* Predictive model of type 2 diabetes remission after metabolic surgery in Chinese patients.

- Int. J. Endocrinol.* **2020**, (2020).
224. Burke, S. J. *et al.* Db / db Mice Exhibit Features of Human Type 2 Diabetes That Are Not Present in Weight-Matched C57BL/6J Mice Fed a Western Diet. *J. Diabetes Res.* **2017**, (2017).
  225. López-Lluch, G. *et al.* Calorie restriction induces mitochondrial biogenesis and bioenergetic efficiency. *Proc. Natl. Acad. Sci. U. S. A.* **103**, 1768–1773 (2006).
  226. Lanza, I. R. *et al.* Chronic caloric restriction preserves mitochondrial function in senescence without increasing mitochondrial biogenesis. *Cell Metab.* **16**, 777–788 (2012).
  227. Gu, C. *et al.* Pancreatic  $\beta$  cells require NeuroD to achieve and maintain functional maturity. *Cell Metab.* **11**, 298–310 (2011).
  228. Hang, Y. *et al.* The MafA transcription factor becomes essential to islet  $\beta$ -cells soon after birth. *Diabetes* **63**, 1994–2005 (2014).
  229. Nishimura, W., Takahashi, S. & Yasuda, K. MafA is critical for maintenance of the mature beta cell phenotype in mice. *Diabetologia* **58**, 566–574 (2015).
  230. Ediger, B. N. *et al.* Islet-1 is essential for pancreatic  $\beta$ -cell function. *Diabetes* **63**, 4206–4217 (2014).
  231. Swisa, A. *et al.* PAX6 maintains  $\beta$  cell identity by repressing genes of alternative islet cell types. *J. Clin. Invest.* **127**, 230–243 (2017).
  232. Mitchell, R. K. *et al.* The transcription factor Pax6 is required for pancreatic  $\beta$  cell identity, glucose-regulated ATP synthesis, and Ca<sup>2+</sup> dynamics in adult mice. *J. Biol. Chem.* **292**, 8892–8906 (2017).
  233. Gutiérrez, G. D. *et al.* Pancreatic  $\beta$  cell identity requires continual repression of non- $\beta$  cell programs. *J. Clin. Invest.* **127**, 244–259 (2017).
  234. Gao, T. *et al.* Pdx1 maintains  $\beta$  cell identity and function by repressing an  $\alpha$  cell program. *Cell Metab.* **19**, 259–271 (2014).
  235. Buteau, J. & Accili, D. Regulation of pancreatic  $\beta$ -cell function by the forkhead protein FoxO1. *Diabetes, Obes. Metab.* **9**, 140–146 (2007).
  236. Huang, J. L. *et al.* Genetic deletion of Urocortin 3 does not prevent functional maturation of beta cells. *J. Endocrinol.* **246**, 69–78 (2020).
  237. Hassler, J. R. *et al.* The IRE1 $\alpha$ /XBP1s Pathway Is Essential for the Glucose Response and Protection of  $\beta$  Cells. *PLoS Biol.* **13**, (2015).
  238. Sheng, C. *et al.* Reversibility of  $\beta$  -Cell-Specific Transcript Factors Expression by Long-Term Caloric Restriction in db/db Mouse. *J. Diabetes Res.* (2016) doi:10.1155/2016/6035046.
  239. Weinberg, N., Ouziel-Yahalom, L., Knoller, S., Efrat, S. & Dor, Y. Lineage tracing evidence for in vitro dedifferentiation but rare proliferation of mouse pancreatic  $\beta$ -cells. *Diabetes* **56**, 1299–1304 (2007).
  240. Billestrup, N. & Otonkoski, T. Dedifferentiation for Replication of Human  $\beta$ -Cells. *Diabetes* **57**, 1457 LP – 1458 (2008).
  241. Parnaud, G. *et al.* Proliferation of sorted human and rat beta cells. *Diabetologia* **51**, 91–100 (2008).
  242. Puri, S. *et al.* Replication confers  $\beta$  cell immaturity. *Nat. Commun.* **9**, (2018).
  243. Guida, C. *et al.* PYY plays a key role in the resolution of diabetes following bariatric surgery in humans. *EBioMedicine* **40**, 67–76 (2019).
  244. Monteiro, R. & Azevedo, I. Chronic inflammation in obesity and the metabolic syndrome. *Mediators Inflamm.* **2010**, (2010).

245. Villarreal-Calderón, J. R. *et al.* Interplay between the Adaptive Immune System and Insulin Resistance in Weight Loss Induced by Bariatric Surgery. *Oxid. Med. Cell. Longev.* **2019**, (2019).
246. Rao, S. R. Inflammatory markers and bariatric surgery: A meta-analysis. *Inflamm. Res.* **61**, 789–807 (2012).
247. Poitou, C. *et al.* Bariatric surgery induces disruption in inflammatory signaling pathways mediated by immune cells in adipose tissue: A RNA-seq study. *PLoS One* **10**, 1–23 (2015).
248. Roberts, H. M. *et al.* Impact of Bariatric Surgical Intervention on Peripheral Blood Neutrophil (PBN) Function in Obesity. *Obes. Surg.* **28**, 1611–1621 (2018).
249. Frikke-Schmidt, H. *et al.* Weight loss independent changes in adipose tissue macrophage and T cell populations after sleeve gastrectomy in mice. *Mol. Metab.* **6**, 317–326 (2017).
250. Subramaniam, R. *et al.* Sleeve Gastrectomy and Roux-en-Y Gastric Bypass Attenuate Pro-inflammatory Small Intestinal Cytokine Signatures. *Obes. Surg.* **29**, 3824–3832 (2019).
251. Harris, D. A. *et al.* Sleeve gastrectomy enhances glucose utilization and remodels adipose tissue independent of weight loss. *Am. J. Physiol. - Endocrinol. Metab.* **318**, E678–E688 (2020).
252. Biobaku, F., Ghanim, H., Monte, S. V., Caruana, J. A. & Dandona, P. Bariatric surgery: Remission of inflammation, cardiometabolic benefits, and common adverse effects. *J. Endocr. Soc.* **4**, 1–17 (2020).
253. Russell, M. A. & Morgan, N. G. The impact of anti-inflammatory cytokines on the pancreatic  $\beta$ -cell. *Islets* **6**, (2014).
254. Rützi, S. *et al.* IL-13 improves beta-cell survival and protects against IL-1 $\beta$ -induced beta-cell death. *Mol. Metab.* **5**, 122–131 (2016).
255. Chong, M. M. W., Thomas, H. E. & Kay, T. W. H.  $\Gamma$ -Interferon Signaling in Pancreatic B-Cells Is Persistent But Can Be Terminated By Overexpression of Suppressor of Cytokine Signaling-1. *Diabetes* **50**, 2744–2751 (2001).
256. Du, J. peng *et al.* IFN- $\gamma$  secretion in gut of Ob/Ob mice after vertical sleeve gastrectomy and its function in weight loss mechanism. *J. Huazhong Univ. Sci. Technol. - Med. Sci.* **36**, 377–382 (2016).
257. Renga, B., Mencarelli, A., Vavassori, P., Brancaleone, V. & Fiorucci, S. The bile acid sensor FXR regulates insulin transcription and secretion. *Biochim. Biophys. Acta - Mol. Basis Dis.* **1802**, 363–372 (2010).
258. Popescu, I. R. *et al.* The nuclear receptor FXR is expressed in pancreatic  $\beta$ -cells and protects human islets from lipotoxicity. *FEBS Lett.* **584**, 2845–2851 (2010).
259. Achel Valdez, I. *et al.* Proinflammatory Cytokines Induce Endocrine Differentiation in Pancreatic Ductal Cells via STAT3-Dependent NGN3 Activation. *Cell Rep.* **15**, 460–470 (2016).
260. Zhang, G. *et al.* Elevated expression of serum amyloid A 3 protects colon epithelium against acute injury through TLR2-dependent induction of neutrophil IL-22 expression in a mouse model of colitis. *Front. Immunol.* **9**, 1–11 (2018).
261. Ather, J. L. & Poynter, M. E. Serum amyloid A3 is required for normal weight and immunometabolic function in mice. *PLoS One* **13**, (2018).
262. Brelje, T. C. *et al.* Effect of homologous placental lactogens, prolactins, and growth hormones on islet B-cell division and insulin secretion in rat, mouse, and human islets: implication for placental lactogen regulation of islet function during pregnancy. *Endocrinology* **132**, 879–887 (1993).
263. Kondegowda, N. G., Zhang, X., Williams, K., Mozar, A. & Vasavada, R. C. Growth Factor Mediated Regulation of Beta Cell Survival. *Open Endocrinol. J.* **4**, 78–93 (2011).
264. Huang, B. *et al.* Placenta-Derived Osteoprotegerin Is Required for Glucose Homeostasis in Gestational

- Diabetes Mellitus. *Front. Cell Dev. Biol.* **8**, 1–12 (2020).
265. Goyvaerts, L. *et al.* Prolactin receptors and placental lactogen drive male mouse pancreatic islets to pregnancy-related mRNA changes. *PLoS One* **10**, (2015).
  266. Wang, X. *et al.* Glucose-Lipid Metabolism in Obesity with Elevated Prolactin Levels and Alteration of Prolactin Levels After Laparoscopic Sleeve Gastrectomy. *Obes. Surg.* **30**, 4004–4013 (2020).
  267. Sorensen, G. L. Surfactant protein D in respiratory and non-respiratory diseases. *Front. Med.* **5**, (2018).
  268. Stidsen, J. V. *et al.* Surfactant protein D deficiency in mice is associated with hyperphagia, altered fat deposition, insulin resistance, and increased basal endotoxemia. *PLoS One* **7**, (2012).
  269. Schraenen, A. *et al.* Placental lactogens induce serotonin biosynthesis in a subset of mouse beta cells during pregnancy. *Diabetologia* **53**, 2589–2599 (2010).
  270. Zhuang, G. Z. *et al.* Carbonic anhydrase-8 regulates inflammatory pain by inhibiting the ITPR1-cytosolic free calcium pathway. *PLoS One* **10**, 1–24 (2015).
  271. Pepin, M. E. *et al.* Prolactin receptor signaling regulates a pregnancy-specific transcriptional program in mouse islets. *Endocrinology* **160**, 1150–1163 (2019).
  272. Johnston, N. R. *et al.* Beta Cell Hubs Dictate Pancreatic Islet Responses to Glucose. *Cell Metab.* **24**, 389–401 (2016).
  273. van der Meulen, T. *et al.* Virgin Beta Cells Persist throughout Life at a Neogenic Niche within Pancreatic Islets. *Cell Metab.* **25**, 911-926.e6 (2017).
  274. Hudish, L., Lorberbaum, D. & Sussel, L. FISHing for beta cells. *Dev. Cell* **48**, 7–8 (2019).
  275. Wolf1, F. A., Angerer, P. & Theis, F. J. SCANPY: large-scale single-cell gene expression data analysis. *Genome Biol.* **19**, (2012).

## Acknowledgements

First of all, I want to thank my advisor Prof. Dr. Heiko Lickert for making this research project possible and for his excellent scientific support. I especially appreciated Heikos contagious enthusiasm for diabetes research as well as the inspiring working atmosphere I have experienced at the **Institute of Diabetes and Regeneration**. I also wish to thank the members of my thesis committee, Prof. Dr. Johannes Beckers, and PD Dr. Marcel Scheideler for their encouragement and scientific support on my research projects.

My special thanks goes to Dr. Anika Böttcher and Dr. Ansarullah, my direct supervisors and mentors who continuously supported me in any way. Thank you, Anika and Ansar, for sharing all your experience and expertise with me as well as for your positive attitude and encouragement during challenging phases of this doctorate project.

I also wish to express my gratitude to our collaborators at the **Institute of Computational Biology**, Prof. Dr. Dr. Fabian Theis and Subarna Palit. Thank you Subarna, for your indispensable work! I also want to thank my 'VSG team', Subarna and Ansar, for the exceptional team work, all the fun time we had in virtual meetings and finally for finishing our research manuscript. My sincere appreciation to Dr. Annette Feuchtinger at the **Institute of Analytical Pathology** for great and smooth collaboration. Additionally, I wish to thank Prof. Dr. Kerstin Stemmer from the **Institute of Diabetes and Obesity** for sharing her expertise on VSG with me, for her conceptual support of this study and investing the time on performing surgeries for this project.

Sincere thanks to Ines Kunze and Jürgen Schultheiß for excellent technical assistance, and the rest of our 'gut group' Dr. Anika Böttcher, Dr. Michael Sterr, Dr. Alexandra Aliluev, Dr. Felizitas Gräfin von Hahn, Veronika Vollmuth and Tobias Greisle for great team work and the good time we had during the last 5 years. I wish to thank Dr. Carina Yang and Dr. Aimée Bastidas-Ponce for discussing and proof-reading this thesis.

A big thanks to my 'IDR girls' Anna Blöchinger and Dr. Katharina Wißmiller for the mutual support and wonderful time together!

Finally, a heartfelt thanks goes to my family and friends, my parents and sisters, who are always there for me, to Sigrid, and especially to Stefan for his patience and support as well as to my little son Paul.

# Publications

Lena Oppenländer\*, Subarna Palit\*, Kerstin Stemmer, Tobias Greisle, Michael Sterr, Annette Feuchtinger, Ciro Salinno, Aimée Bastidas-Ponce, Anika Böttcher, Ansarullah, Fabian J. Theis and Heiko Lickert:

## **Vertical sleeve gastrectomy triggers fast $\beta$ -cell recovery upon overt diabetes.**

In revision at **Molecular Metabolism**.

Alexandra Aliluev\*, Sophie Tritschler\*, Michael Sterr, Lena Oppenländer, Julia Hinterdobler, Tobias Greisle, Martin Irmeler, Johannes Beckers, Na Sun, Axel Walch, Kerstin Stemmer, Alida Kindt, Jan Krumsiek, Matthias H. Tschöp, Malte D. Luecken, Fabian J. Theis, Heiko Lickert and Anika Böttcher:

## **Diet-induced alterations in ISC function underlies obesity and pre-diabetes.**

In press at **Nature Metabolism** 2021.

Ansarullah\*, Chirag Jain\*, Fataneh Fathi Far\*, Katharina Wißmiller\*, Sarah Homberg\*, Felizitas Gräfin von Hahn\*, Aurelia Raducanu, Silvia Schirge, Michael Sterr, Sara Bilekova, Johanna Siehler, Julius Wiener, Lena Oppenländer, Amir Morshedi, Aimee Bastidas-Ponce, Gustav Collden, Martin Irmeler, Johannes Beckers, Annette Feuchtinger, Michal Grzybek, Christin Ahlbrecht, Regina Feederle, Oliver Plettenburg, Timo D. Müller, Matthias Meier, Matthias H. Tschöp, Ünal Coskun and Heiko Lickert:

## **Inceptor counteracts insulin signalling in $\beta$ -cells to control glycaemia.**

**Nature** 2021.

Anika Böttcher, Maren Büttner, Sophie Tritschler, Michael Sterr, Alexandra Aliluev, Lena Oppenländer, Ingo Burtscher, Steffen Sass, Martin Irmeler, Johannes Beckers, Christoph Ziegenhain, Wolfgang Enard, Andrea C. Schamberger, Fien M. Verhamme, Oliver Eickelberg, Fabian J. Theis and Heiko Lickert:

## **Non-canonical Wnt/PCP signalling regulates intestinal stem cell lineage priming towards enteroendocrine and Paneth cell fates.**

**Nature Cell Biology** 2021.

Thomas Grund, Yan Tang, Diego Benusiglio, Ferdinand Althammer, Sophie Probst, Lena Oppenländer, Inga D. Neumann and Valery Grinevich:

## **Chemogenetic activation of oxytocin neurons: Temporal dynamics, hormonal release, and behavioral consequences.**

**Psychoneuroendocrinology** 2019.

\* These authors contributed equally to the publication